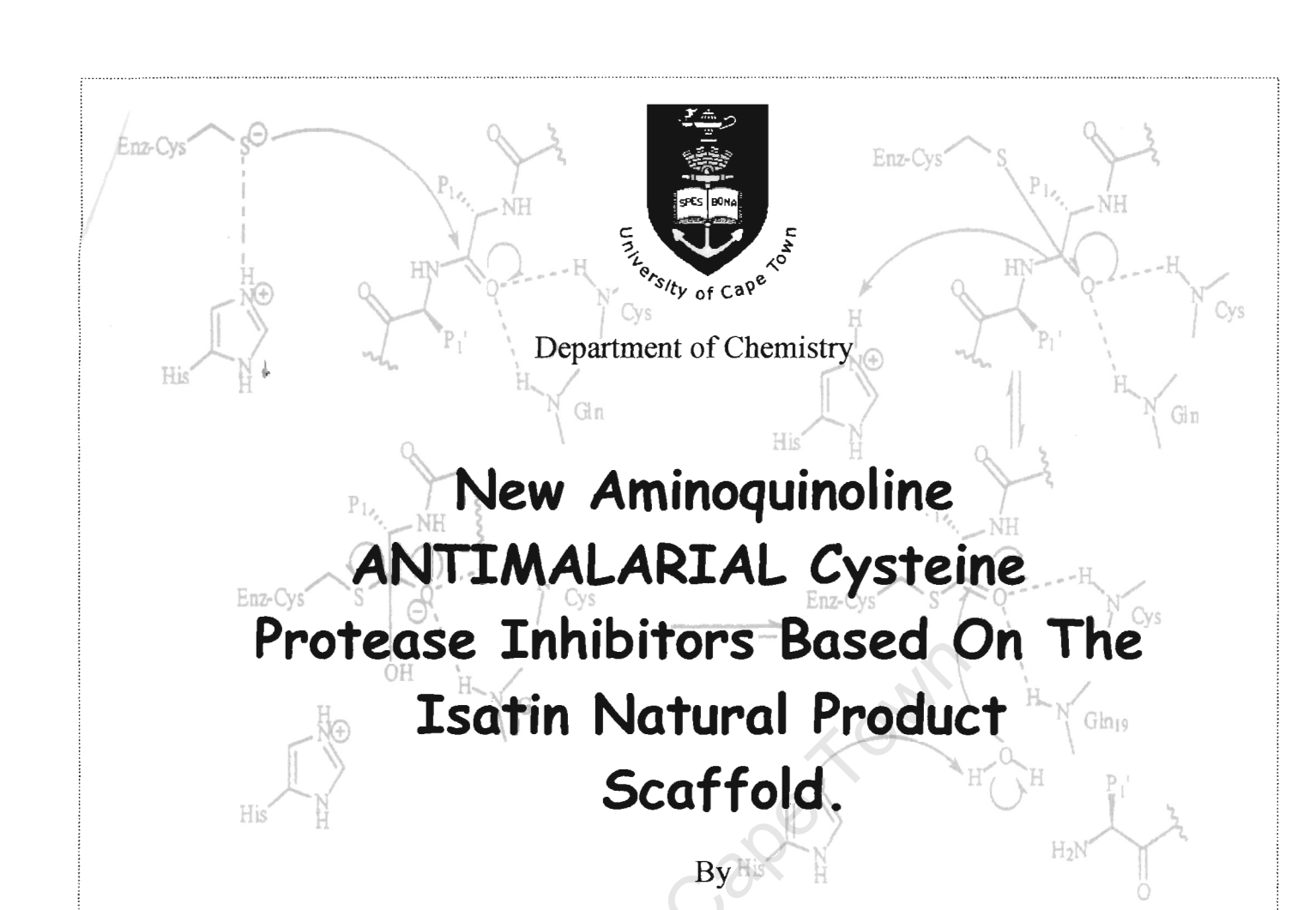

Department of Chemistry

New Aminoquinoline ANTIMALARIAL Cysteine Protease Inhibitors Based On The Isatin Natural Product Scaffold.

By

Nelson Axe Ntuli

A thesis presented for the degree of

MASTER OF SCIENCE

In the subject

CHEMISTRY

Supervisor:

Associate Professor Kelly Chibale

JANUARY 2005

CONTENTS

ACKNOWLEDGEMENTS

I would like to thank my supervisor Associate Professor Kelly Chibale for giving me the opportunity, guidance, advice, encouragement and support throughout the course of this work.

Thanks to all my colleagues in the group I worked with especially Dr. A. Nchinda, Dr Frank Chouteau, Chitalu Musonda, Freddy Munyololo, Mlungiseleli Ganto, Alex Chipeleme & Fereidoon Daryaee for advice and ideas.

Also thanks to Pete Roberts and Noel Hendricks for NMR experiments, Arthur Joseph for maintenance, Pierro Benincasa for microanalysis, Dr. Louis Fourie (University of Potchefstroom) and Tommy van der Merwe (University of Witswatersrand) for mass spectra measurements and collaborators who assisted in the biological testing of synthesized compounds, Prof. Philip J. Rosenthal and Jiri Gut (School of Medicine, University of California San Francisco, USA), for inhibition of falcipain-2 and growth of cultured malaria parasites (W2 strain) *in vitro*; My sincere gratitude also goes to the South African National Research Foundation and the University of Cape Town for financial support.

Lastly, I would like thank Father Alan Kay, my whole big family of Mamvelase; especially; Thembekile, Mathole, Zamisa, Agnes Phi, all my brothers and sisters especially Thandazile, Ntuthuko, Ncedile & Sizwe, the late Nomusa, Mqiniseni, Mbongi, Samukelo, & Thembisile to whom I dedicate this work.

ABSTRACT

Presented in this thesis is the work on *New 4-Aminoquinoline Antimalarial Cysteine Protease Inhibitors Based On The Natural Product Isatin Scaffold.*

Many antimalarial drugs including chloroquine are no longer effective against the disease, as their efficacy has been decreased by the spread of drug resistant strains. This loss has been a major barrier to the effective treatment of malaria and has necessitated an urgent need to discover new antimalarial drugs.

New 4-aminoquinoline isatin derivatives have been designed and synthesised. Isatin was used as a biologically validated starting point for the design of chemical libraries directed at the intended target due to its privileged nature. Included in the design of these isatin derivatives is the thiosemicarbazone moiety previously demonstrated to inhibit cysteine proteases from multiple protozoan parasites.

Synthesized compounds were tested against the enzyme falcipain-2 (Rec-FP-2) as well as the parasite source of this protease, *Plasmodium falciparum* (P.f. W2). The results of structure activity relationship studies demonstrate the influence of substituents at position 5 of the isatin scaffold. With respect to the chain length, a two carbon methylene spacer between the aminoquinoline and isatin moieties, was found optimum. A 5-bromo isatin derivative with this spacer, compound **79b**, was found to be the most active with an IC_{50} value of 163.5 nM against the W2 parasite strain and second most active against the enzyme (IC_{50} = 3.65 μM).

Another class of derivative was designed and synthesized to include the β-amino alcohol moiety, a known antimalarial pharmacophore. It was hypothesized that incorporation of a β-amino alcohol fragment would lead to improved antimalarial activity. β-Amino alcohol compound **89** was indeed found to be substantially more active (IC_{50} P.f. W2 ~ 19 nM) than the corresponding compound **79c** (IC_{50} P.f.W2 ~ 206 nM) without the amino alcohol fragment. Relative to chloroquine, compound **89** is also substantially more active (IC_{50} for chloroquine in P.f. W2 ~ 300 nM). However, the activity of compound **89** against FP2 was modest (IC_{50} = 16.8 μM) suggesting a lack of strong correlation between inhibition of FP2 and antimalarial activity *in vitro*, which may in turn suggest other mechanisms may be involved.

ABBREVIATIONS

DTT	Dithiothreitol
DMSO	Dimethylsulfoxide
DNA	Deoxyribonucleic acid
Et	Ethyl
equiv.	Equivalent
GR	Glutathione reductase
GSH	Glutathione
GSSG	Glutathione disulfide
h	Hour
Hb	Haemoglobin
His	Histidine
HRMS	High Resolution Mass Spectrometry
IC_{50}	Inhibitory concentration to inhibit 50 % of enzyme activity or parasite growth
IR	Infrared
mol	Mole
Me	Methyl
MS	Mass Spectrometry
NMR	Nuclear Magnetic Resonance
P	*Plasmodium*
RBC	Red Blood Cell
rt	Room temperature
SAR	Structure-Activity Relationship
S_N2	Nucleophilic bimolecular substitution
SHAM	Salicylhydroxamic acid
T.	*Trypanosoma*
T. b	*Trypanosoma brucei*

TLC	Thin layer chromatography

The following abbreviations are used in the EXPERIMENTAL section;

s	singlet
br	broad
br s	broad singlet
d	doublet
dd	double of doublets
t	triplet
q	quartet
quint	quintet
m	multiplet
δ	chemical shift
Anal.	Analytical
cm^{-1}	wavenumbers
EI	Electron impact
mp	Melting point
m/z	mass to charge ratio
R_f	Retention factor

CHAPTER 1

INTRODUCTION

1.1 HISTORY OF MALARIA

Malaria was thought to be common in ancient Greece, Egypt, India, and China, where it was actually described and recorded [1]. The disease was named "*mal' aria*" as it was believed to be connected to "bad air" surrounding stagnant water [1]. Malariologists were fascinated by the malaria pigment since Meckel (1847) first identified a certain pigment in the blood and spleen of an insane person, but no connection was made [2]. Later Virchow (1849) was able to connect the pigment to malaria when he studied and described pigmented bodies in the blood of a patient with chronic malaria. Hischl (1850) verified and confirmed the presence of pigment with intermittent fevers [3]. Carbone isolated the malaria pigment from the autopsied spleen of a 33-year-old man in 1891[4]. Since then, the literature is filled with controversy over the pigment's composition.

1.2 IMPORTANCE OF MALARIA.

Malaria is the most serious and important parasitic disease in the world, ranking fifth in terms of numbers of deaths due to infectious diseases [5]. Approximately 2 billion people are at risk from this disease in tropical and subtropical areas of the world [6]. About 300-500 million people are infected with the disease every year, leading to 1.5 to 3 million deaths [3], the majority of which happen in young children [5].

Today the disease has become very crucial and widespread due to many factors. It has spread into areas that were previously not affected as a result of changing land utilization, especially plantation agriculture. This includes regions such as highland areas of East Africa. A map below (Figure 1) shows that almost 90 % of these deaths occur in Sub-Saharan Africa.

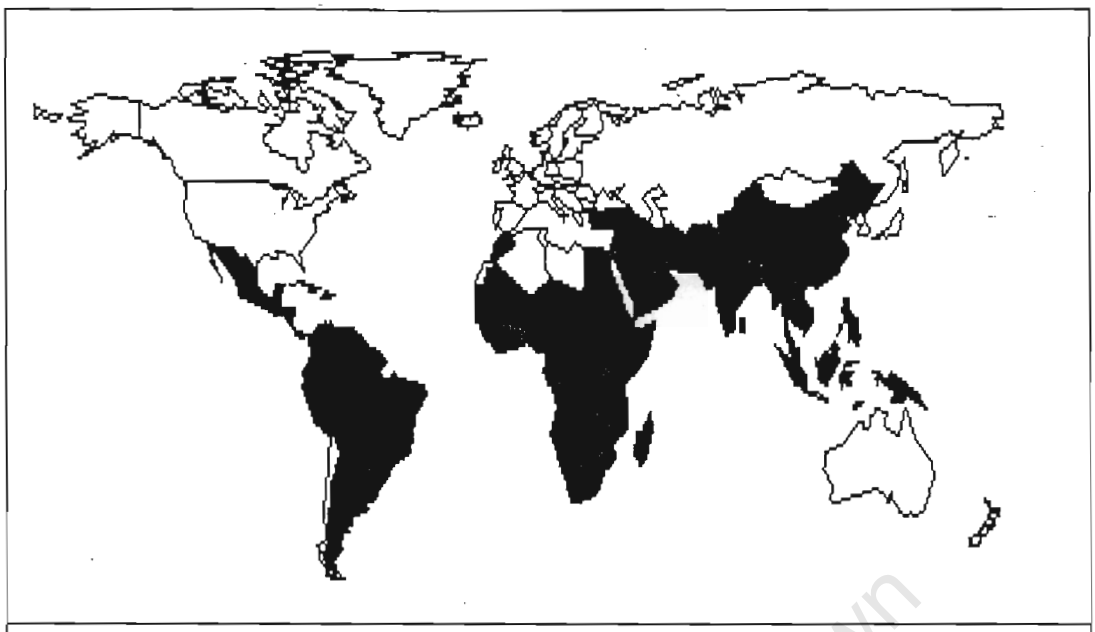

Figure 1: A map showing the current worldwide distribution of malaria.

The other factor is that many antimalarial drugs including chloroquine, are no longer effective against the disease, as their efficacy has been decreased by the spread of drug resistant strains [6]. This loss in efficacy has been a major barrier to the effective treatment of malaria and has posed an urgent challenge to discover new antimalarial drugs.

1.3 LIFE CYCLE OF THE MALARIA PARASITE.

Malaria is caused by four species of the genus *Plasmodium*, namely *P. falciparum*, *P. vivax, P. ovale* and *P. malariae* [6]. Almost all fatalities are due to *P. falciparum* infections and it is therefore the most important species, but *P. vivax* also causes significant morbidity [5]. Fortunately the biology of *P. falciparum* is the most well understood of the four species as techniques for maintaining it in culture have been available for two decades [5].

The life cycle of *P.falciparum* has three overall stages namely; mosquito, liver and blood stages [6] (see Figure 2). Gametocytes are reproduced sexually in the gut of the mosquito leading to the formation of zygotes that hide themselves in the gut lining of the mosquito.

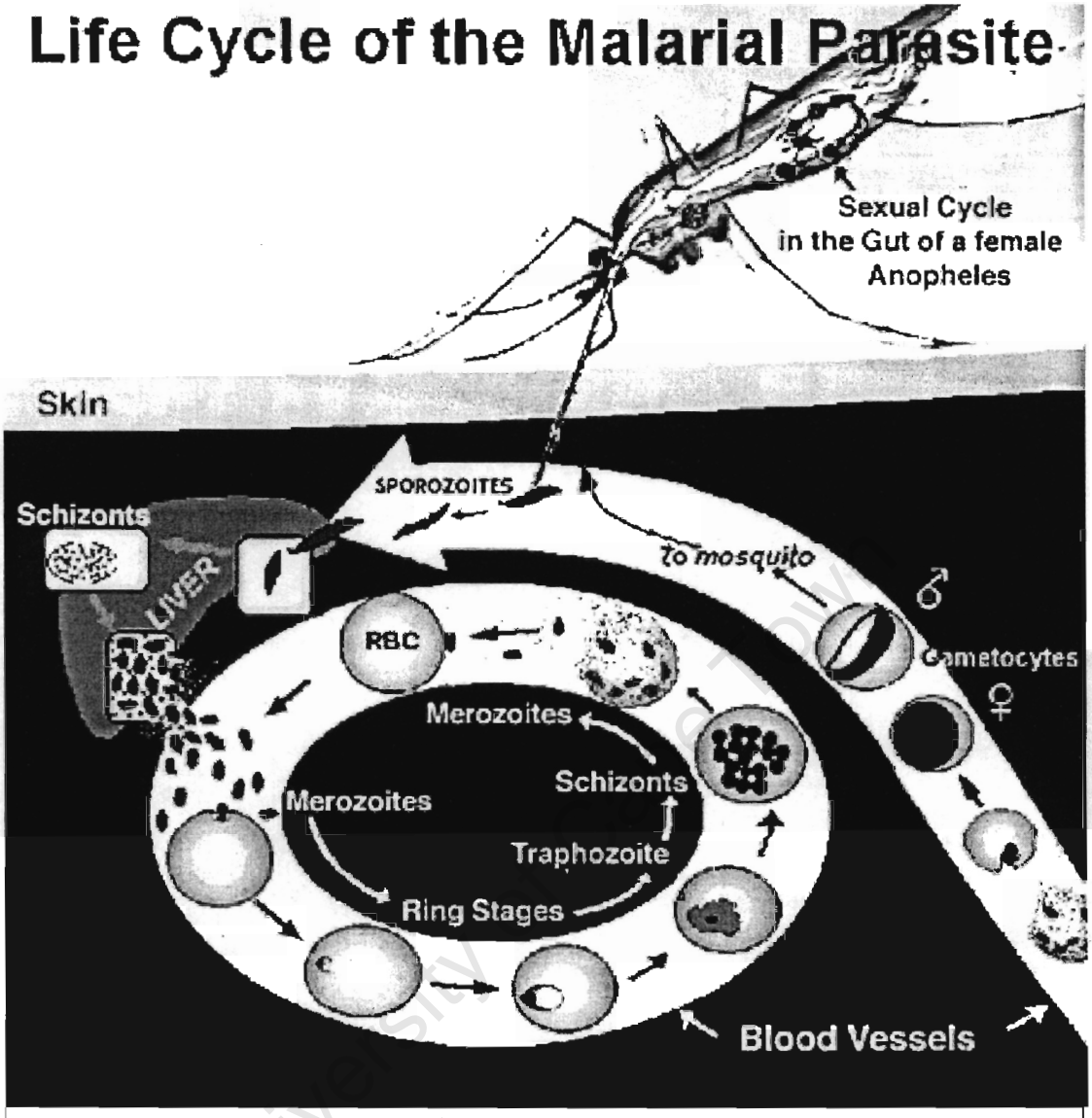

Figure 2: Life cycle of malaria parasite [4].

The zygotes then develop into oocysts to form sporozoites after some time, which migrate to the salivary glands of the mosquito. When an infected mosquito bites a human host, these sporozoites enter the blood stream and quickly make their way to the liver, invading hepatocytes.

The parasites multiply asexually as tissue schizonts during a period of development of about a week, and then enter the blood stream as merozoites. These merozoites invade red blood cells, entering into the blood cycle consisting of ring, trophozoite and blood

schizont stages. The reproduction (asexual) in the red blood cells leads to further merozoites increasing the parasitaemia. Some of the merozoites develop into gametocytes upon entering the cell and may be taken up by mosquitoes to complete the cycle. The signs of the disease are associated with the blood stage and any potential drug must specifically act against this stage of the life cycle [5].

1.4 ANTIMALARIAL CHEMOTHERAPY

1.4.1 Quinolines

Quinoline antimalarials and related aryl alcohols originated from quinine **1** (Figure 3) an active ingredient that was isolated from the *Cinchona* bark. Quinine was first imported in Europe from Peru for antimalarial use in the seventeenth century [7]. The use of quinine was found to result in toxicity such as tinnitus and it requires a three-times-a-day administration over a period of 7 days.

Thus, opportunities presented by its structural elucidation led to the development of the fully synthetic chloroquine **2** and later amodiaquine **3**, cheap antimalarials administered over a 3 day period [8]. As shown in Figure 3, a quinoline moiety acts as a template for the synthetic agents chloroquine/amodiaquine and related drugs. Amodiaquine retains a high degree of efficacy against the disease. However, the drug was linked to the occurrence of occasional agranulocytosis in adult travelers using the drug [9] and was also found to be inactive against chloroquine resistant strains.

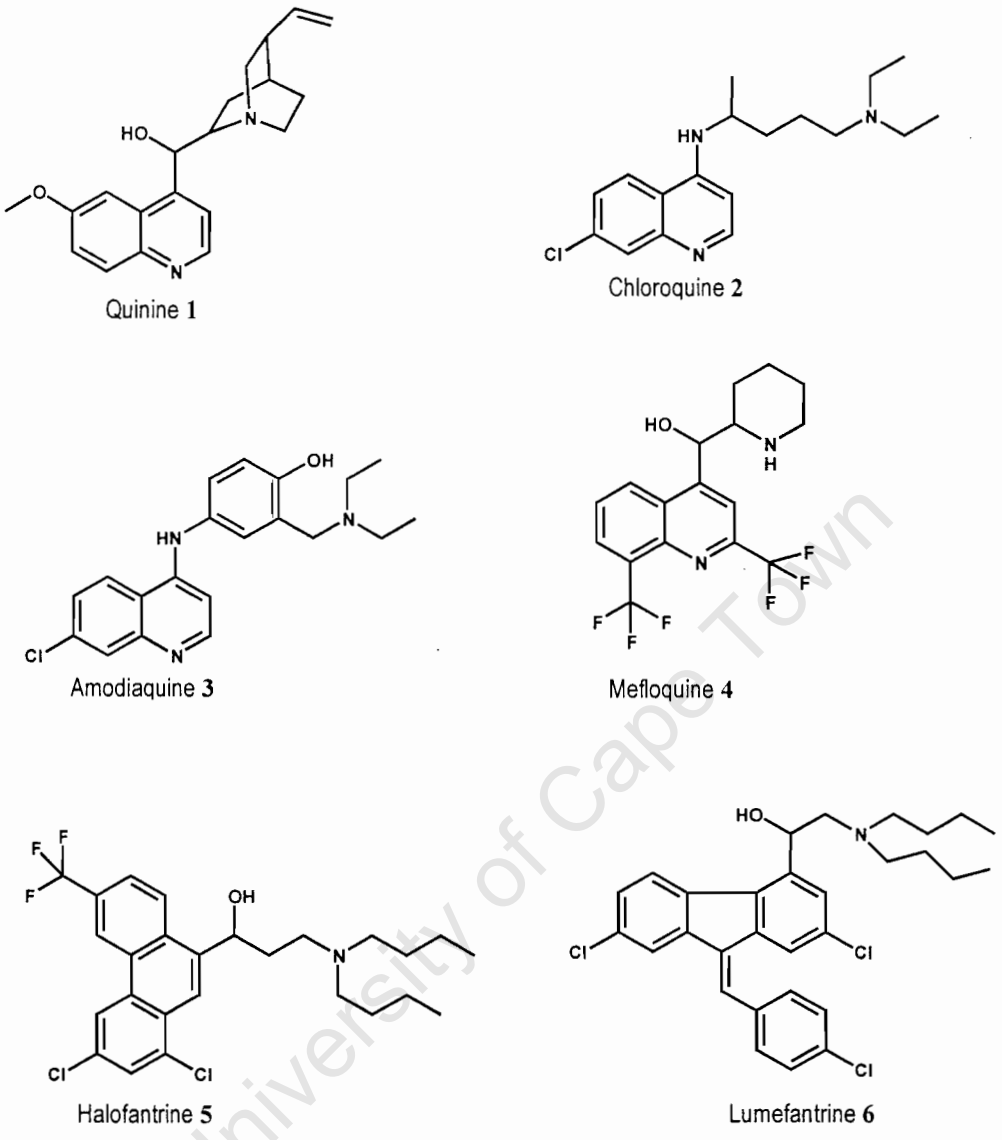

Figure 3: Antimalarials used clinically.

Mefloquine **4**, halofantrine **5** and lumefantrine **6** are structurally related amino alcohol drugs that are active against chloroquine resistant strains, but resistance can develop rapidly to each of these drugs. In addition, halofantrine has some side effects to people with a history of heart disease [9].

With the rise of parasites resistant to these antimalarials, it became a necessity to search for other synthetic and natural product-based agents. Inspection of the data from Chinese herbal remedies led to the investigation of extracts of *Artemisia annua* (Wormwood).

1.4.2 Artemisinins

Artemisia annua is a particular plant that has been used for centuries in China as an antimalarial [10] known as 'Quinghaosu'. In 1972, from this particular plant an active ingredient was isolated and identified as a sesquiterpene endoperoxide called artemisinin **7** (see Figure 4a).

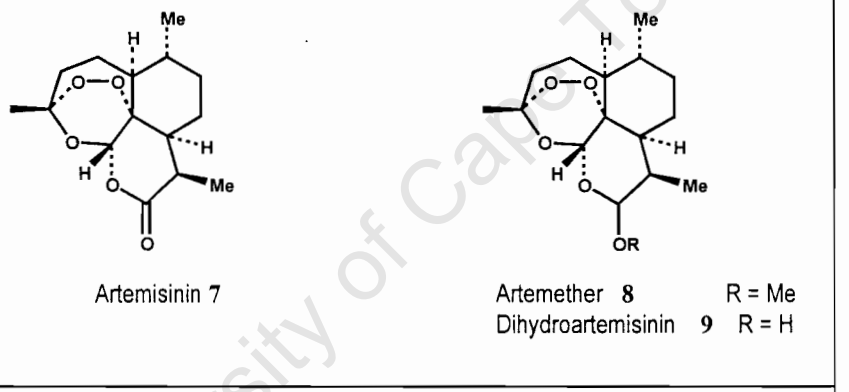

Figure 4a: Artemisinin Antimalarials.

Many semi-synthetic compounds were made using the base structure of artemisinin to optimize the pharmacology. This led to the identification of artemether **8**. As a potent antimalarial agent that is now used throughout the world, artemether is a simple modification of the actual active metabolite, dihydroartemisinin **9**. Despite modifications to improve solubility and distribution, the active constituent ended up to be the same molecule [11].

1.5 NATURAL PRODUCTS AS SOURCES OF NEW DRUGS

1.5.1 History and Role of Natural Products

Plants have formed the basis of sophisticated traditional medicine systems for thousands of years. More recently, natural products have been a good source of most important lead compounds, especially against infectious diseases. The most important lead compound against malaria is the alkaloid quinine **1**, isolated from the *Cinchona* bark in the 1800's [11], which was used as a template for chloroquine **2** and mefloquine **4** as explained before. More recently, artemisinin **7**, isolated from the Chinese plant *Artemisia annua*, has been used successfully against malaria that has become resistant to chloroquine.

Some medicines were discovered by accidental observations, for example penicillin. Alexander Fleming discovered it when he noticed that his bacterial cultures were killed by the mold (Penicillium), which produces penicillin, which kills many kinds of bacteria. Chemical modification of known drugs can often lead to improved drugs. The natural product Penicillin G **a** (Figure 4b) is broken down by bacterial beta-lactamases. However, the modification of Penicillin G by adding two $-OCH_3$ groups, leads to methicillin **b**, which is resistant to lactamase.

Another alkaloid that was isolated in the 1800's along with quinine is morphine **c**, which was first commercialized in 1826. Morphine, which occurs in opium poppies is a powerful analgesic, but has serious side effects such as respiratory depression, constipation, and dependence liability. Over thousands of chemical structures related to morphine have been synthesized in an attempt to get an analgesic with fewer side effects. Sometimes a little chemical modification may have a huge influence on the activity. For example, nalorphine **d** partially antagonizes (exhibits some morphine-like activity, and at higher concentration, antagonizes morphine effects) morphine, whereas naloxone **e** is an antagonist.

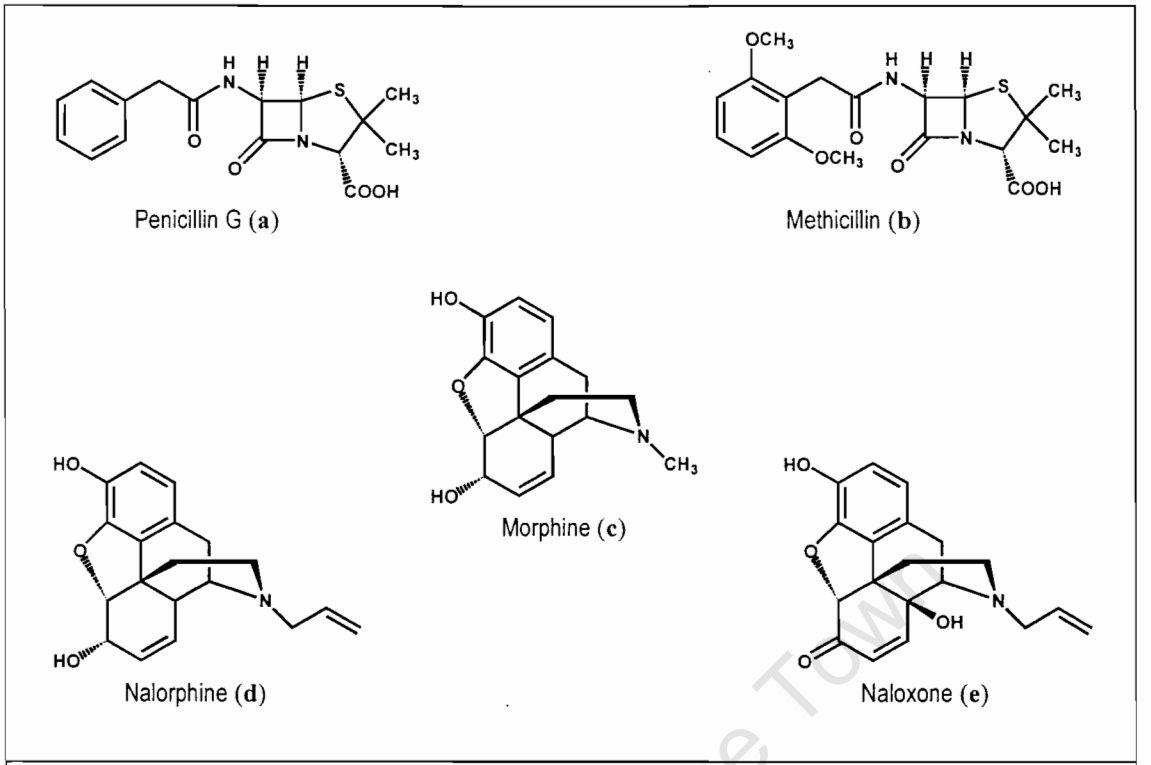

Figure 4b: Natural products with medicinal properties.

A previous study has shown that natural products play a very essential role in the drug discovery, development process and health care systems [12]. Over 75 % of these drugs respectively, were shown to be of natural origin in the area infectious diseases, based on the numbers of new drugs approved by regulatory agencies. This is as reported in Annual Reports of Medicinal Chemistry from 1983 to 1994 the United States Food and Drug Administration (FDA) is an example of a regulatory agency [12]. Presently, at least 119 chemical substances, derived from 90 plant species, can be considered as important drugs that are in use in one or more countries [13]. 74 % of these 119 drugs were discovered as a result of chemical studies directed at the isolation of the active substances from plants used in traditional medicine. It is evident that natural products still play a major role in drug treatment; it has been shown recently that over 50 % of the most-prescribed drugs in the US had a natural product either as the drug, or as part of the agent [14].

1.6 ISATIN AS A NATURAL PRODUCT SCAFFOLD FOR BIOLOGICALLY ACTIVE MOLECULES

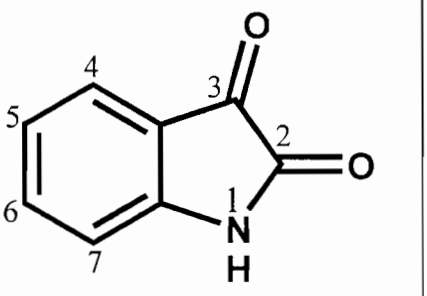

Figure 5: Isatin (1H-indole-2, 3-dione).

In 1941, isatin (1*H*-indole-2, 3-dione) was first made by Erdman and Laurent as a product from oxidation of indigo by nitric and chromic acids [15]. Isatin is naturally available, in plants of the genus *Isatis* [16] and has also been obtained as a component of the secretion from the parotid gland of *Bufo* frogs. In humans, isatin is a metabolic derivative of adrenaline [18-20].

Various isatin derivatives are known to possess a range of pharmacological properties including antiprotozoal activities [21, 22]. Isatins have recently been used in the inhibition of cysteine and serine proteases [23, 24]. Isatins are therefore biologically validated starting points for the design and synthesis of chemical libraries directed at these targets [25]. As a privileged natural product scaffold, derivatives synthesized around the basic structure of isatin should yield medicinally active compounds with high hit rates at significantly reduced library size compared to large classical libraries obtained from combinatorial chemistry efforts based on non-privileged templates [26].

1.7 SYNTHESIS OF ISATINS

1.7.1 The Sandmeyer's Methodology

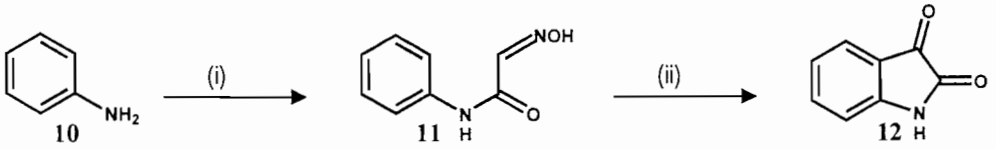

Scheme 1: Sandmeyer's Methodology (i) $Cl_3CCH(OH)_2$, $NH_2OH.HCl$, Na_2SO_4 (ii) H_2SO_4, H_2O.

The most frequently used method for the synthesis of isatins is the one developed by Sandmeyer (Scheme 1). This involves the reaction of aniline **10** with chloral hydrate and hydroxylamine hydrochloride in aqueous sodium sulphate to form an isonitrosoacetanilide **11**. After isolation, the isonitrosoacetanilide is treated with concentrated sulfuric acid to yield more than 75 % of isatin **12** [27].

1.7.2 The Stolle's Proceedure

This procedure by Stolle is the most essential alternative to Sandmeyer's. The Stolle procedure involves reacting anilines with oxalyl chloride to form oxalylanilides, which can be cyclized in the presence of a Lewis acid such as aluminium chloride or $BF_3.OEt_2$ [28]. Dimethoxyanilines such as **13** have been observed to undergo spontaneous cyclization to yield dimethoxyisatins (Meloisatin) **14** in the absence of a Lewis acid [29] as shown in Scheme 2.

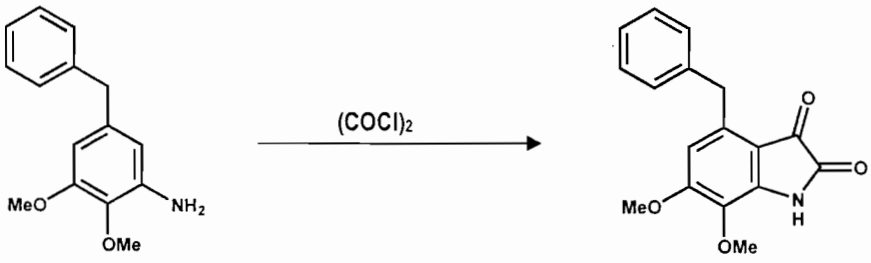

13 14

Scheme 2: Stolle's procedure, an alternative to Sandmeyer's.

This method seems to be the best alternative for obtaining these derivatives, since aminophenols were found to be poor substrates leading to unsuccessful reactions [30].

1.7.3 The Martinet Isatin Synthesis

An aminoaromatic compound **15** is reacted with an oxomalonate ester or its hydrate in the presence of an acid to give a (3-hydroxy-2-oxindole) **16**. The carboxylic acid derivative then undergoes oxidative decarboxylation to yield the desired isatin **17** (Scheme 3).

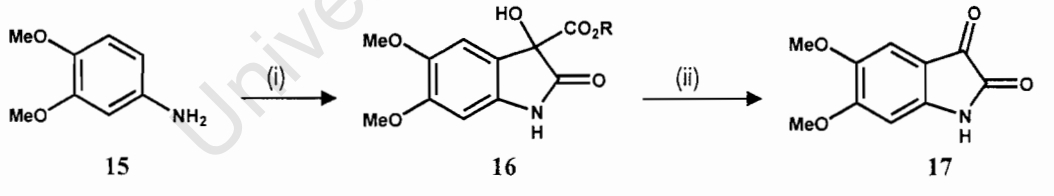

15 16 17

Scheme 3: The Martinet Isatin Synthesis. (i) Oxomalonate ester, H_3O^+ (ii) Oxidative decarboxylation.

1.7.4 The Glassman Proceedure

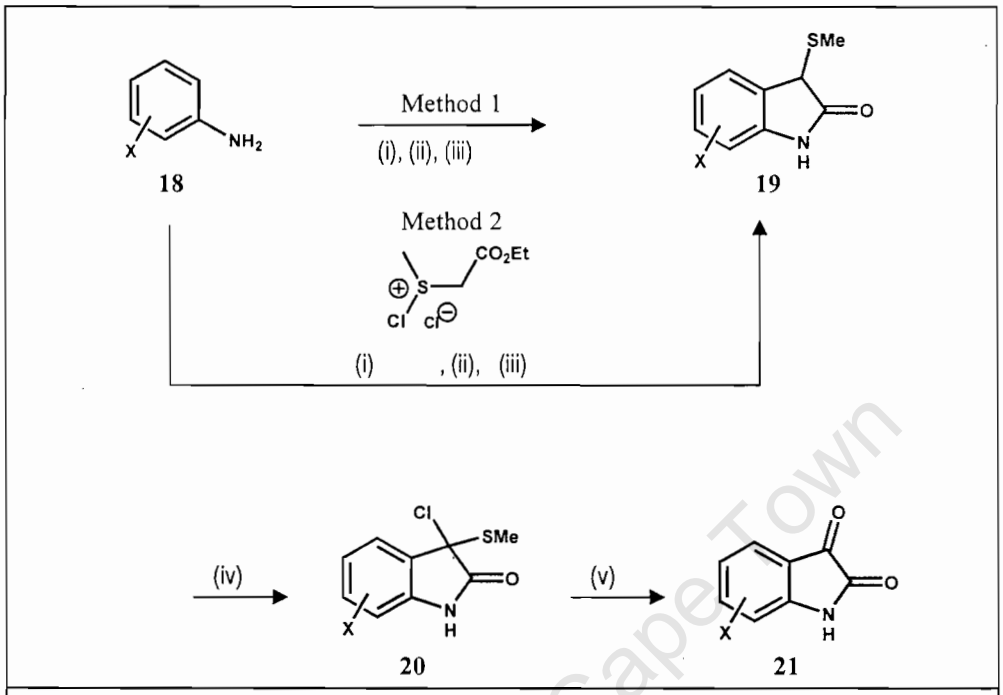

Scheme 4: Method 1: (i) tBuOCl, $MeSCH_2CO_2Et$, (ii) Et_3N (iii) H_3O^+ Method 2: (ii) Et_3N, (iii) H_3O^+ (iv) NCS, (v) HgO/BF_3 or $H_2O/THF/\Delta$.

This alternative method consists of the formation of intermediate 3-methylthio-2-oxindole **19** or **20** [31-33] from the aniline derivative **18** (Scheme 4). The intermediate is then oxidised to yield (40-81 %) of the corresponding substituted isatin **21**.

1.8 CHEMISTRY OF ISATINS

1.8.1 *N*-Methylene Amino Derivatives

N-Methyleneamino isatins (Mannich bases) can be synthesised through performance of the Mannich reaction. Mannich bases are prepared by reacting an isatin with a primary or secondary amine. This reaction type can also be carried out with isatin derivatives such as

isatin-thiosemicarbazones. A series of corresponding *N*- Mannich bases was synthesized by reacting isatins with formaldehyde and diphenyl amine (Scheme 5).

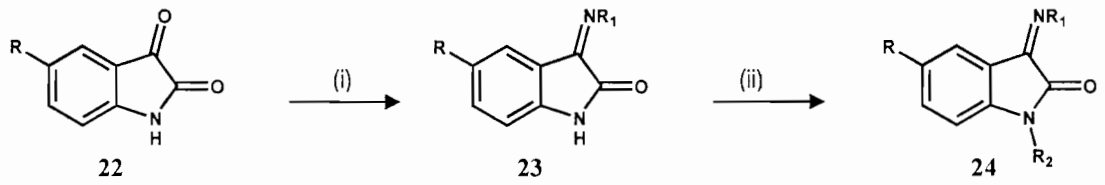

Scheme 5: Synthesis of N-Mannich bases (i) R_1-NH_2 (ii) HCHO, $NH(C_6H_5)_2$ where R = H, Cl, Br, CH_3, NO_2; R_1 = –NH-C(S)-NH_2, -BzCl, $BzCH_3$, $BzOCH_3$ (ii) -NH_2–NH-C(S)-NH_2 and R_2 = H, -CH_2-N$(C_6H_5)_2$.

1.8.2 *N*-Acylation

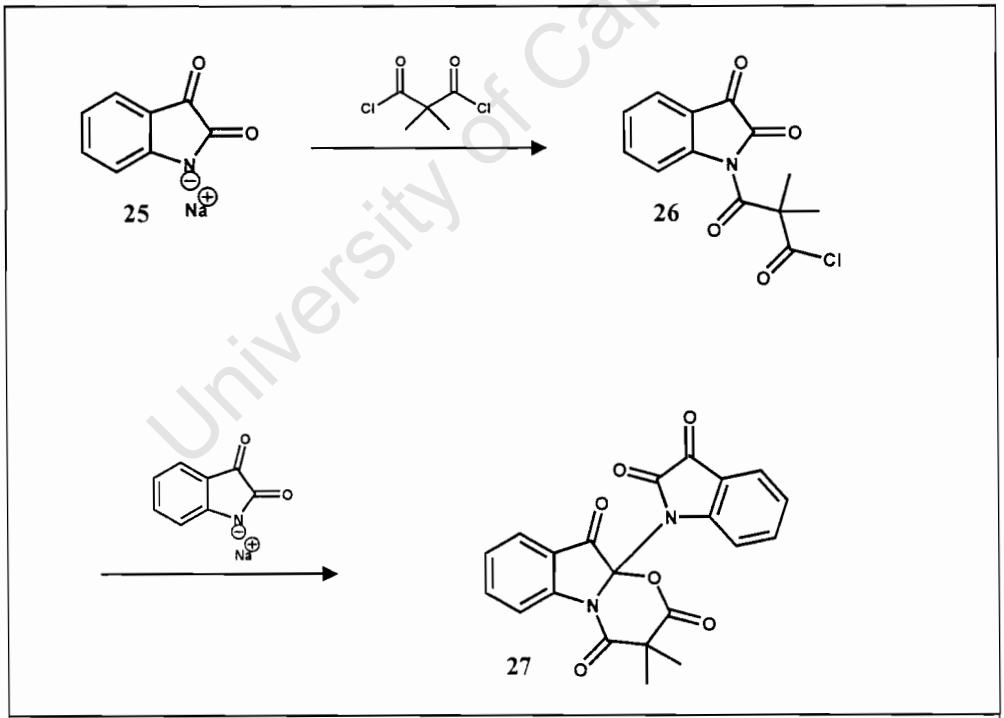

Scheme 6: N-Acylation of Isatins.

Acylation may be carried out using perchloric acid, triethylamine or pyridine in benzene without an additive [34]. Scheme 6 shows that this reaction is achieved by converting an isatin to sodium isatide **25** using NaH in toluene under reflux followed by reaction with acyl chlorides [35]. The use of diacyl chlorides such as oxalyl, octanedioyl or nonanedioyl chlorides [36], yields *N*-acylisatin **26**. Attempts to use 2, 2-dimethylmalonyl chloride to furnish 2, 2-dimethylmalonyl-bis-isatin failed, and led instead to an unusual tricyclic compound **27** which was characterized by spectroscopic methods and by X-ray diffraction [37].

1.8.3 Reactivity of the Aromatic Nucleus

Isatins with substituents attached to the aromatic ring can be obtained from anilines with corresponding functionality. Attachment of substituents to the aromatic ring can also be achieved through electrophilic aromatic substitution. Bromination of isatin **28** with *N*-bromoacetamide in acetic acid (Scheme 7) gives 5-bromoisatin **29** in a high yield [38].

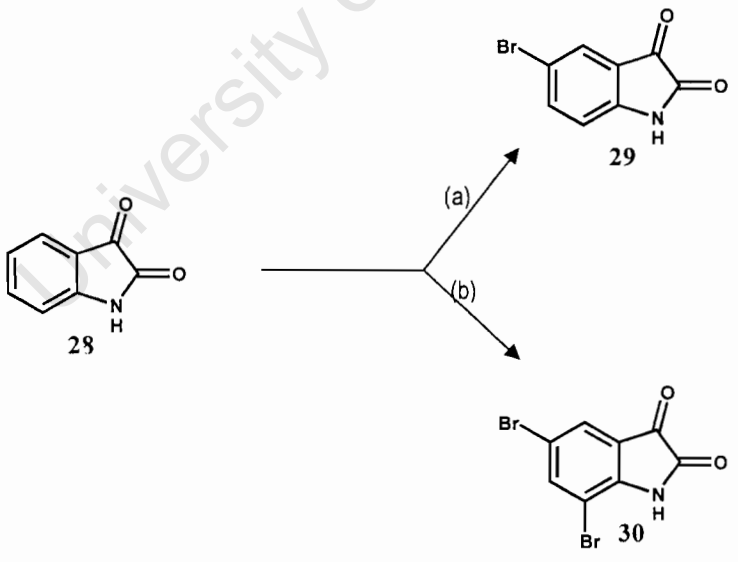

Scheme 7: Bromination of isatin (a) N-bromo acetamide, CH_3COOH, 90 %; (b) Br_2, 95 % warm EtOH, 80 %.

5, 7-Dibromoisatin **30** can also be synthesized using bromine in the presence of warm 95 % ethanol in 80 % yield [37].

CHAPTER 2

CYSTEINE PROTEASES
AND THEIR INHIBITORS

2.1 WHY CYSTEINE PROTEASES?

The specific cysteine protease inhibitor E-64 partially inhibited the denaturation of the hemoglobin molecule and blocked the separation of haem from globin when incubated with cultured malaria parasites. This was demonstrated by the fact that most of the haemoglobin that accumulated in these parasites appeared to be partially denatured. This implies that there are enzymes likely also involved in haemoglobin denaturation in addition to the cysteine protease falcipain. The enzyme falcipain has been shown to hydrolyse globins (step 4a in Figure 22, page 39), as inhibitors of this cysteine protease have been shown to inhibit the hydrolysis of globins [39]. But the partial block in haemoglobin denaturation that was clearly shown likely contributes to the antimalarial effects of cysteine protease inhibitors. Haem retention within haemoglobin molecules was also evaluated in protease inhibitor-treated parasites. Haemoglobin (native and partially denatured), which accumulated in these parasites, was seen to retain large quantities of haem. Thus falcipain plays an important role of separating haem moieties from haemoglobin in addition to haemoglobin degradation.

From all the studies done so far, it is clear that, firstly, inhibition of falcipain activity starves the parasite of amino acids. Secondly, falcipain inhibition may limit parasite small portion [39] supplies of iron required for the synthesis of iron-containing proteins [40], including ribonucleotide reductase [41], and for synthesis of parasite-derived haem [42]. Thirdly, a block in the separation of haem and globin may allow the persistence of potentially toxic haem-globin complexes. The persistence of these complexes would be expected to limit haemozoin formation, as it was shown that the specific cysteine protease inhibitor is E-64 or antimalarials chloroquine or artemisinin but not pepstatin.

Pepstatin, the general inhibitor of aspartic proteases was shown to inhibit haemozoin formation in cultured parasites [43]. As free haem is toxic to malaria parasites, the antimalarial effect of chloroquine has been explained by haem-chloroquine complexation [44]. Thus, haemoglobin complexes that accumulate under these conditions may be toxic to the parasite.

All the above suggest that cysteine proteases are potential targets for antimalarial chemotherapy and inhibitors such as E-64 are promising antimalarial drugs.

2.2 CATALYTIC MECHANISM OF CYSTEINE PROTEASES

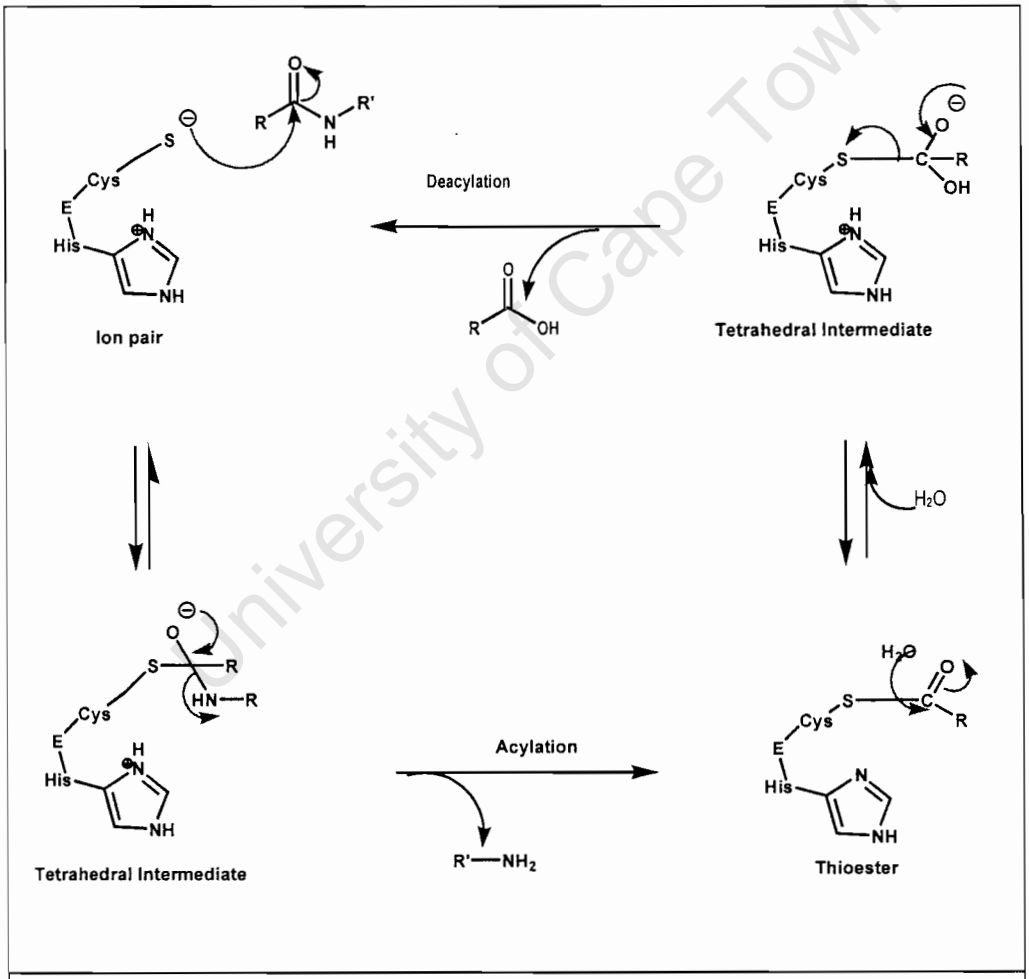

Scheme 8: Catalytic mechanism of papain-like cysteine proteases [45].

Cysteine proteases catalyse the hydrolysis of amide bonds in peptides and proteins through nucleophilic attack by the active-site cysteine thiol on the amide carbonyl (Scheme 8). Most inhibitors of cysteine proteases have taken advantage of this mechanism of amide bond hydrolysis and contain an electrophilic functionality, such as a carbonyl or Michael acceptor that reacts with the active-site cysteine residue.

During peptide hydrolysis, the nucleophilic cysteine thiolate attacks the carbonyl carbon of the scissible bond of the bound substrate and forms a tetrahedral intermediate, which is stabilized by the so-called oxyanion hole. The tetrahedral intermediate transforms into an acyl enzyme (enzyme-substrate thiol ester) with simultaneous release of the C-terminal portion of the substrate (acylation). This step is followed by hydrolysis of the acyl enzyme with water, forming a second tetrahedral intermediate, which finally splits into enzyme and the *N*-terminal portion of the substrate (deacylation).

2.3 CLASSIFICATION OF BINDING SITES

The diagram below (Figure 6) is the active site cleft of papain [46]. Both structures in Figure 6 are pictures of the papain structure but viewed a little differently from the top along the active site cleft of papain. The active binding sites of papain-like enzymes are located to the left and right of the active site cleft as seen below (Figure 6).

Classified or defined in this subsection are binding sites S1, S2, S3, S1', and S2'. P1, P1', P2, P2', P3 are residues of the substrate in the active site as shown in the diagram below. There is evidence that common S3'and S4 binding sites do not exist [46].

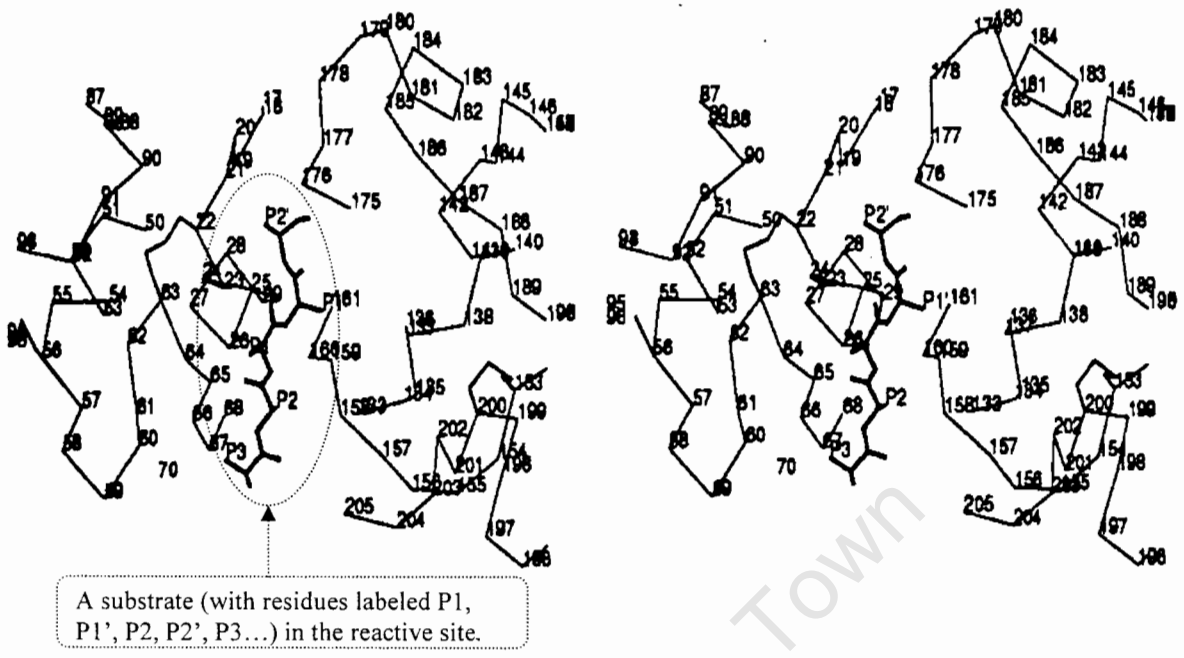

Figure 6: The active site cleft of papain. Both images viewed from the top along the active site cleft [46].

On the left of the active site, the 59-67 residues loop constitutes the area within which P3 residues attach, termed the S3 binding site. The S2' binding site is formed by the 25-19 loop. The form of the S1 is also a loop; however, it is constructed from parts embracing the S3 and S2'. For a well-defined binding site, interaction of the substrate with the enzymes involves both main-chain as well as the side-chain atoms. The P3 residues are not well defined as they differ from substrate to substrate unlike the P2' residue binding site for example.

The S2 and S1' substrate binding sites are the ones showing diversity and selecting against the substrates and inhibitors. It therefore seems likely that protein substrates will bind into the core substrate binding region from the S2 to the S1' site in the same way as small molecule synthetic compounds. The location of the substrate binding sites beyond S3 and S2' is uncertain [46].

2.4 CHEMISTRY OF CYSTEINE PROTEASE ACTIVE SITE THIOL

Cysteine proteases represent proteins with an exceptional biochemistry because of the unique chemical characteristics of the active site thiol group. The enzyme active site thiol has three distinct chemistries namely; nucleophilicity, redox activity and metal binding. These properties make cysteine an essential building block of several proteins and a key catalytic component of enzyme function.

2.4.1 Nucleophilicity

The cysteine protease active site has a thiol group that is nucleophilic, implying that it is attracted to electrophilic centers. Some antimalarials are designed to mechanistically react with the enzyme cysteine protease, by taking advantage of the thiol nucleophilicity.

2.4.2 Redox Activity

Considering redox activity, cysteine residues with sulfur in numerous oxidation states have been identified in proteins among them cysteinyl radical, cysteine disulphide, cysteine sulfenic acid, cysteine sulfinic acid, cysteine sulfonic acid and others (Figure 7).

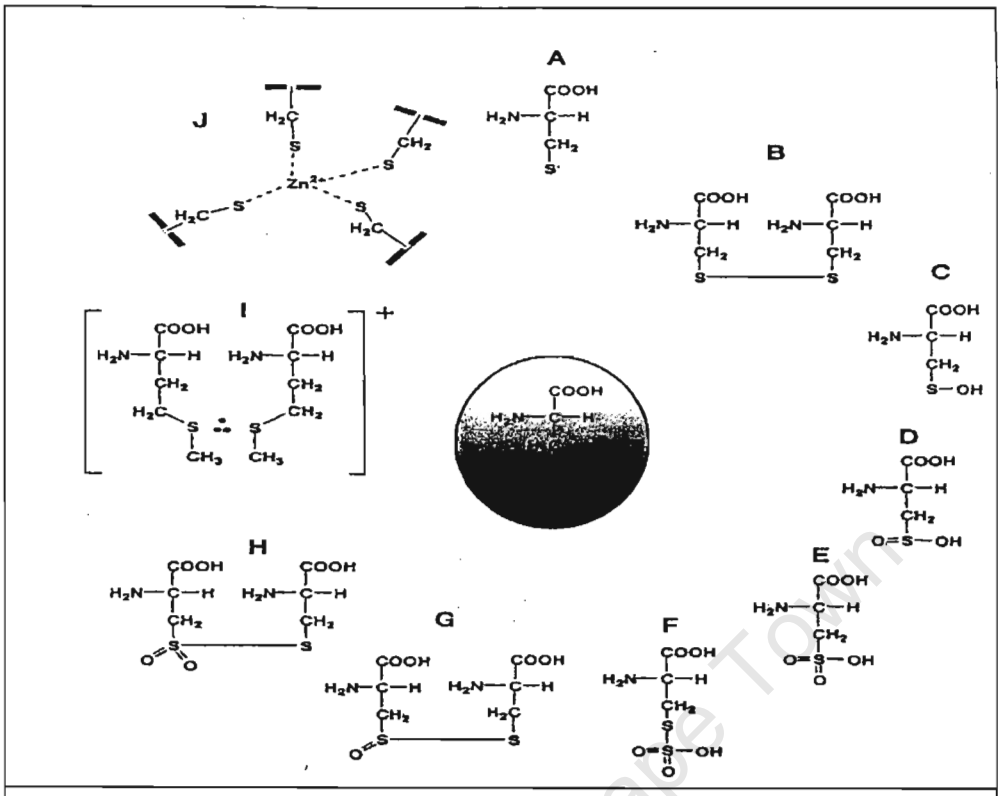

Figure 7: Important posttranslational cysteine and methionine modifications found in peptides and proteins [47]. **A** Cysteinyl radical (-1), **B** Cysteine disulfide (-1), **C** Cysteine sulfenic acid (0), **D** Cysteine sulfinic acid (+2), **E** Cysteine sulfonic acid, **F** Cysteine-S-sulfate (+5), **G** cystine-S-monoxide(+1), **H** Cystine-S-dioxide (+3), **I** Methionine disulfide radical cation with a three electron bond (-3/2), and **J** A tetrahedral $ZnCys_4$ complex (-2) [47].

Changes in the sulfur oxidation state of cysteine influences the activity of many proteins. There is a variety of redox mechanisms and resulting oxidation states found for cysteine *in vivo*. Electron transfer from cysteine is observed between its thiol group and metal ions such as Cu^{2+} and Fe^{3+}. Cysteine proteases are susceptible to these oxidative stressors, forming a variety of posttranslational modifications [47]. The one-electron oxidation of cysteine by Cu^{2+} or Fe^{3+} ions and radical species such as the hydroxyl radical, superoxide, and nitric oxide initially results in (thiyl, $RS^{\bullet}$) radical formation. The latter can combine with a second radical to form nonradical species such as disulfides (RSSR), sulfenic acids (RSOH), sulfinic acids (RS(O)OH, or in the case of NO, an S-nitrosylated cysteine (RSNO) (Figure 7).

The auto-inhibition process is recognized to be the oxidation of two cysteine residues (Cys61 and Cys328) at the active site to cysteinyl radicals. The reaction is inititiated by one-electron transfer from cysteine to Cu^{2+}, forming Cu^{+} and the first cysteinyl radical. The hydroxyl radical produced by the reaction of Cu^{+} and H_2O_2, regenerating Cu^{+}, then reacts with the second cysteine residue, forming another cysteinyl radical and water. The resulting two cysteinyl radicals dimerise to form a disulfide. This is confirmed by incubation with DTT, which restores enzymatic activity [48].

2.4.3 Metal Binding

Sulfur can accommodate a large number of bonds and geometries resulting in very diverse structures with the same metal through the changes in its oxidation state. Cysteine can perform as a monodentate ligand to bind metals such as from *Azotobacter vinilandii* containing a [4Fe-4S] cluster where each iron is coordinated to a separate cysteine ligand. Cysteine can function as a bidentate bridging ligand, as found in the active site of the [NiFe] hydrogenase from *Desulfovibrio vulgaris* Miyazakis F, which contains four cysteine sulfur and four non-protein sulfide (S^{2-}) ligands coordinated to the cluster. Cysteine can also bind more than one type of metal in a cluster as seen in the recently characterised carbon monoxide dehydrogenase from *Carboxydothermus hydrogenoformans*, which contains an active site [Ni-4Fe-5S] cluster where each metal is ligated by a separate cysteine. Lastly, cysteine can function as a bridging ligand between different subclusters. This is exemplified by hydrogenase from *Clostridium pasteurianum*, which contains an [4Fe-4S] subcluster coordinated to three cysteine and has a fourth coordinating cysteine ligand that bridges to the [2Fe] subcluster.

2.5 INHIBITOR CLASSES

A variety of cysteine protease inhibitor templates have been discovered. These inhibitor templates may be divided broadly into three mechanistically distinct groups, namely irreversible, reversible and slow turnover inhibitors.

2.5.1 Reversible Inhibitors

1, 3-Bis(acyl) diaminoketone Inhibitors: The design of this series of inhibitors was based upon the observation that tripeptide aldehydes leupetin **31** and Z-leu-leu-CHO **32** (Figure 8) had bound in opposite directions within the active site of papain[49, 50].

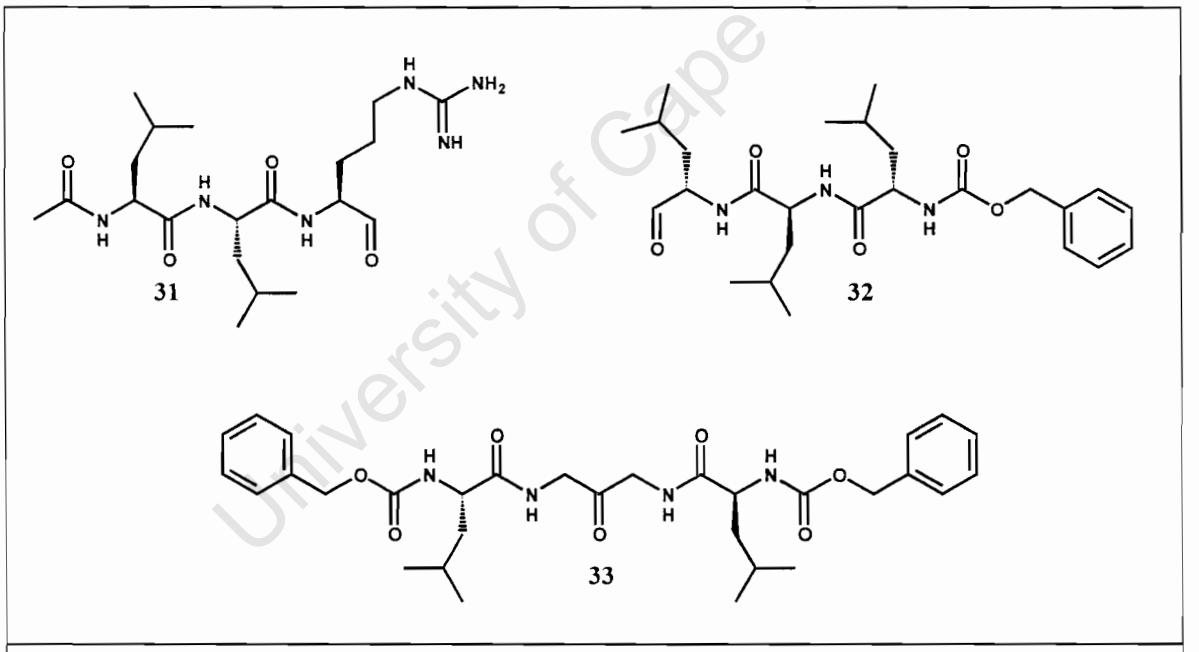

Figure 8: 1,3-Bis(acyl) diaminoketone Inhibitors.

Molecular modelling experiments based on these cocrystal structures generated the C2 symmetric ketone **33**, which was characterised as a reversible and competitive inhibitor of cathepsin K.

Cyclic Diaminoketone Inhibitors: These inhibitors are a conformationally constrained version of **33** [51]. The C2 symmetric inhibitors **34** and **35** (Figure 9) are weak inhibitors of cathepsin K [52].

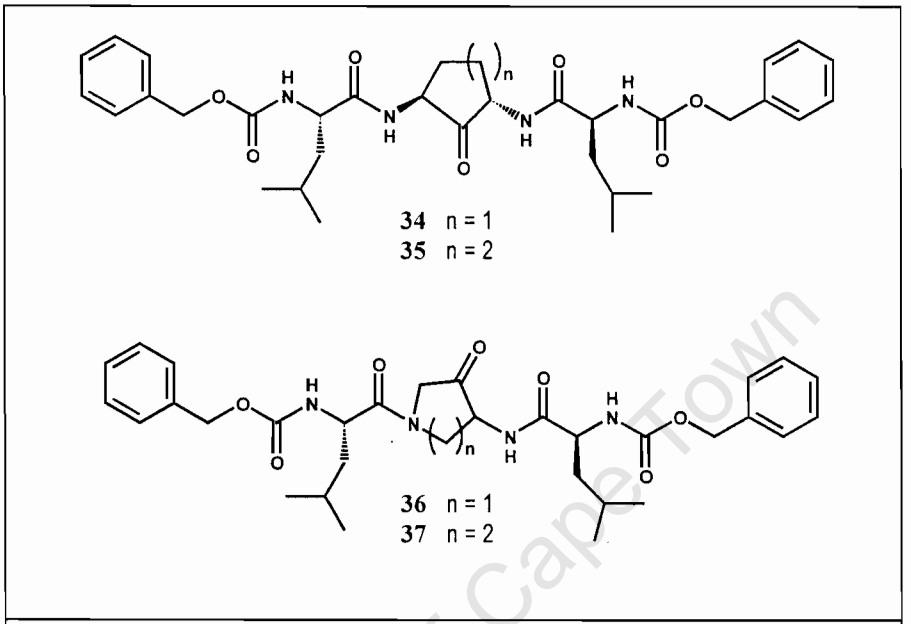

Figure 9: Cyclic Diaminoketone Inhibitors.

Both **36** and **37** were selective for cathepsin K versus cathepsin B ($K_{i,\,app}$'s = > 1,000 and 440 nM) and were less selective over cathepsin L ($K_{i,app}$'s = 39 nM, and 16 nM). These ketone based analogs have been characterized as reversible and competitive inhibitors [52].

α-Heteroatom Ketone Inhibitors: This class of inhibitors was designed in an effort to eliminate the metabolic liabilities associated with aldehyde based inhibitors such as **32**, which had shown good in vitro and in vivo efficacy against cathepsin K [53]. Ethyl ketone analogue **38** was a 18.5 nM inhibitor while incorporation of a phenylpentyl group provided **39** (Figure 10), which was an 4 nM inhibitor of interleukin-1β converting enzyme (ICE) [52].

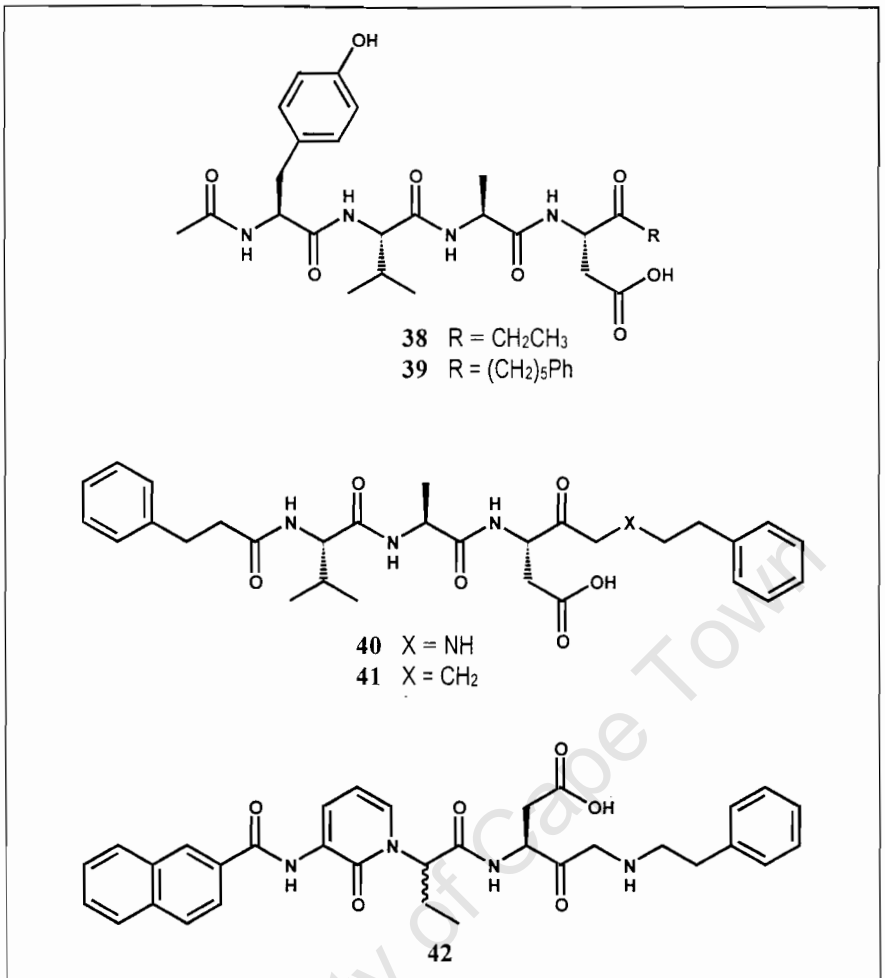

Figure 10: α-Heteroatom Ketone Inhibitors.

The increased potency of **39** over **38** was attributed to the ability of the alkylphenyl moiety to access the hydrophobic binding pocket in the P1' to P2' subsites of the enzyme active site [52]. Aminomethylketone derivative **40** (4.7 nM inhibitor) is 25 fold more potent than the carbon analogue **41** (100 nM inhibitor). Incorporation of the pyridine based P3-P2 val-ala peptidomimetic gave rise to **42**, which is a 0.37 nM inhibitor of ICE [52].

4-Heterocyclohexanones: This class of inhibitors is based upon increased reactivity of the ketone carbonyl of the 4-heterocyclohexanone ring system [54].

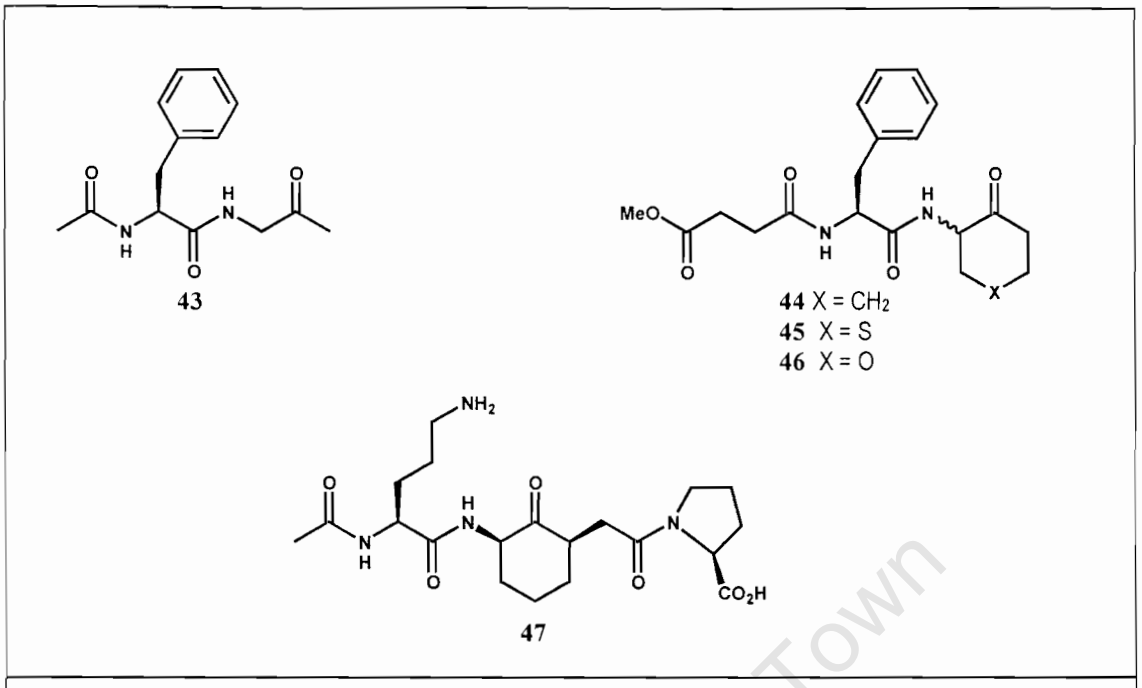

Figure 11: 4-Heterocyclohexanones.

The more active diastereomer of the cyclohexanone derived compound **44** (Figure 11) was a 78 μM inhibitor of papain. Compound **44** was 20 times more potent than the acyclic derivative **43** highlighting the contribution that ring strain plays in effecting the reactivity of the carbonyl group. Incorporation of heteroatoms in the 4-position of **44** gave the tetrahydrothiopyranone **45** and 4- tetrahydropyranone **46** which were 26 μM and 11 μM inhibitors of papain respectively. The utility of this inhibitor strategy has been extended by the synthesis of **47**, which is a 6.6 μM inhibitor of the lysosomal cysteine protease cathepsin B [55].

Aryl Ketone Based Inhibitors: A series of reversible 2-benzothiazole ketone inhibitors of human rhinovirus 3C protease [56]. The 2-benzothiazole ketone **48** (Figure 12) is a reversible inhibitor of rhinovirus 3C protease (Ki = 0.065 μM) with modest antiviral activity (EC50 = 3.2 μM, HRV serotype-14) [52].

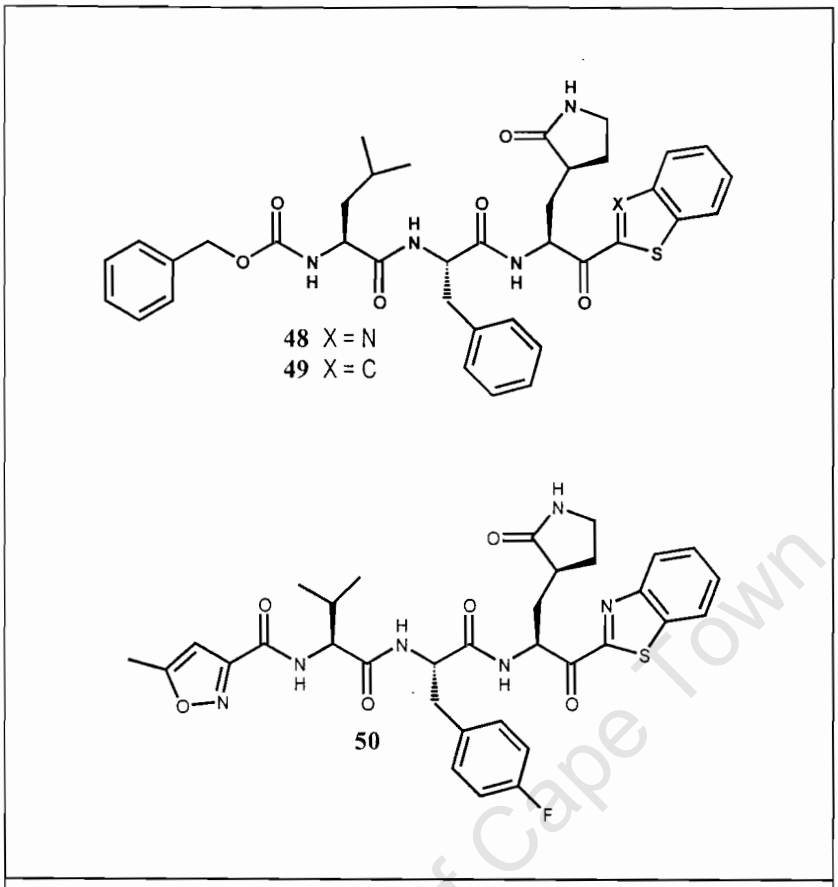

Figure 12: Aryl Ketone Based Inhibitors.

The related benzo[b]thiophene derivative **49** was far less potent than **48** with a Ki = 4.7 μM. The 2-benzothiazole ketone electrophile of **48** was incorporated into a recently identified tripeptidyl inhibitor template **50**, which is a 4.5 nM inhibitor of human rhinovirus serotypes [52].

2, 3 Dioxindoles (Isatins): The isatin moiety has seen recent application in the inhibition of the rhinovirus 3C protease as well as the selective inhibition of caspases 3 and 7. Molecular modelling and structure-based design led to the identification of 1-methyl isatin-5-carboxamide **51** (Figure 13), which is a 51 nM inhibitor of human rhinovirus 3C protease.

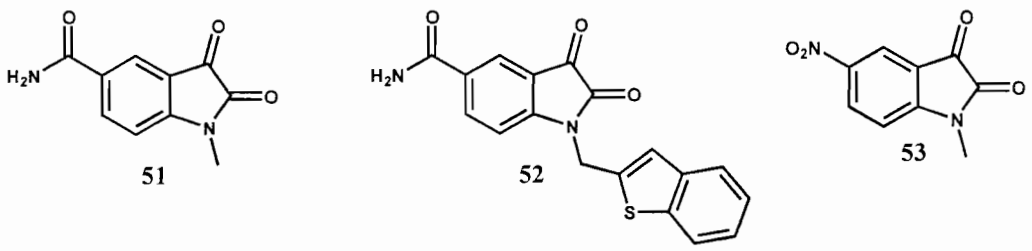

Figure 13: 2, 3 Dioxindoles (Isatins).

It is also selective for HRV-14 3CP versus several rhinovirus serotypes. Incorporation of the benzo[b]thiophene produced **52** which is a 2 nM inhibitor. The 5-nitro-1-methyl isatin **53** was identified by high throughput screening as a 500 nM inhibitor of human caspase-3 [57].

2.5.2 Irreversible Inhibitors

α, β Unsaturated Esters: The X-ray co-crystal structure of **54** (Figure 14) bound within the active site of the protease showed that the inhibitor was attached to the protein *via* a 1, 4 Michael addition of the active site cysteine to the β-carbon of the acrylate. Analogue **56** that incorporates several preliminary modifications suggested by the HRV-14 3CP, cocrystal structure was 32 times more potent than **54**. Replacement of the Leu-Phe amide nitrogen by a ketonemethylene provided analogues **55** and **57**.

A combination of several of the modifications discussed above has led to the identification of **58**, which is a potent inhibitor of HRV-14-3CP. Compound **58** displayed a combination of favourable biological and chemical properties. This compound has recently entered clinical trials as a delivered antirhinoviral therapy for the common cold [58, 59].

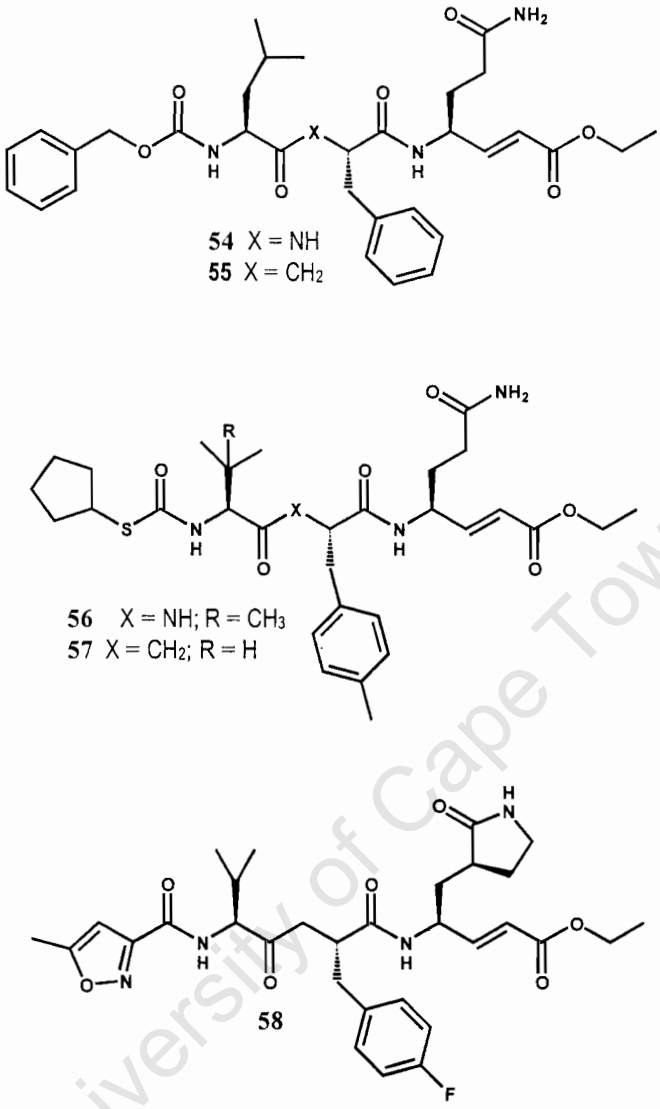

Figure 14: α, β-Unsaturated Esters

Peptidyl Vinyl Sulfones: An extension of the peptidyl Michael acceptor design embodied by the α, β unsaturated ester inhibitors has been designed based upon both the hydrogen bonding capabilities and the polarizable nature of the vinyl sulfone moiety. The prototype vinyl sulfone **59** (Figure 15) has recently been shown to be an effective inhibitor of cathepsin S *in vivo* [60].

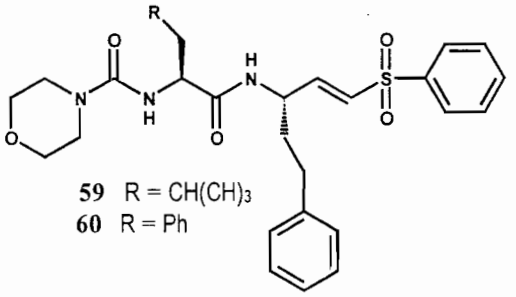

Figure 15: Peptidyl Vinyl Sulfones

Vinyl sulfone **60**, which incorporates a P_2 phenylalanine, is an effective inhibitor of *cruzain*, the trypanosomal cysteine protease from *T.cruzi* (causative agent of Chagas disease). Analogue **60** is also an inhibitor of falcipain (IC_{50} = 0.08 μM) a cysteine protease of *Plasmodium falciparum* [61].

(Acyloxy) Methyl Ketones: These have been used as templates for the inhibition of a variety of cysteine proteases [62, 63]. Inhibitors such as **61** (Figure 16) have been shown to inhibit cathepsin B and **62** inhibits cathepsin S. These inhibitors have three components that may be used in order to achieve potent and selective inhibition. The three components are, peptidyl recognition sequence specificity and reactivity of the carbonyl moiety of these inhibitors towards the cysteine thiol group and the dependence of the rate of enzyme inhibition on the pKa of the carboxylate leaving group. Several other leaving groups have been incorperated into this template and their mechanism of inhibition has been studied.

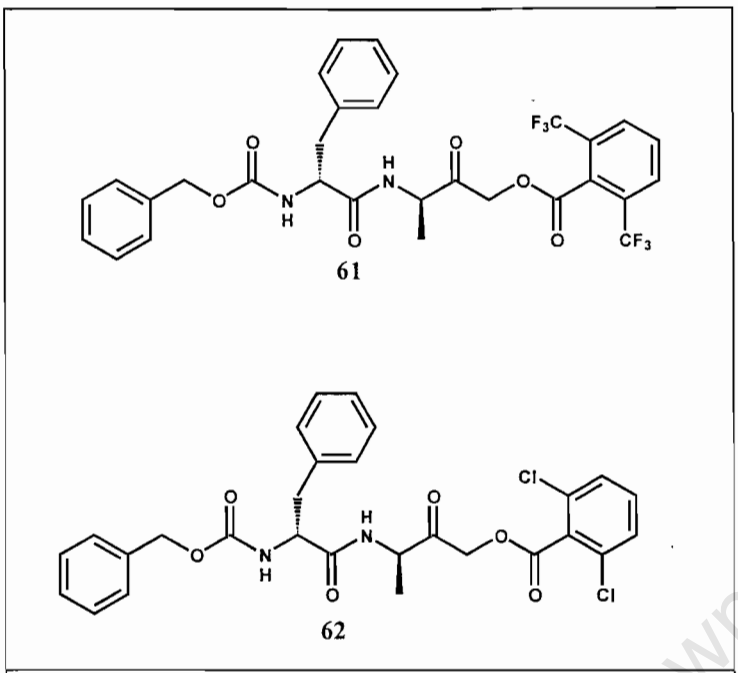

Figure 16: (Acyloxy) methyl Ketones.

Aza-Peptides: A series of these amides, which utilize both primed and unprimed side chain binding elements, have recently been shown to be virtually reversible inhibitors of papain [64]. These pseudo-substrates were designed so that, upon attack of the active site cysteine, they would produce a thioacyl-enzyme intermediate, which would hydrolyze slowly relative to the parent peptide substrate. The rate of papain inactivation by aza-peptide **63** and **64** (Figure 17) was reported to have a K_{on} = $13M^{-1}s^{-1}$. Analogue **65**, which incorporates a leaving group capable of interacting with the S1' binding pocket, inactivates papain at a rate 17 times that of **63**. The thioacyl enzyme intermediate formed between papain and **65** is hydrolysed with a $t_{1/2}$ = 12 hours making these inhibitors essentially irreversible [52].

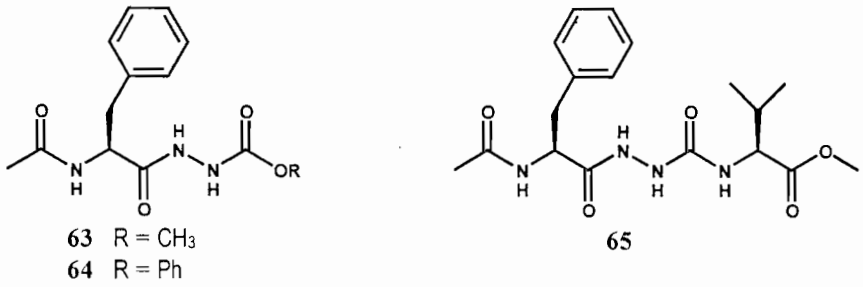

63 R = CH_3
64 R = Ph

65

Figure 17: Aza-Peptides.

2.5.3 Slow Turnover Inhibitors

Peptidyl Carbazate Esters: Synthesis and evaluation of peptidyl carbazate esters of this class have been recently reported [65]. The carbazate ester **66** (Figure 18) has been reported to be a transient inhibitor of HRV 3CP.

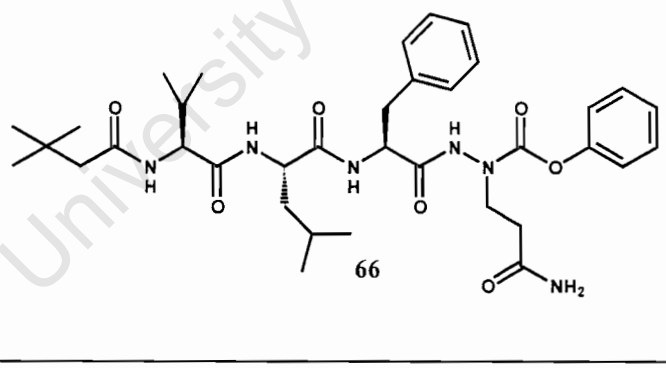

66

Figure 18: Peptidyl Carbazate Esters.

The enzyme is initially inhibited quickly but not completely and what is suggested by the data is that formation of the intermediate thioacyl enzyme between **66** and HRV 3CP is rapid but then hydrolyses slowly.

Acyl-Bis-Hydrazides: Nitrogen substitution of the central diamino propane scaffold of the reversible ketone based inhibitor 33 (Figure 8, page 23) has led to a series of acyl-bis hydrazide inhibitors of cathepsin K [66].

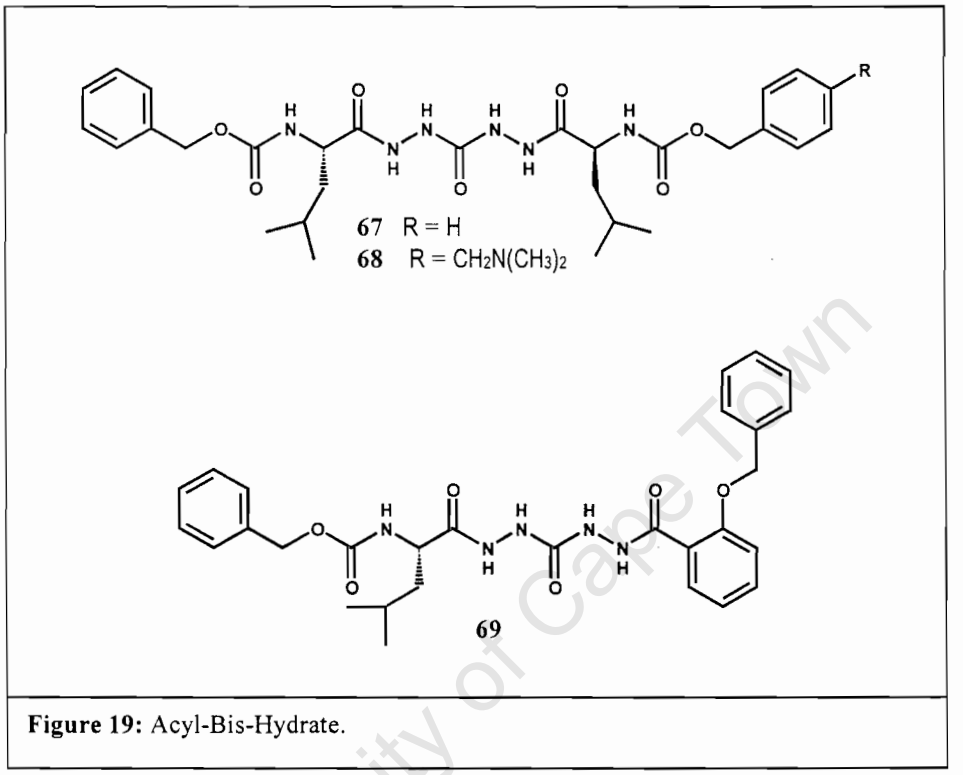

Figure 19: Acyl-Bis-Hydrate.

Both **67** and **68** (Figure 19) are potent inhibitors of cathepsin K in a cell based osteoclast resorption assay with IC_{50} values of 0.34 and 0.12 μM respectively. Inhibitor **69**, in which the *o*-benzyloxybenzoyl moiety was shown to be an effective replacement for the Z-leucine of **67**, was a potent and selective inhibitor of cathepsin K.

Diacyl Hydrazines: Replacement of one of the acylhydrazide moieties of **67** with a thiazole amide bond isostere provided **70** (Figure 20) which is a potent and selective inhibitor of cathepsin K.

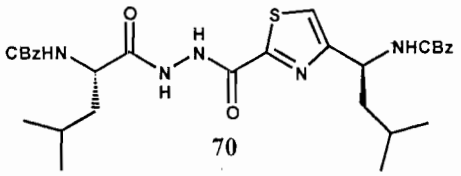

70

Figure 20: Diacyl Hydrazides

The mode of inhibition of **70** was shown to be initially rapidly reversible with a subsequent slow turnover step [66].

In conclusion, potent and selective inhibitors of cysteine proteases have continued to evolve, through the application of iterative structure based design and the development of high throughput combinatorial synthesis methodologies.

2.6 FROM HAEMOGLOBIN TO HAEMOZOIN - BIOCHEMISTRY OF THE FOOD VACUOLE.

2.6.1 Haemoglobin (Hb) Degradation

2.6.1.1 Separation of Hb Components

The intraerythrocytic malaria parasites reside and grow within a cell that is rich in a cytosolic protein, haemoglobin. The parasite requires amino acids to develop but it has a limited ability to synthesise them *de novo* [67]. The parasite takes up host haemoglobin and degrades it in a specialized acidic (pH in the range 5.2-5.6) food vacuole (Figure 21) that is within the parasite. Haemoglobin, the major protein utilised by *P. falciparum* for nutrient supply during its blood stage, is taken up initially by trophozoites and early schizonts, the most metabolically active stages [68]. The process begins with erythrocyte cytoplasm being ingested by cytosomes and shuttled in vesicular transport, to the specialized proteolytic organelle called the digestive vacuole [39]. Upon its delivery, hemoglobin-rich erythrocyte cytosol is subjected to an acidic pH in the food vacuole.

As 25% to 75% of erythrocyte haemoglobin is degraded, a bulk of amino acids is produced and then used for parasite protein synthesis [67]. During Hb degradation, haem is yielded as a by-product, which is then converted to haemozoin, also known as malaria pigment to prevent toxicity of haem to the parasite [69]. Processing of haem may also give rise to free iron for the biosynthesis of iron-containing proteins [40] and parasite-derived haem [42].

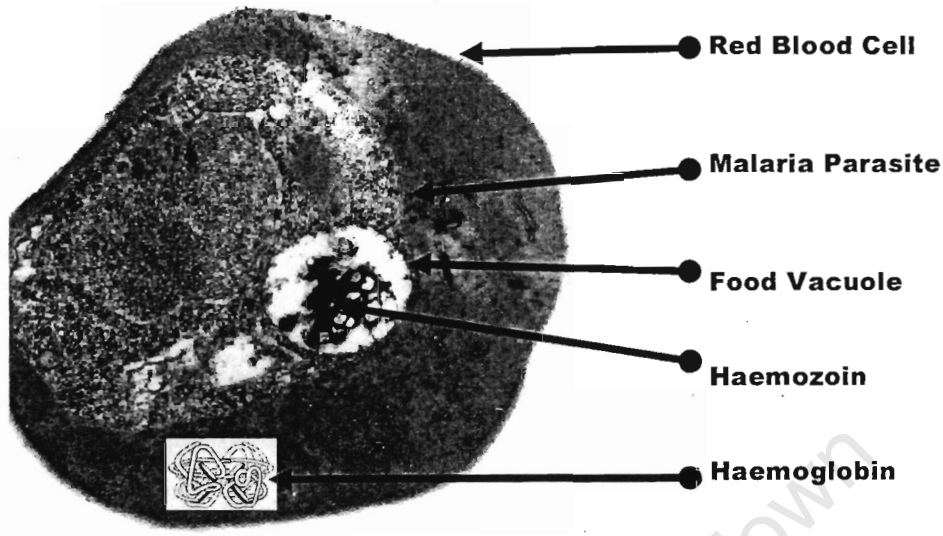

Figure 21: Parasitised Red Blood Cell.

This is supported by the observation that small amounts of iron are released from haem after incubation at the pH of the food vacuole [68]. A fraction of not more than 5 % haem may be degraded [70] but there hasn't been definitive evidence regarding this aspect. At least 95 % of the iron observed at the trophozoite stage is definitely incorporated into haemozoin [70].

Thus, essential processes of haemoglobin catabolism and haem conversion are likely targets for a number of compounds with antimalarial activity, including well-established drugs and promising new agents. Even though the two are linked they may be treated separately.

2.6.1.2 Controversy on Proteases Involved in Hb Degradation

There has been a lot of controversy around this topic, especially the first step (hydrolysis of native Hb). The conclusion of one study is that haemoglobin degradation is an ordered process, initiated by plasmepsin I cleaving native heamoglobin at the hinge region that appears important for the integrity of the haemoglobin tetramer, and therefore unraveling the molecule [71]. Plasmepsin II appears to be able to cleave some of the native haemoglobin but not the denatured molecule [71].

Cysteine protease can make further cleavage once the aspartic proteases have initiated proteolysis [71]. It was demonstrated that falcipain cannot degrade native haemoglobin without reducing conditions that first denature the hemoglobin molecule [72]. In another study reducing conditions were predicted to be present in the food vacuole and falcipain was shown to cleave native haemoglobin [73]. The presence of the reducing conditions is debatable since the redox potential of the food vacuole has not been measured. Autoxidation of haemoglobin takes place in the red blood cell cytoplasm causing oxidative damage [74,75], which is prevented by antioxidants present including catalase [76], which may be available at a high concentration enough to prevent haemoglobin denaturation in the food vacuole [72].

Haemoglobin has been demonstrated to be denatured once subjected to acidic pH between 4.0-4.5 by spetrophotometric [40] and electrophoretic [39] methods, but this process is very slow in the vacuole pH (5.2-5.6). Therefore, the activity of enzymes tends to be necessary for proper separation of heme and globin. It is then concluded that the evidence points to plasmepsins being required to denature Hb for falcipain activity [72]. Besides, plasmepsins I and II comprise at least 50% of the total globin-degrading activity of the vacuole and non-reducing assay conditions, and are expected to be capable of haemoglobin breakdown even when the cysteine protease is inactive [72].
When haemoglobin is digested by plasmepsins I and II *in vitro*, a total of 16 cleavages with an average size of about 30 amino acids have been observed [71].

2.6.1.3 Conclusion on the Process of Hb Degradation

Despite the controversy on the process of Hb degradation in the acidic food vacuole, in this thesis by combining information from different studies a conclusion has been drawn. Arriving at this conclusion was not easy since all the contributions from different studies [39, 69, 71-80] had to be accommodated. Although this picture (Figure 22) may not be final, so far it can be concluded that:

Haemoglobin degradation is said to be a very organized [71] process involving at least three classes of enzymes that mediate this process namely:

- four aspartic proteases (plasmepsins I, II and IV and histo-aspartic protease/ HAP).
- two cysteine proteases (falcipain, 2 and 3)
- a zinc metalloprotease also known as falcilysin

Some of the above enzymes have been purified and characterized [71, 77]. Hb is ingested by means of a cytostome, which spans a double membrane between the RBC and parasite cytoplasm. Hb containing vesicles are pinched off from the cytostome and travel to the digestive vacuole where the Hb is broken down (Figure 22). Plasmepsin I is active in degrading native Hb into denatured Hb, plasmepsin II then further digest the Hb to form globin fragments plus haem. Specifically, the initial attack is made between α33Phe and 34Leu residues by the aspartic proteases, and then subsequent cleavages at several other sites can be made. The 33 -34 bond is located in the hinge region of haemoglobin.

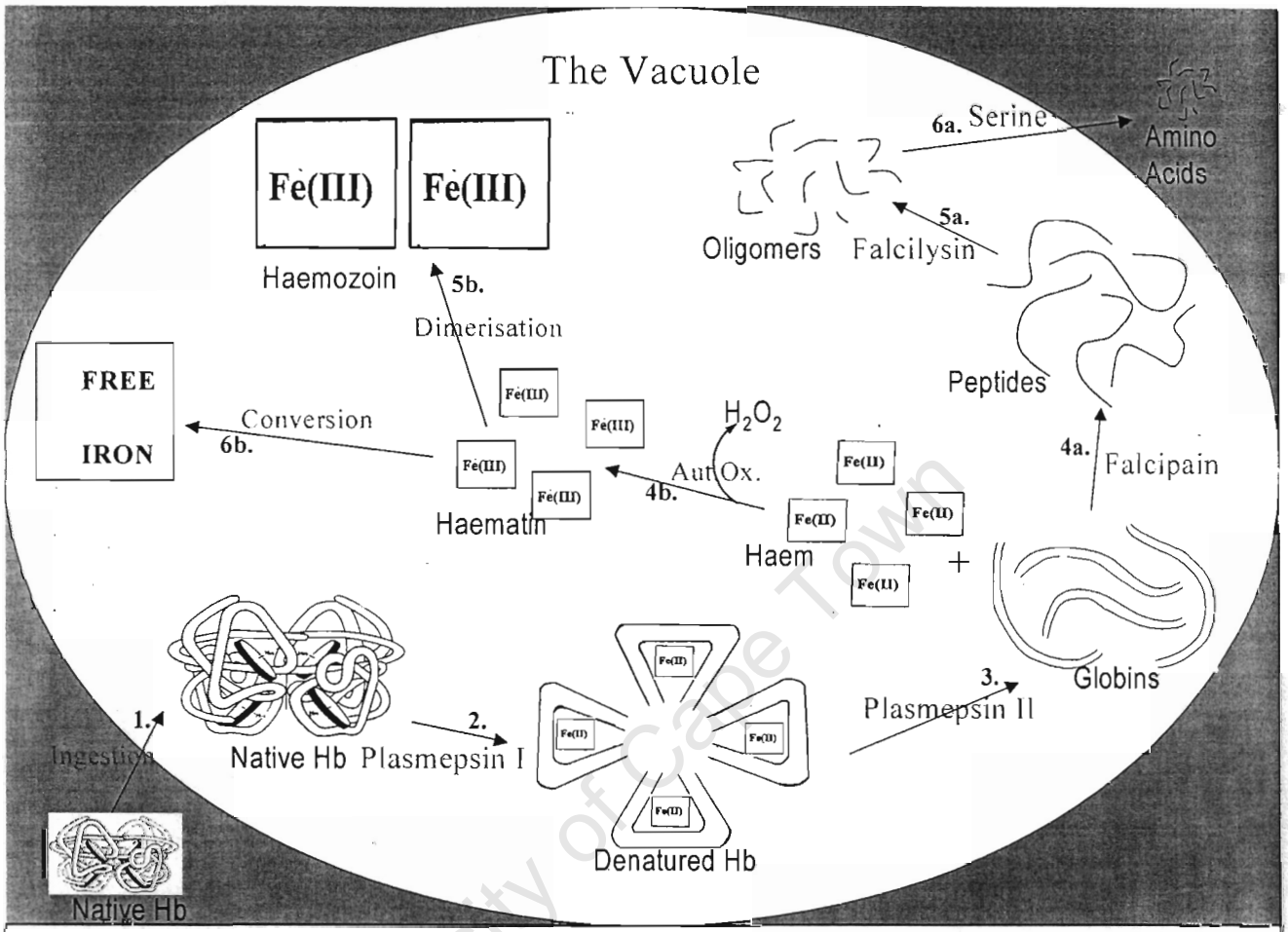

Figure 22: Schematic representation showing Hb degradation. (1) ingestion of native Hb by means of a cytostome; (2) separation of Hb tetramer into monomers (denatured Hb); (3) separation of each monomer into haem and globins; (4a) hydrolysis of globins into peptides; (5a) hydrolysis of peptides into oligomers; (6a) hydrolysis of oligomers into amino acids; (4b) autoxidation of haem into haematin; (5b) dimeriasation of haematin into haemozoin; (6b) conversion of haematin into free iron.

Cleavage in this area is likely to cause unravelling of the tetramer (Figure 23 and 24), exposing other sites for proteolytic attack by aspartic and other proteases continuing degradation [77].

The globin fragments are further hydrolysed by falcipain-2 into peptides. These peptides are then broken down into smaller fragments/ oligomers by falcilysin. Small peptides are transported out of the food vacuole to the cytoplasm where they are further broken down to amino acids by serine proteases. In the process of Hb degradation, haem in the ferrous

form is released as a by-product and autoxidised to α haematin (H_2O-Fe(III)PPIX), in ferric form. This leads to the production of hydrogen peroxide through the one electron oxidation of Fe(II) [5]. The α-haematin, which is toxic to the parasite, is converted into an insoluble pigment called haemozoin. Most (about 95 %) of the iron resulting from this process is converted to haemozoin [70] and the rest (not more than 5 %) is degraded possibly to free iron but no definitive evidence has been found to support this.

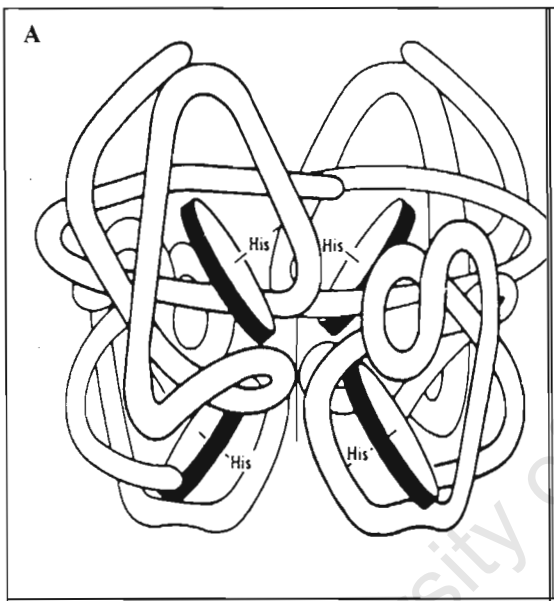

Figure 23: Simplified form of Haemoglobin

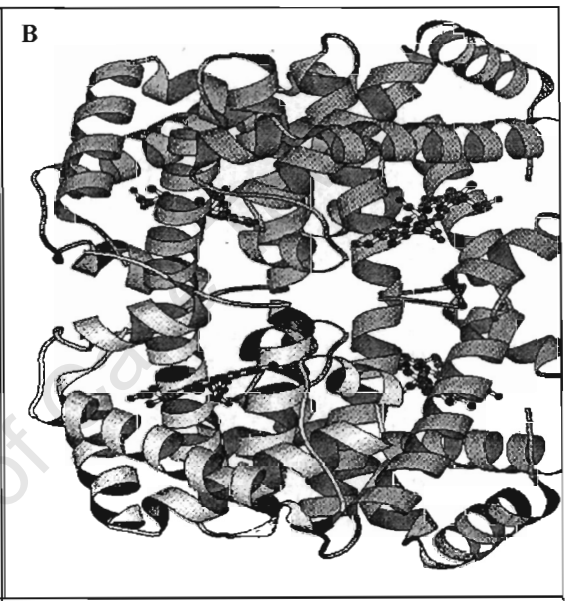

Figure 24: Ribbon presentation of Haemoglobin

Noted to be striking was the difference in specificity of the aspartic proteases against native compared with fragmented or unwound haemoglobin [77]. Isolated α chains are less folded and much less tertiary structures than native haemoglobin [78]. When they are used as substrates the same 33-34 cleavage is made, but other breaks appear at the same time. Fragment 1-105, a peptide arising from cleavage at the 105-106 bond, is observed early on without previous cleavage at 33-34. Thus the enzyme is highly site selective when confronted with folded protein, and not nearly as selective when given unwound protein [77].

2.6.2 Mechanism of Action of Chloroquine

Quinoline antimalarials in current use include chloroquine, amodiaquine, mefloquine, quinidine and primaquine. They are believed to function by forming complexes with haematin. This was first recognised in the 1980's and led to proposal that haematin is the target of chloroquine [6]. The result of this interaction has not been definitely demonstrated, but there is considerable evidence that formation of such complexes blocks formation of haemozoin preventing removal of haematin from the parasite.

Little is known about the structures of these complexes. The complexes between 4-aminoquinolines and haematin are almost certainly so-called π-π complexes. This means there is a co-planar interaction between the aromatic ring of the quinoline and the porphyrin system. Interaction between chloroquine and hydroxoferriprotoporphyrin IX has been studied using proton NMR, and it has been suggested that a dimer of haematin interacts with the quinoline nucleus of chloroquine mainly by means of hydrophobic interactions [79]. The interaction of quinine with a metal free porphyrin (uroporphyrin I) was also investigated. This was used to demonstrate that the iron atom is not essential for the interaction. The result is a broadening of all the resonance lines in the proton NMR spectrum and shift of various protons upon the addition of uroporphyrin to quinine. All the protons were shifted to high field but the largest shifts were observed for the quinoline ring protons, demonstrating that this part of the molecule interacts most closely with the porphyrin. Similarly, the induced chemical shifts on the protons of the bicyclic quinuclidine side chain of quinine were reported to be small compared to those observed for the quinoline protons.

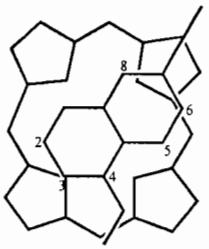

Figure 25: Structural models depicting the interaction of chloroquine with a phorphyrin.

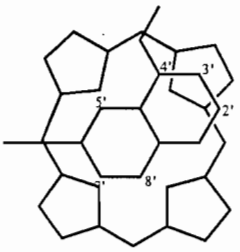

Figure 26: Structural models depicting the interaction of quinine with a phorphyrin.

A similar result is obtained from the ^{13}C NMR spectrum suggesting that the quinoline ring is stacked above the periphery of the porphyrin, in a π-π type interaction with the 2', N, 10', 8' edge facing the center of the porphyrin. It also indicates that the 9-OH group is coordinated to the Fe(III) ion, being appropriately positioned only when iron(III) ion is present in the porphyrin core.

From the structural models in Figure 25 and 26, the following can be observed: (i) The quinoline is centered above the porphryrin. (ii) Bulky substituents of quinoline are kept away from the porphyrin core. Thus shifs in proton and ^{13}C NMR peaks can provide useful information on the interaction of quinolines with porphyrins. There is still a question as to which part of the porphyrins are involved, a question that has not been investigated. This would require the use of a diamagnetic model of Fe(III)PPIX, such as Zn(II)PPIX.

2.6.3 Haematin Polymerization

2.6.3.1 Mechanism of Haemozoin Formation

As mentioned previously, upon protolysis, the required amino acids are yielded and haem is released as a by-product into the digestive vacuole where the iron of the haem is oxidized from the ferrous (+2) state to the ferric (+3) state [4]. To balance the metabolic

needs for amino acids against the toxic haem effects, the parasites have evolved a detoxification mechanism, which involves the incorporation of haem into an insoluble aggregation of haem known as haemozoin[4] (Figure 27 and 28).

It was suggested that aggregation of haem does not happen spontaneously, but that something is facilitating this aggregation [80]. Four mediating processes were suggested by different researchers namely; 1) a haem polymerase [81], 2) haem-derived material [80], 3) phospholipids [82], 4) a nucleating template protein [83]. Native haemozoin formation was previously suggested to be catalysed by a parasite-dependent activity, along with a speculated haem polymerase enzyme [81]. Acetonitrile extracts of native haemozoin, free of detectable haem cause rapid haem polymerization [84]. A similar active fraction with phospholipid-like chromatographic properties could be readily extracted from β-haematin chemically synthesized from commercially available haem, by heating a haem chloride solution to 70 °C at acid pH [82]. These properties were found to support haem polymerization at 37 °C like haemozoin. It was then reasoned that if this activity was due to haem-derived material rather than enzyme, then it should be possible to extract a solubilized haem-polymerized activity from synthetic β-haematin [80]. This was confirmed by experiments that showed that acetonitrile extracts from synthetic β-haematin, trophozoite lysate and haemozoin can all support haem polymerization equally, and they are all inhibited by chloroquine [80]. Rapid polymerization of haem is promoted by phospholipids and therefore may play a role in the formation of haemozoin by the malarial parasite [82]. Although phospholipids may account for the acetonitrile extracts, it is not clear whether the polymerization of haem within malaria-infected erythrocytes is effected solely by activity of these lipids [82].

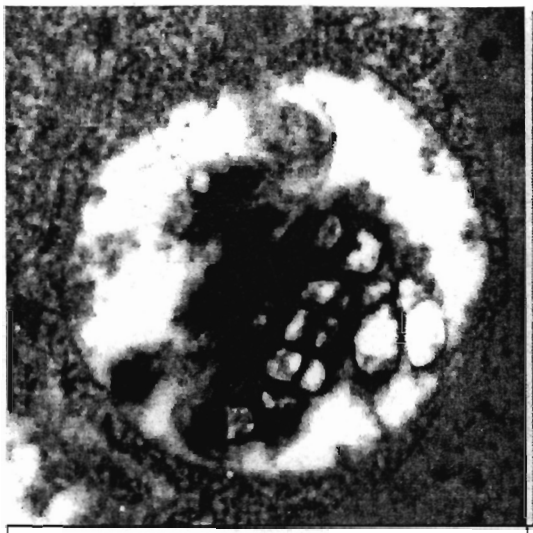

Figure 27: Haemozoin Crystals in the Food Vacuole.

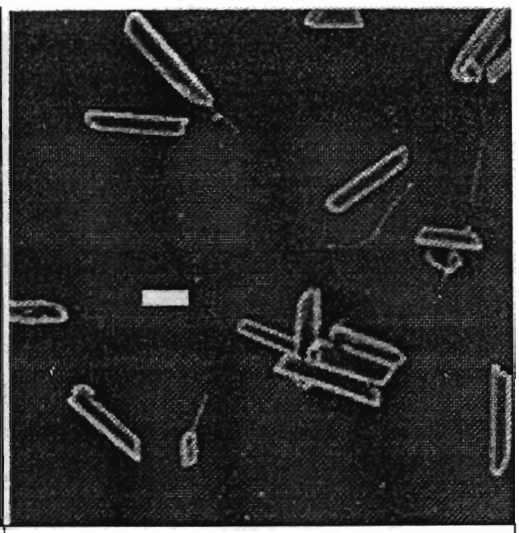

Figure 28: Crystallized Haemozoin [84].

A lot of suggestions concerning the catalysis of haem polymerization have been raised, that may imply that haemozoin as a polymer is formed so easily. The big question that remains is the initiation of haem polymerization? The answer could be that the protein is instrumental. If it exists, the protein will not work as 'haem polymerase' but rather as a structural focus [82].

2.6.3.2 The Structure of Haemozoin - Malaria Pigment

The structure of haemozoin fascinated malaria researchers after Carbone isolated the pigment. A number of models were proposed about the structure of the material. The long-standing model of haemozoin's structure shown below is the first model proposed. It is a coordination polymer of Fe(III)PPIX's in which an oxygen from a propionate group from one unit serves as an axial ligand to the five coordinate ferric ion of another (Figure 29). This was strongly supported by IR and Ramman spectroscopies for the Fe-O (propionate) linkage.

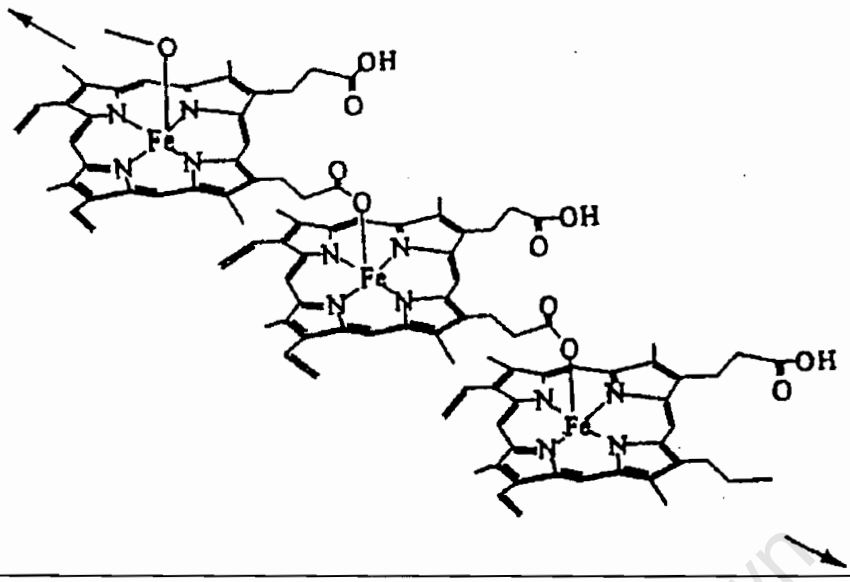

Figure 29: Spectroscopical based model of haemozoin as a linear coordination polymer of heme units linked by a propionate linkage.

A second model proposed by Bohle and co-workers [86] was a dimerization of two linear polymer chains hydrogen-bonded through propionic groups (Figure 30).

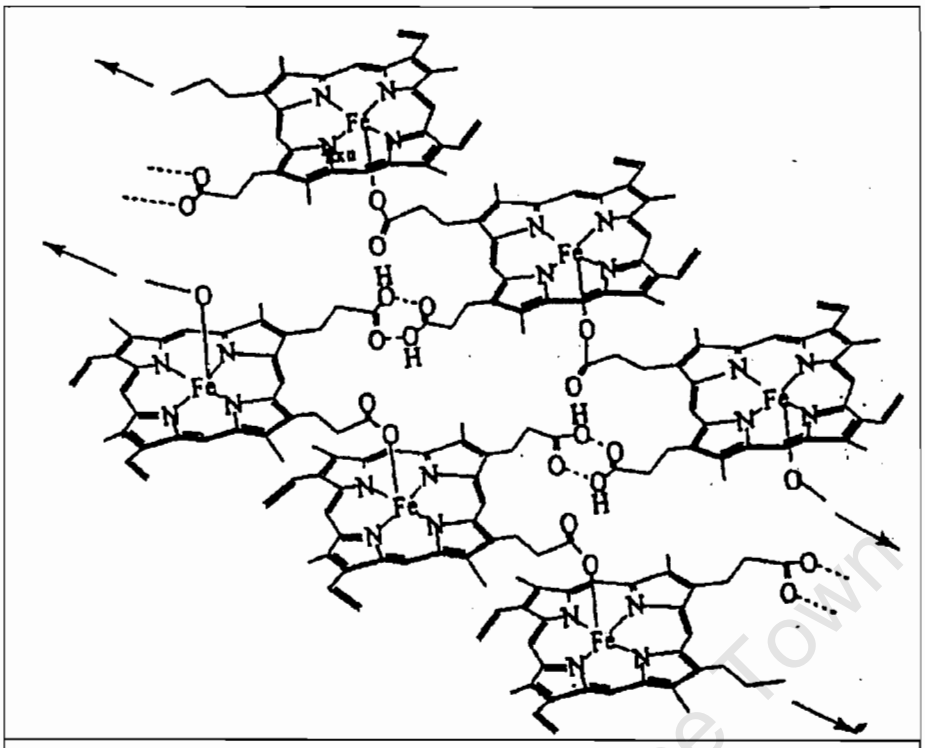

Figure 30: Haemozoin model, a dimerization of two linear polymer chains hydrogen-bonded through propionic groups.

Another proposal by Pagola for the correct structure of haemozoin was a dimer of haem units linked by reciprocating iron-carboxylate bonds to one of the propionic side chains of each prophyrin. In addition the dimers are hydrogen-bonded into chains forming an extended crystalline network (Figure 31). For many years the structure of haemozoin was believed to be a polymeric form of Fe(III)PPIX until the crystal structure was solved from the high resolution X-ray powder diffraction pattern [85].

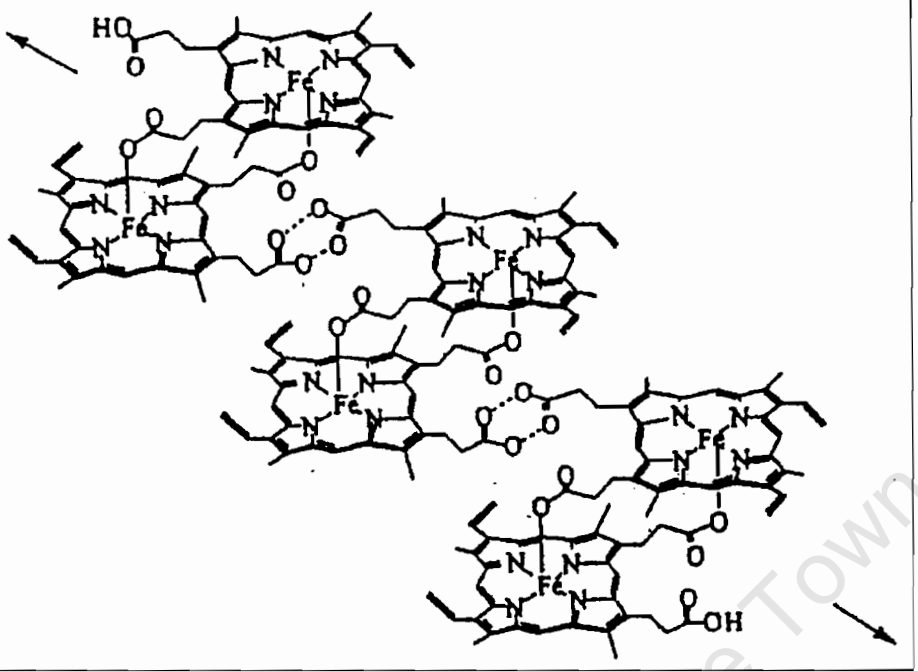

Figure 31: Haemozoin model: a dimer of haem units linked by reciprocating iron-carboxylate bonds to one of the propionic side chains of each prophryin.

The pigment was eventually found to be a dimer (Figure 32) and therefore the previous proposals of the pigment being a polymer have been misleading.

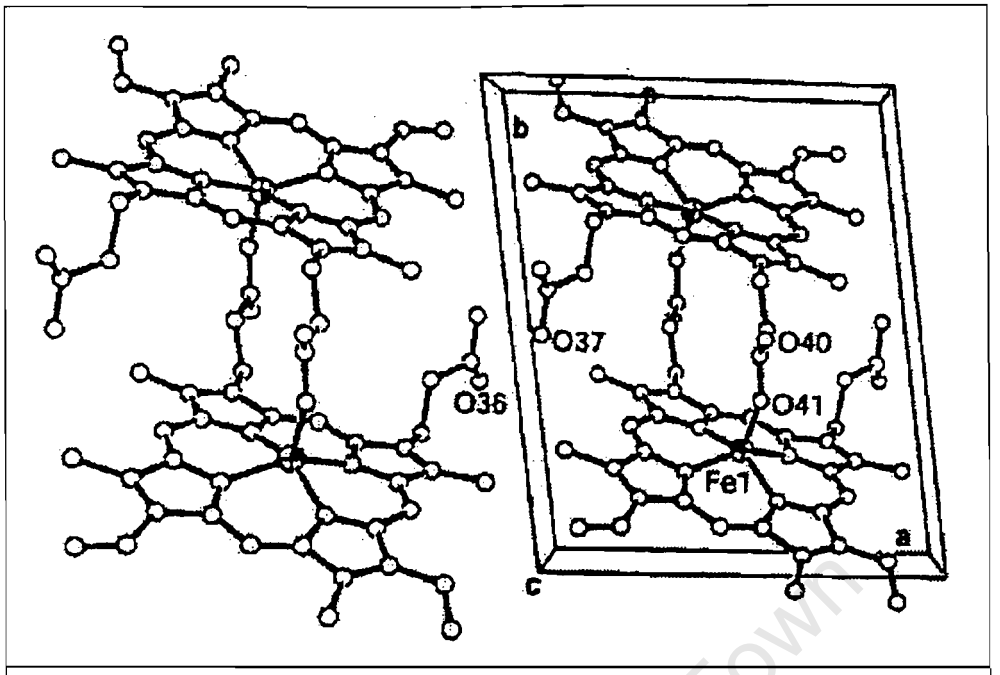

Figure 32: The molecular structure of haemozoin [85].

2.6.3.3 The Structure of β-Haematin

Synthetic haemozoin known as β-Haematin has been demonstrated to be structurally (Figure 32) identical to the natural haemozoin [86]. Synthetically, it is prepared by heating a haem chloride solution to 70 °C at acid pH with the presence haemozoin/β-haematin 'haem polymerase'[80]. A lot of suggestions concerning the catalysis of haem polymerization have been raised, that may imply that the formation haemozoin as a dimer may not be a real reaction but a simple transformation.

2.7 OBJECTIVE OF THIS MSC STUDY

To potentially overcome or slow down drug resistance in malaria using a multi-therapeutic strategy in which quinoline inhibitors of haemozoin formation are combined with other antimalarial pharmacophores such as β amino alcohol and electrophilic cysteine protease inhibiting moieties such as thiosemicarbazones.

2.8 AIMS OF THIS MSC STUDY

i) Synthesis and structure-activity relationship studies of isatin derivatives of aminoquinoline-thiosemicarbazones and an aminoquinoline-β-amino alcohol-thiosemicarbazone.

ii) Characterization of the synthesized compounds by spectroscopic and analytical techniques.

iii) In collaboration with the School of Medicine, University of California San Francisco (USA) to evaluate synthesized compounds for inhibition of falcipain-2 and malaria parasites *in vitro*.

CHAPTER 3

RESULTS & DISCUSSION

3.1 DESIGN AND SYNTHESIS OF VARIOUS CLASSES OF POTENTIAL ANTIMALARIAL ISATIN-DERIVED CYSTEINE PROTEASE INHIBITORS.

3.1.1 *N*-methyl Isatin Thiosemicarbazones.

Thiosemicarbazones are a class of small molecules that have been evaluated over the last 50 years as antivirals [87], anticancer therapeutics [88], and as well as for their parasiticidal action against *Plasmodium falciparum* [89] and *Trypanosoma cruzi* [90]. A series of thiosemicarbazones was recently shown to inhibit a *Trypanosoma cruzi*-derived cysteine protease, cruzain [91]. The potential of isatin thiosemicarbazone derivatives to inhibit parasitic cysteine proteases has already been demonstrated [26].

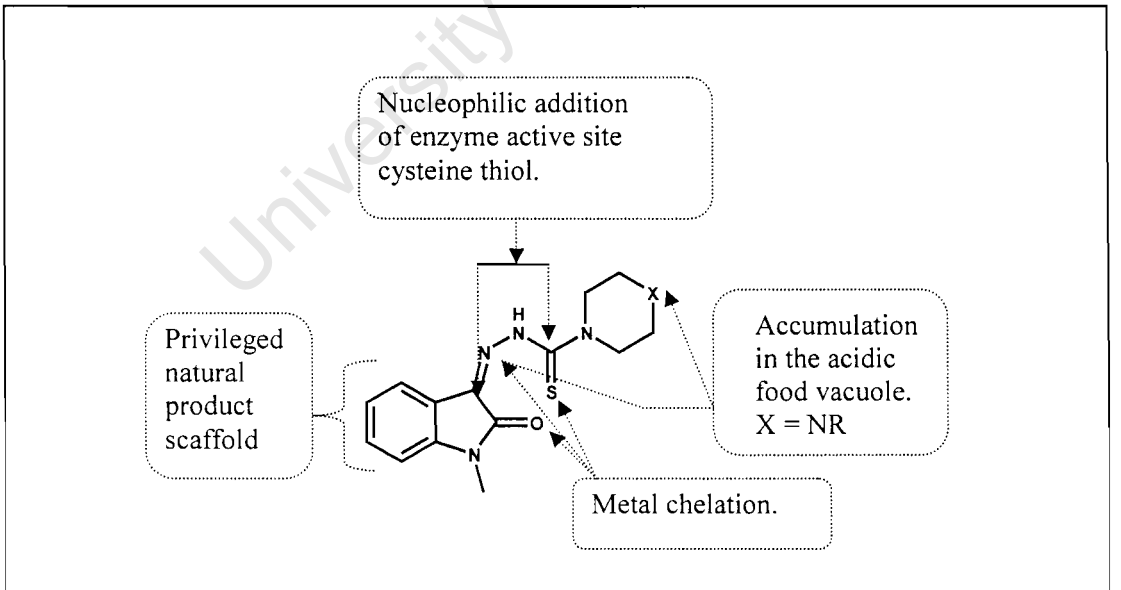

Figure 33: Rational design for *N*-methyl isatin thiosemicarbazones as antimalarial cysteine protease inhibitors.

The design (Figure 33) above was initially intended for SAR studies to probe the effect of including and/or excluding a 4-aminoquinoline unit. The rationale for the inclusion of a thiosemicarbazone unit in the design is based on the three possible mechanisms of inhibition of a cysteine protease as follows:

1) Thiosemicarbazones that are non-peptidic have been recently identified as potent anti-trypanosomal inhibitors of *cruzain* [91]. The inhibition of *cruzain* by thiosemicarbazones has been mechanistically proposed to be *via* attack (Scheme 9) of the enzyme-thiolate anion on the thiol carbonyl resulting in formation of a tetrahedral adduct. The electrophilicity of the thio-carbonyl is enhanced by protonation of thiosemicarbazone sulfur by His 159 driving the attack, and this is supported by experimental and computer modeling results [91].

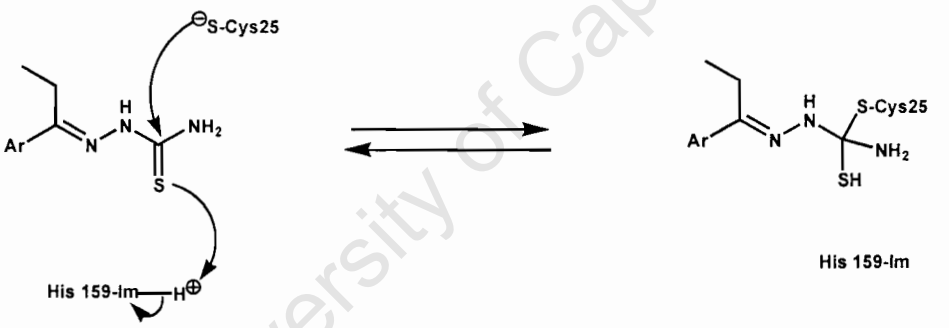

Scheme 9: Mechanistic inhibition of the cysteine protease cruzain by thiosemicarbazones

2) Peptidyl semicarbazones inhibit cysteine proteases via the formation of a tetrahedral adduct (Scheme 10) by attack of the active site thiolate on the imine carbon of the semicarbazone [92].

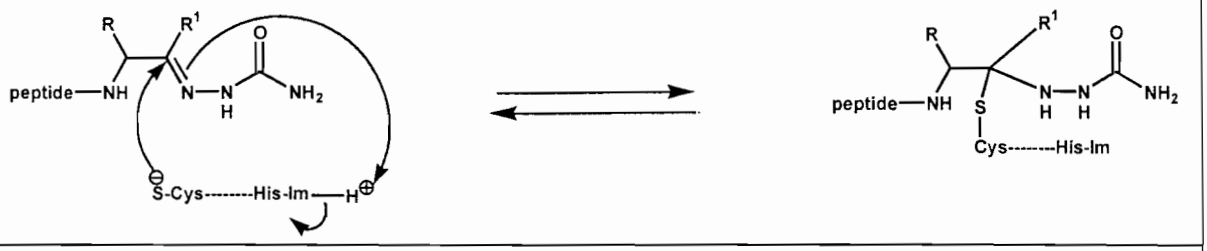

Scheme 10: Mechanistic inhibition of cysteine protease by peptidyl semicarbazones

This attack is driven by polarization of the enzyme-cysteine thiol group by a histidine group that is in close proximity. This polarisation also allows deprotonation under neutral to weakly acidic pH conditions.

3) Thiosemicarbazones are metal chelators (*via* the sulfur and hydrazinic nitrogen atoms) which may act as metal-interactive inhibitors of cysteine proteases [93].

Isatins have recently been used in the inhibition of cysteine and serine proteases as mentioned before. As a privileged natural product scaffold, derivatives synthesized around the basic structure of isatin should yield medicinally active compounds with high hit rates at significantly reduced library size compared to large classical libraries obtained from combinatorial chemistry efforts based on non-privileged templates [26]. The ketone functionality adjacent to the aromatic ring on the isatin scaffold provides a diversity point for accessing the corresponding thiosemicarbazones [26]. Cyclic amines especially those bearing a protonatable nitrogen (X = NR) have been introduced, to increase accumulation of the molecules in the parasite acidic food vacuole *via* pH trapping.

3.1.2 The 4-Aminoquinoline Derivatives.

This class of compounds (Figure 34) was designed on the basis of a multitherapeutic strategy in which a haematin binding 7-chloro-4-aminoquinoline moiety is attached to a cysteine protease inhibiting electrophilic warhead (imine C=N and thiocarbonyl C=S) and/or metal chelating unit.

Quinolines are heteroaromatic molecular structures occurring naturally in coal tar and other products of fossil fuel [94]. Derivatives of quinolines have been used widely in the treatment malaria since the discovery of quinine, the first quinoline antimalarial natural product. Quinine led to the discovery of synthetic derivatives such as chloroquine, mefloquine, and amodiaquine as mentioned before. It is postulated that quinoline antimalarials accumulate in the parasite's acidic food vacuole and inhibit β-haematin formation.

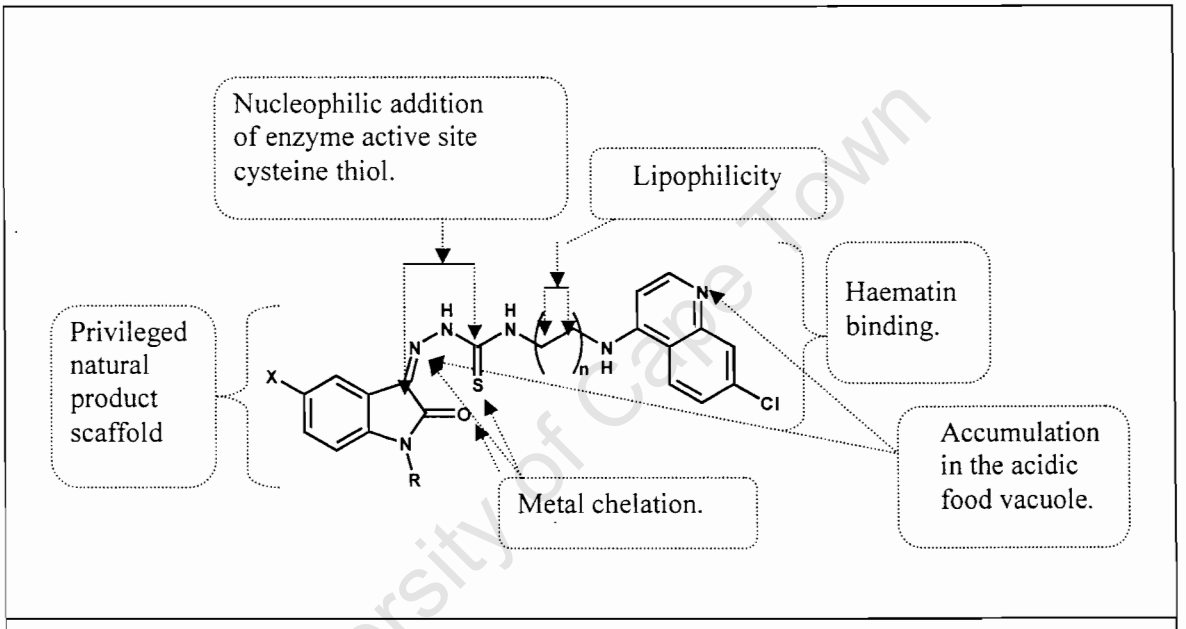

Figure 34: Rational design for 4-aminoquinolines derivatives as antimalarial cysteine protease inhibitors.

Lipophilicity is important in the effective antimalarial activity of metal (iron) chelators. Adequate lipophilicity is essential for these derivatives to cross the parasite membrane and enter the acidic vacuole where they accumulate via pH trapping. Thus introducing a variable alkyl spacer between the isatin thiosemicarbazone and 4-aminoquinoline moieties would permit studies of the effects of lipophilicity and antimalarial activity within a homologous series.

As already mentioned, the potential of isatin thiosemicarbazone derivatives to inhibit parasitic cysteine proteases has been demonstrated [26]. Results presented showed that combination of the thiosemicarbazone moiety with substitution at position 5 of the isatin scaffold is certainly worth pursuing [26]. In the present study, the effect of substituents at this position will also be investigated.

3.1.3 The 4-aminoquinoline β-mino Alcohol Isatin Derivative.

In addition to the features described in Figure 34, an amino alcohol fragment was introduced at the N position of the isatin (Figure 35). It was envisaged that incorpoation of the β-amino alcohol unit would lead to improve antimalarial activity.
This is on the basis of the fact that the β-amino alcohol moiety is well known antimalarial bioactiphore or pharmacophore. It is present in clinically established antimalarial agents such as quinine, quinidine, mefloquine and halofantrine. Structure-activity relationship studies have shown that potent antimalarial activity is observed if the hydroxy and amino groups are separated by 2-3 carbon atoms.

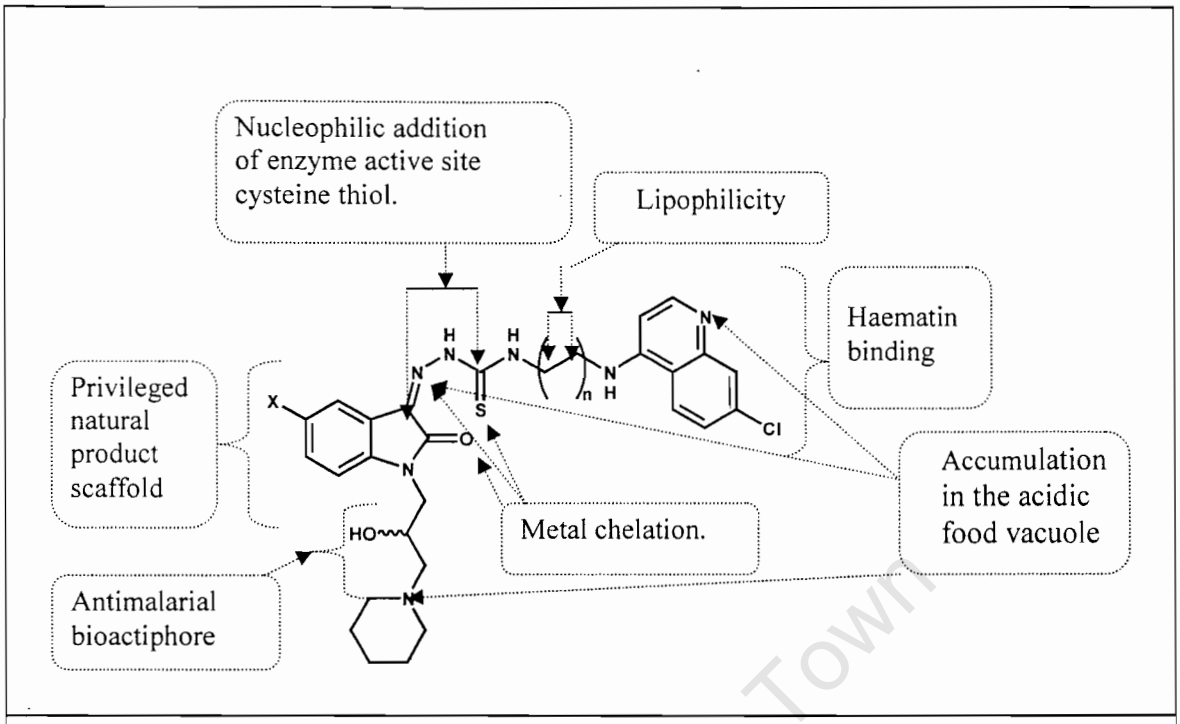

Figure 35: Rational design for 4-aminoquinolines β-amino alcohols derivatives as antimalarial cysteine protease inhibitors.

3.2 SYNTHESIS OF ISATIN DERIVATIVES.

3.2.1 *N*1-Disubstituted *N*-methyl Isatin Thiosemicarbazones.

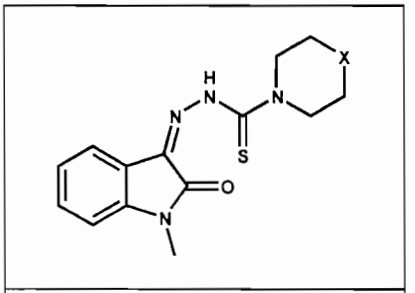

Figure 36: *N*-methyl isatin thiosemicarbazones.

3.2.1.1 Retrosynthetic Analysis.

A simple two-step retrosynthetic analysis (Scheme 11), revealed two commercially available starting materials, cyclic amines and *N*-methylisatin. The other starting material, hydrazinecarbodithioc acid methyl ester (thiosemicarbazide thioester), could be prepared readily using literature procedure (Scheme 12).

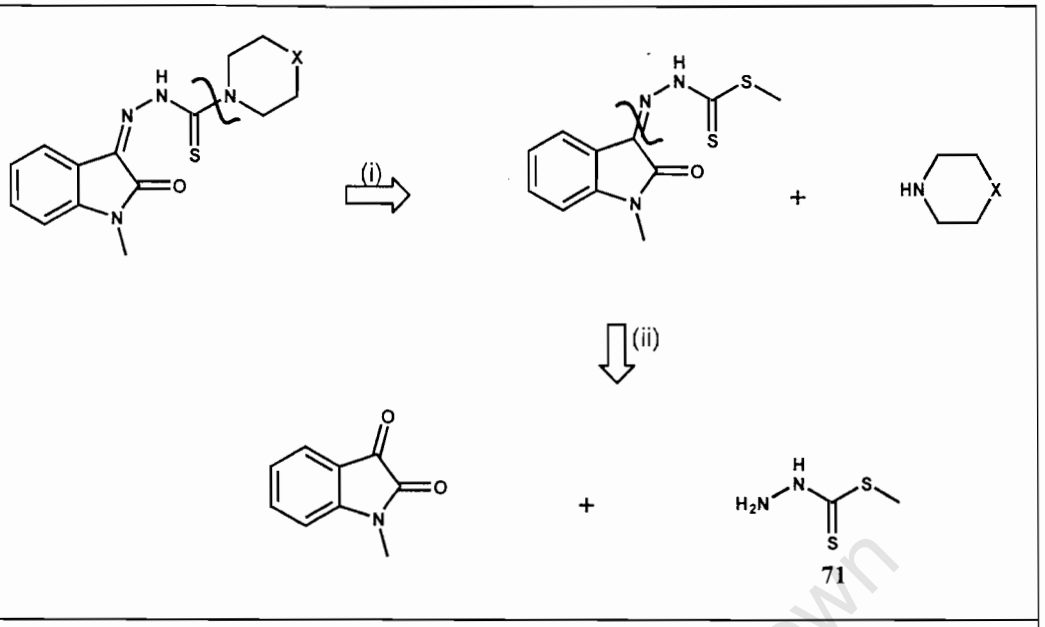

Scheme 11: Retrosynthetic analysis for *N*-methyl isatin thiosemicarbazones: (i) C-N substitution (ii) C-N imine formation.

3.2.1.2 Synthesis of Hydrazinecarbodithioic Acid Methyl Ester **71**.

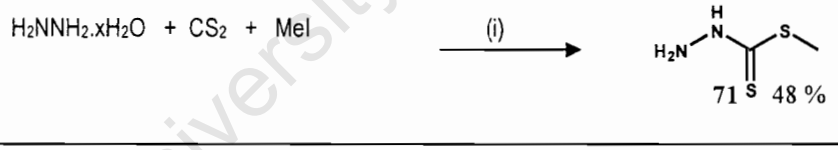

Scheme 12: Synthesis of hydrazinecarbodithioic acid methyl ester. (i) KOH / H_2O.

As shown above in Scheme 12, the compound was made by sequential additions [95] of hydrazine hydrate, carbon disulphide and iodomethane, respectively, in a basic medium to give a 48 % isolated yield of the ester **71**.

3.2.1.3 Synthesis of *N*1-Disubstituted *N*-methyl Isatin Thiosemicarbazones.

Isatin has two carbonyl groups (ketone and amide) at position 2 and 3 (see Figure 5, page 9), which differ from each other in terms of reactivity towards nucleophilic addition. Both carbons of the two carbonyl groups are electrophilic, but donation of electrons by nitrogen through the amide bond towards the amide carbonyl decreases the electrophilicity of this carbonyl group. Thus, the ketone carbonyl group is more reactive towards nucleophiles and the reactions are thus chemoselective.

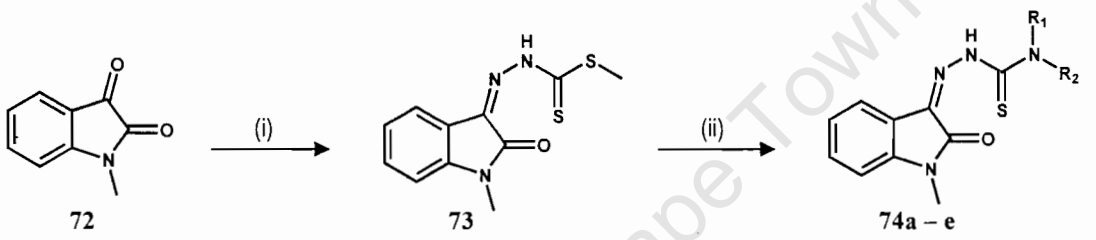

Scheme 13: Synthesis of *N*1-Disubstituted *N*-methyl isatin thiosemicarbazones: (i) Hydrazinecarbodithioic acid methyl ester, Acetic Acid / MeOH, Reflux (ii) Amine / MeOH, Reflux.

As shown above (Scheme 13), the first step is amination with hydrazinecarbothioic acid methyl ester in the presence of a catalytic amount of acetic acid at reflux in methanol. The last step was carried out on intermediate **73** through parallel synthesis using a number of secondary amines to produce compounds **74a - d** in yields ranging from 52 – 72 % (Table 1).

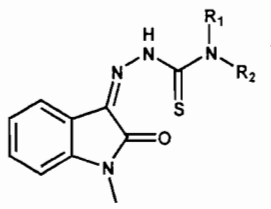

Code	74a	74b	74c	74d
	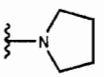	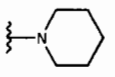	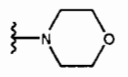	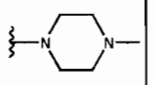
Yield %	52	66	56	72

Table 1: Synthetic yields for cyclic amine derivatives.

3.2.2 4-Aminoquinoline Derivatives.

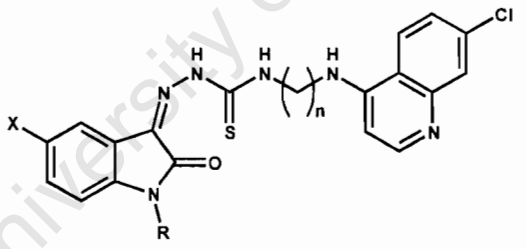

Figure 37: 4-aminoquinoline derivatives.

3.2.2.1 Retrosynthetic Analysis.

Before carrying out the synthesis of 4-aminoquinolines, available starting materials were identified by breaking down the target molecule retrosynthetically as shown below (Scheme 14). It is noteworthy that the key disconnections involved a C-N bond. The key

starting materials were identified as isatins, hydrazinecarbodithioic acid methyl ester, diamines and 4, 7-dichloroquinoline by further disconnecting advanced intermediates including **76a-d**.

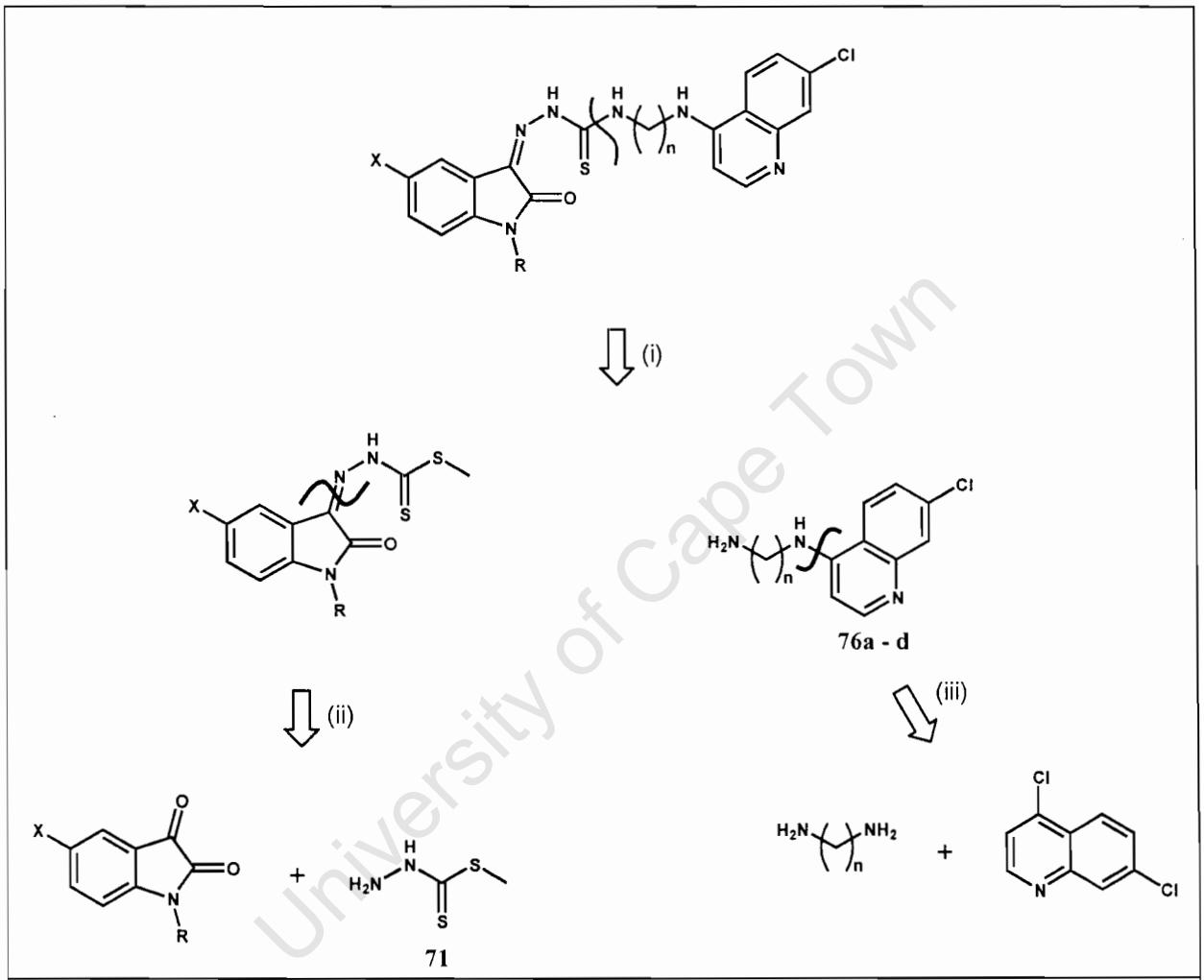

Scheme 14: Retrosynthetic analysis of 4-aminoquinoline derivatives: (i) C-N substitution (ii) C-N imine formation (iii) C-N aromatic substitution.

3.2.2.2 Synthesis of 7-Chloro-quinolin-4-yl Diamine Intermediates **76a – d.**

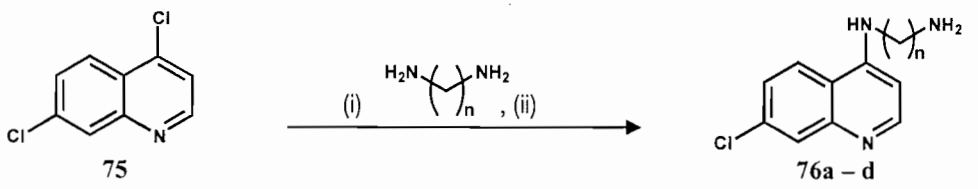

Scheme 15: Synthetic route To 7-chloroquinolines-4-diamine: (i) diamine, (ii) Et_3N, K_2CO_3, 80 °C for 1 h, then 145 °C for 4 h.

The synthesis of compounds **76a – d** above (Scheme 15) involves refluxing in an excess of a diamine in the presence of triethylamine and potassium carbonate to ensure a maximum yield ranging from 80 –95 % as shown in Table 2 below.

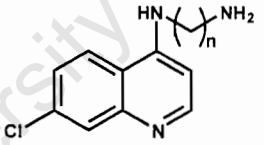

Code	76a	76b	76c	76d
n	2	3	4	6
Yields (%)	89	80	92	95

Table 2: Synthetic yields of 7-chloroquinoline diamines.

3.2.2.3 Synthesis of 4-Aminoquinoline Derivatives.

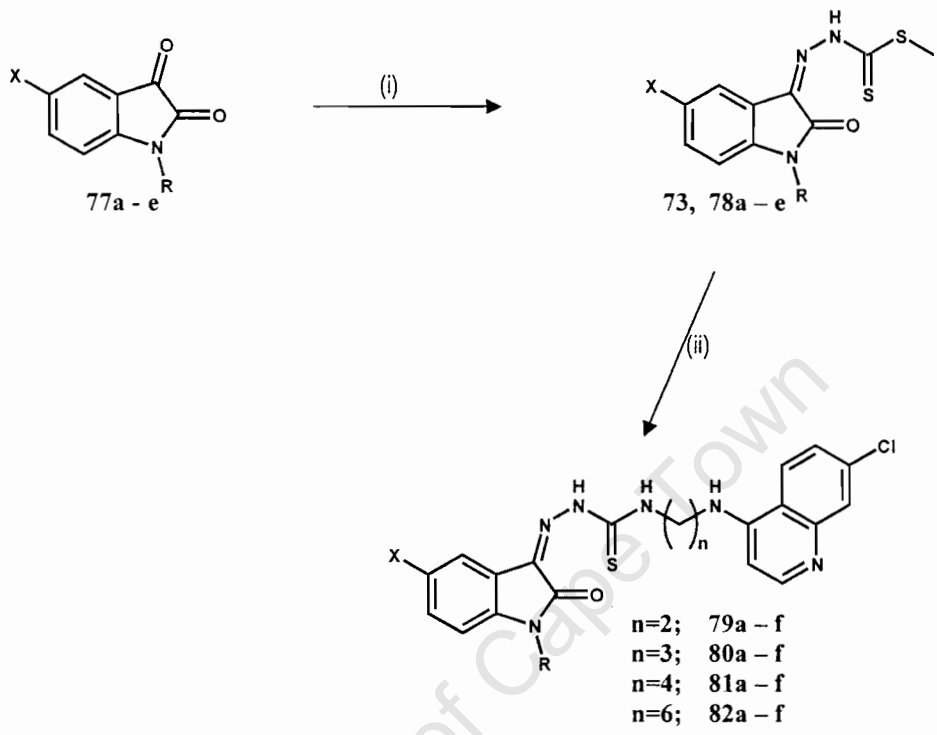

Scheme 16: Synthetic route to 4-aminoquinoline derivatives: (i) Hydrazinecarbodithioic acid methyl ester / MeOH, Reflux (ii) Amine / MeOH, Reflux.

With the same reaction conditions as those employed for Scheme 13 intermediates **73**, **78a – e** and final products **79a – f** to **82a – f** were obtained in good yields as shown in Table 3 and 4.

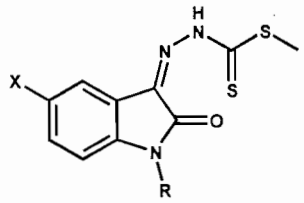

Compound	**78a**	**78b**	**78c**	**73**	**78d**	**78e**
X	Br	Cl	F	H	Me	NO_2
R	H	H	H	Me	H	H
Yield (%)	80	95	71	92	76	87

Table 3: Synthetic yields of isatin thiosemicarbazones.

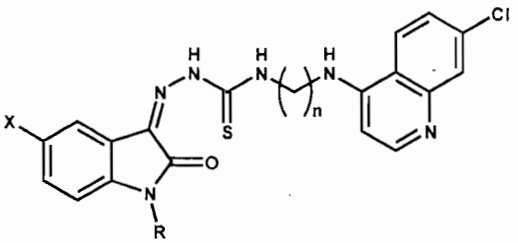

Compound	X	R	n	Yield %
79a	H	Me	2	93
80a	H	Me	3	82
81a	H	Me	4	91
82a	H	Me	6	95
79b	Br	H	2	93
80b	Br	H	3	84
81b	Br	H	4	98
82b	Br	H	6	65
79c	Cl	H	2	94
80c	Cl	H	3	75
81c	Cl	H	4	82
82c	Cl	H	6	78
79d	F	H	2	98
80d	F	H	3	71
81d	F	H	4	99
82d	F	H	6	98
79e	Me	H	2	95
80e	Me	H	3	86
81e	Me	H	4	94
82e	Me	H	6	73
79f	NO_2	H	2	96
80f	NO_2	H	3	72
81f	NO_2	H	4	97
82f	NO_2	H	6	92

Table 4: Synthetic yields of 4-aminoquinolines.

3.2.3 4-Aminoquinoline β-amino Alcohol Derivative.

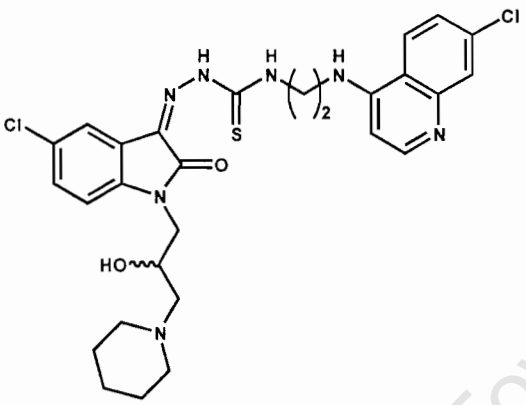

Figure 38: 4-aminoquinoline β-amino alcohol **89**.

3.2.3.1 Retrosynthetic Analysis.

The retrosynthetic analysis for this molecule is depicted in Scheme 17. Most of the key disconnections have already been encountered in the previous schemes. Additional disconnections revolved around the β-amino alcohol fragment, which revealed the epoxide as a key intermediate. Regioselective opening of the epoxide intermediate by the secondary (piperidine) amine required prior protection of the ketone carbonyl, as a ketal, in order to avoid reaction at this site in addition to the desired (epoxide) ring opening reaction.

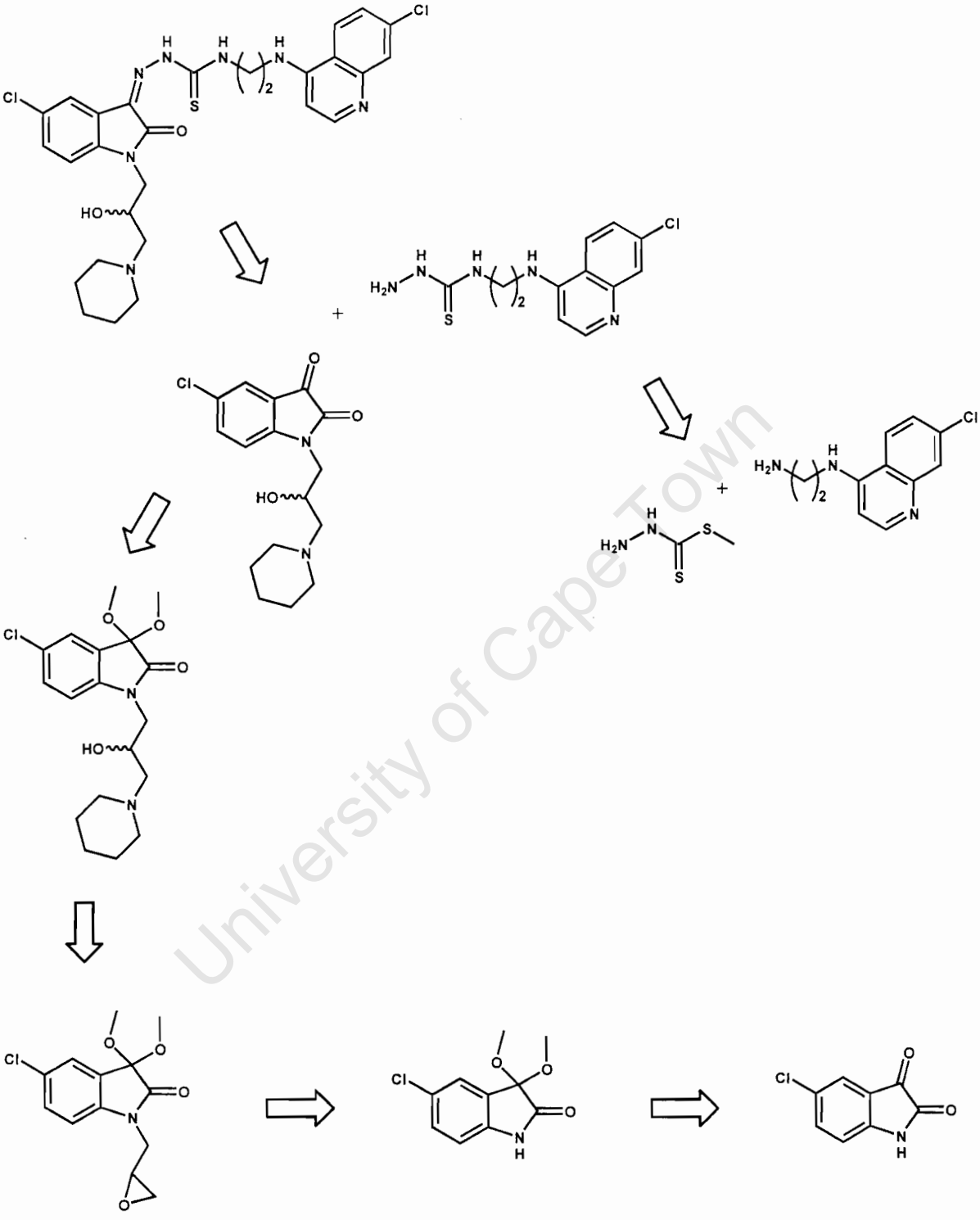

Scheme 17: Retrosynthetic analysis of 4-aminoquinoline β-amino alcohol **89**.

3.2.3.2 Synthesis of Thiourea **83.**

The thio-urea intermediate **83** in scheme 18 below was synthesized in a 52 % yield from the reaction of N^1-(7-chloro-quinolin-4-yl)-ethane-1,2-diamine **76a** and hydrazinecarbodithioic acid methyl ester **71** in methanol under reflux.

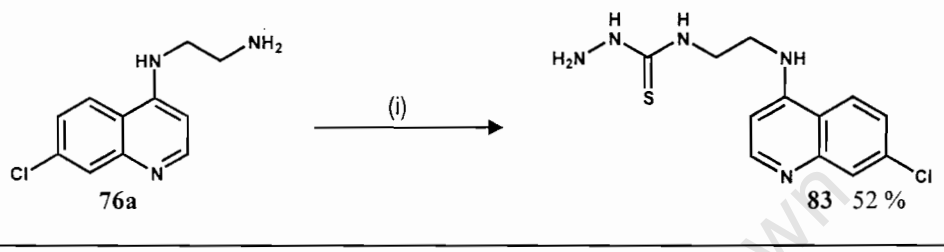

76a **83** 52 %

Scheme 18: Synthetic route for thiourea **83**. (i) **71** / MeOH at Reflux.

3.2.3.3 Synthesis of 4-Aminoquinoline β-amino Alcohol Isatin Derivative **89.**

The five-step synthesis was initiated by protection of the ketone **84**. As already alluded to in the retrosynthetic analysis, this step had to be carried out in order to avoid nucleophilic addition to the carbonyl group in step (iii). Thus, protection was performed using trimethyl orthoformate in the presence of a catalytic amount of *p*-toluene sulfonic acid. The mixture was refluxed in methanol (anhydrous) under nitrogen for 48 hrs to give a 62 % yield of the *ketal* **85** (see Scheme 20 for mechanism).

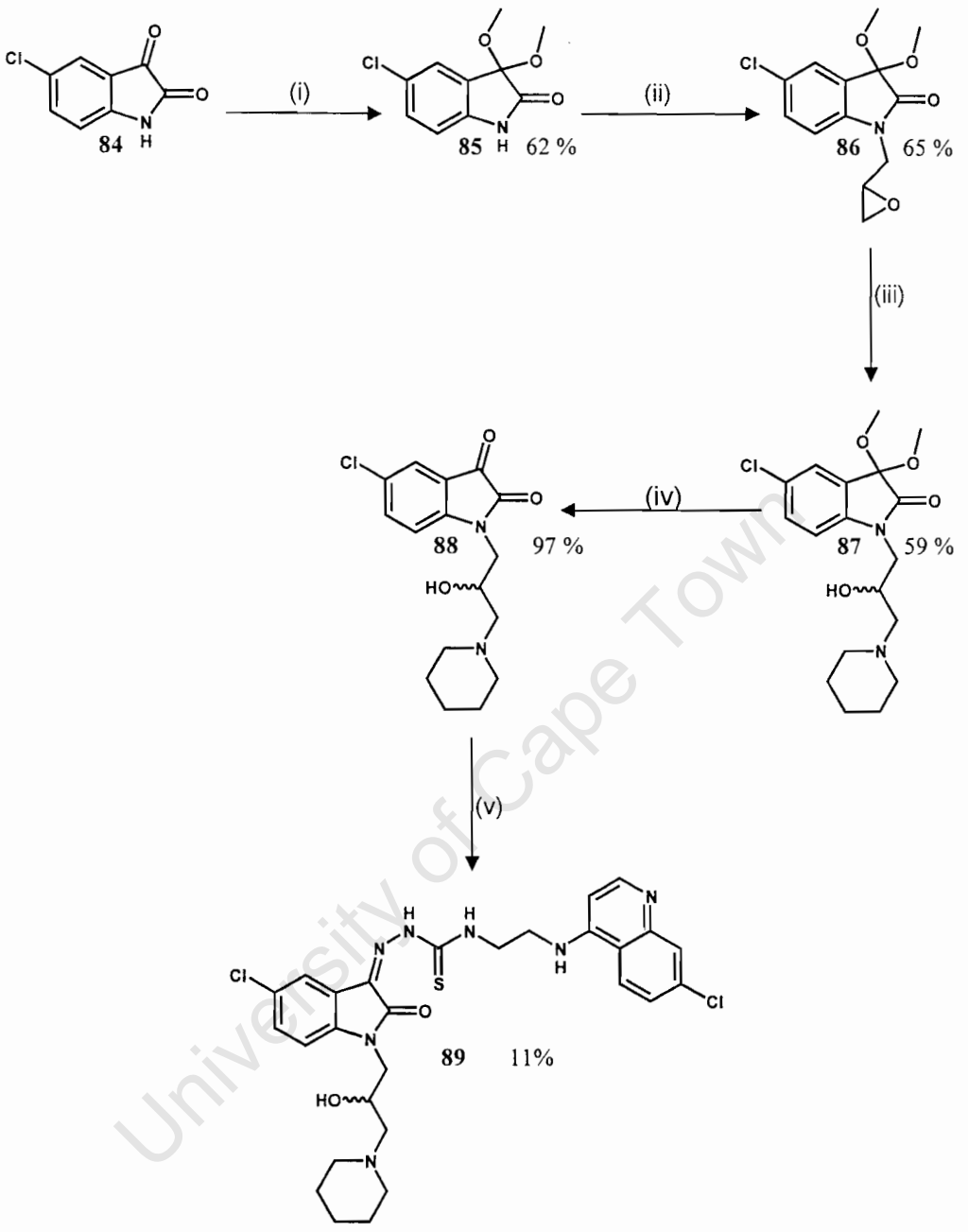

Scheme 19: Synthetic Route to 4-AminoQuinoline (N^1-Amino Alcohol) Derivatives. (i) $CH(MeO)_3$, *p*-TsOH / MeOH, Reflux /N_2, 48 hrs; (ii) KF/Al_2O_3, Epichlorohydrin / DCM, RT, 48 hrs; (iii) Piperidine/MeOH, 65 °C, 12 hrs; (iv) 10 % HCl / Acetone, RT, 3hrs; (v) Thiourea **83** / MeOH, Reflux, 24 hrs.

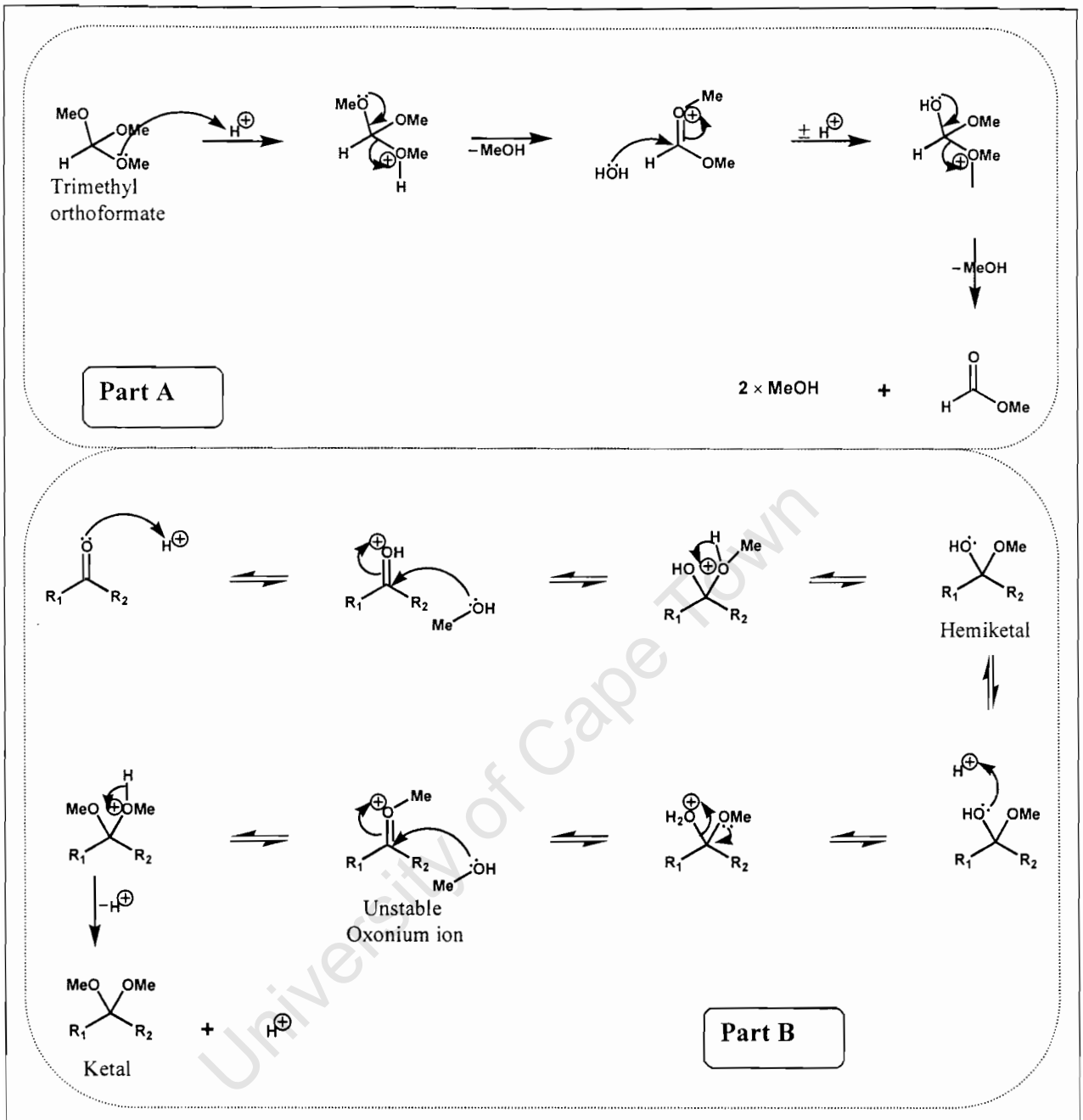

Scheme 20: Ketone Protection Mechanism. Part A is the hydrolysis of trimethyl orthoformate and Part B is the actual ketone protection mechanism.

Trimethyl orthoformate as an orthoester is a source of alcohol (methanol). Orthoesters, in the presence of an acid as catalyst, are hydrolysed by water to yield an ester plus 2 × alcohol (Scheme 20 PartA).

Part A + B in Scheme 20 are only separated for the sake of illustration. The two schemes represent one mechanism, which starts off as if the orthoester is going to hydrolyse but the alcohol (in this case MeOH) released adds to the ketone and acetal formation begins.

Ketal formation is initiated by protonation by *p*-toluene sulfonic acid enhancing the electrophilicity of the carbonyl carbon. This is followed by addition of methanol to form a hemiketal. The hydroxyl group of the hemiketal is then protonated, followed by water elimination, which is taken out of the equilibrium by hydrolysis of the orthoester. An unstable and highly reactive oxonium ion is formed. Methanol is then added to the oxonium ion breaking the π bond, followed by loss of a proton to give the ketal.

Compound **85** was then N-alkylated with 1-chloro-2, 3-epoxypropane (epichlorohydrin) in the presence of KF/Al_2O_3 as a base to yield 65 % of *epoxide* **86**. This was followed by epoxide ring opening (third) step with piperidine, which required refluxing for 12 hrs. In this step, there are two (most and least hindered) electrophilic centers liable for nucleophilic attack to give two possible products (see Figure 43, page 78). However, from the reaction only one product **87** in 59 % yield was obtained. The 2D NMR (Figure 45, page 80) of **87** confirmed attack of the amine at the least hindered terminal electrophilic carbon of the epoxide, as this would be expected on steric grounds.

Removal of the protecting group was carried out at room temperature with 10 % concentrated HCl in acetone for 3 hrs to give the *ketone* **88** in 97 % yield. The ketone was then reacted with **83** (prepared according to Scheme 18) in the presence of a catalytic amount of acetic acid at reflux in methanol for 48 hrs to deliver target compound **89** in 11 % yield.

3.3 CHARACTERIZATION OF SYNTHESISED COMPOUNDS.

3.3.1 ^{1}H NMR Confirmation of Compounds.

Synthesised compounds were confirmed by Mass spectrometry, IR, ^{1}H and ^{13}C and 2D NMR. However, ^{1}H and 2D NMR are discussed in detail in this section for relevant compounds. ^{1}H NMR interpretation of final compounds especially the 4-aminoquinolines required the use of starting material splitting patterns. It must be noted that the letters Q for quinolines and I for isatin were used for proton reference.

3.3.1.1 ^{1}H NMR Interpretation of Isatin Thiosemicarbazones **73, 78a –e**.

Each compound synthesized was confirmed by the ^{1}H NMR splitting patterns and coupling. For example in the series **73, 78a – e** the aromatic protons are easily assigned from the multiplicities and *J* values they give.

In this series of intermediates, **78a** is the representative compound whose ^{1}H NMR is displayed in Figure 39. H4I has a smaller *J* value than H7I due to long range coupling to H6I and gives rise to a doublet with a *J* value of 2.2 Hz. H7I gives rise to a doublet with a *J* value of 8.4 Hz due to vicinal coupling to H6I. On the other hand H6I couples to both H7I (*J* value of 8.4 Hz) and H4I (*J* value of 2.2 Hz) to give a doublet of doublets splitting pattern.

3.3.1.2 ^{1}H NMR Interpretation of 7-Chloro-quinolines-4-yl Diamines **76a – d**.

N^{1}-(7-Chloro-quinolin-4-yl)-ethane-1, 2-diamine **76a** is the representative compound used for illustration in Figure 40. By resonance H3Q is the most shielded while H2Q appears downfield as it is the most deshielded and both protons give rise to a *J* value of 6.0 Hz as they couple to each other. H8Q displays a doublet of *J* equal to 2.1 Hz due to long-range coupling to H6Q, while H5Q has a very large vicinal coupling constant of *J* =

9.2 Hz. H6Q therefore gives a doublet of doublets by coupling to both H8Q (*J* value of 2.1 Hz) and H5Q (*J* value of 9.2 Hz).

3.3.1.3 ^{1}H NMR Interpretation of 4-Aminoquinolines Derivatives **79a – f** to **82a – f**.

The information gained from Figures 39 and 40 was quite useful in assigning the protons of derivatives **79a - f** to **82a – f**. However, H6Q and H6I give rise to similar splitting patterns and coupling constants. Since H6I appears first (around 6.90 ppm) in the spectrum of **78a** and H6Q appears second (around 7.39 ppm) in the spectrum of **76a**, the two protons for this compound in Figure 41 were therefore assigned as in these starting materials. H8Q in compound **79f** (Figure 41) and related (some nitro derivatives) compounds surprisingly is the most deshielded proton. This is quite opposite to what is expected by reasonance wherein H2Q would be the most deshielded. As shown in Figure 41, H8Q displays a long range coupling (*J* = 2.5 Hz) to H6Q. H2Q (as assigned) has a larger coupling (*J* = 5.4 Hz), which matches with that of H3Q.

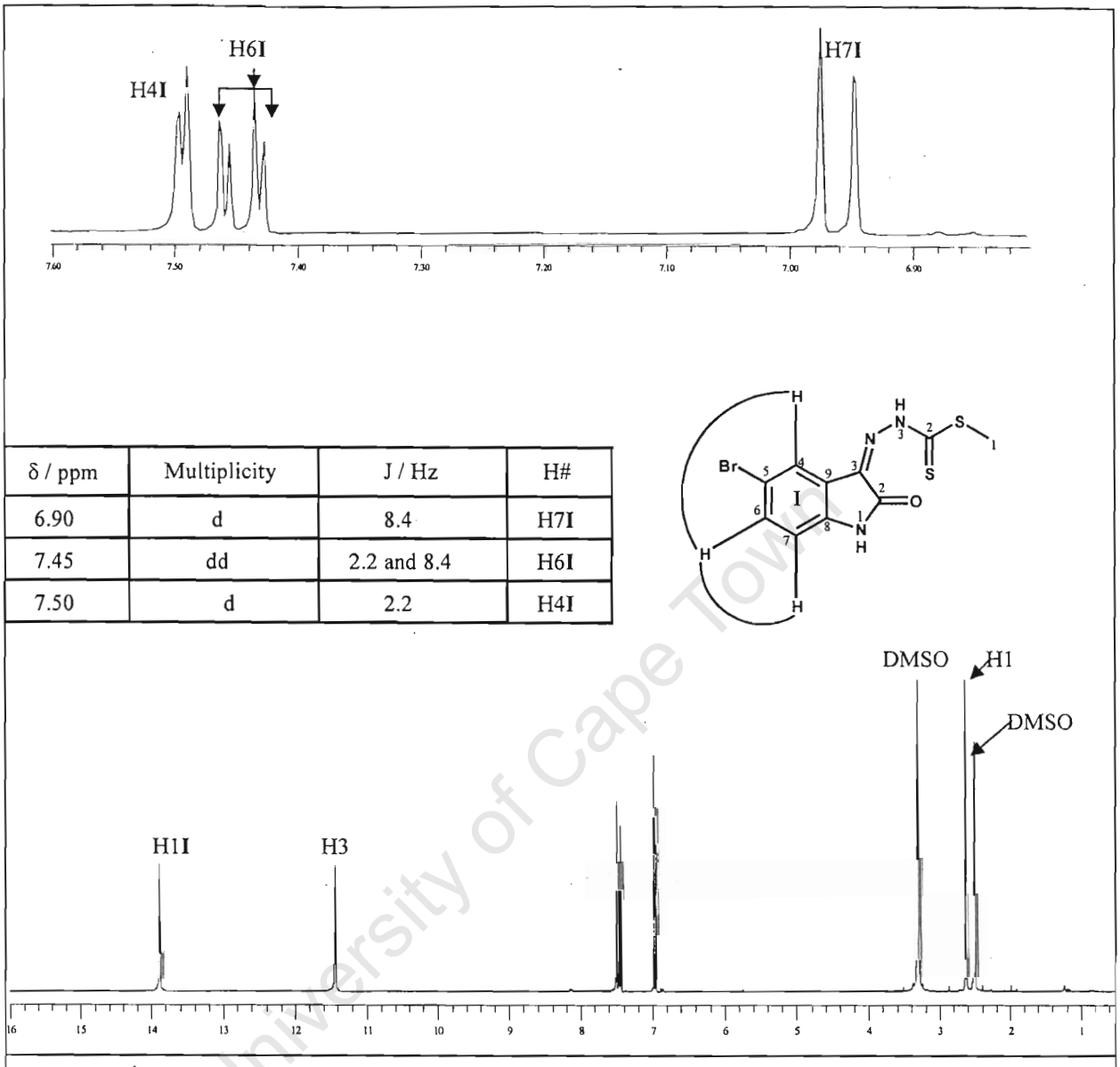

δ / ppm	Multiplicity	J / Hz	H#
6.90	d	8.4	H7I
7.45	dd	2.2 and 8.4	H6I
7.50	d	2.2	H4I

Figure 39: ^{1}H NMR Interpretation of isatin thiosemicarbazone **78a**.

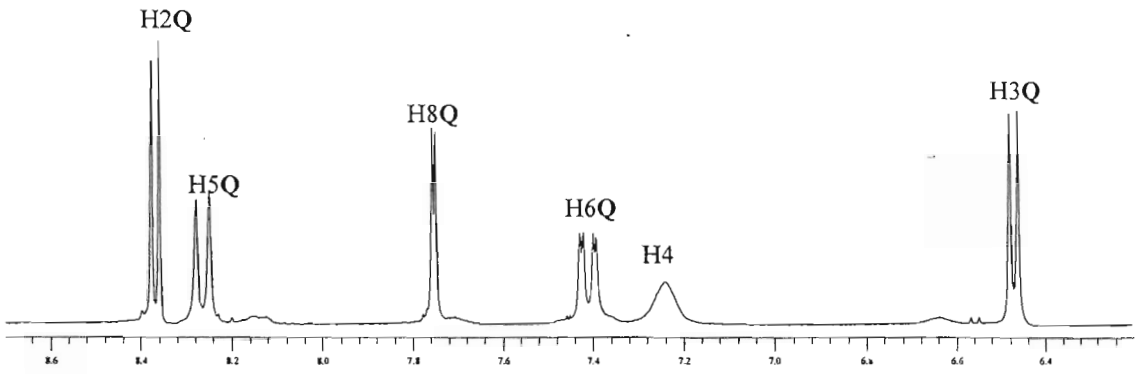

δ / ppm	Multiplicity	J / Hz	H#
6.56	d	6.0	H3Q
7.39	dd	2.1 and 9.2	H6Q
7.77	d	2.1	H8Q
8.10	d	9.2	H5Q
8.35	d	6.0	H2Q

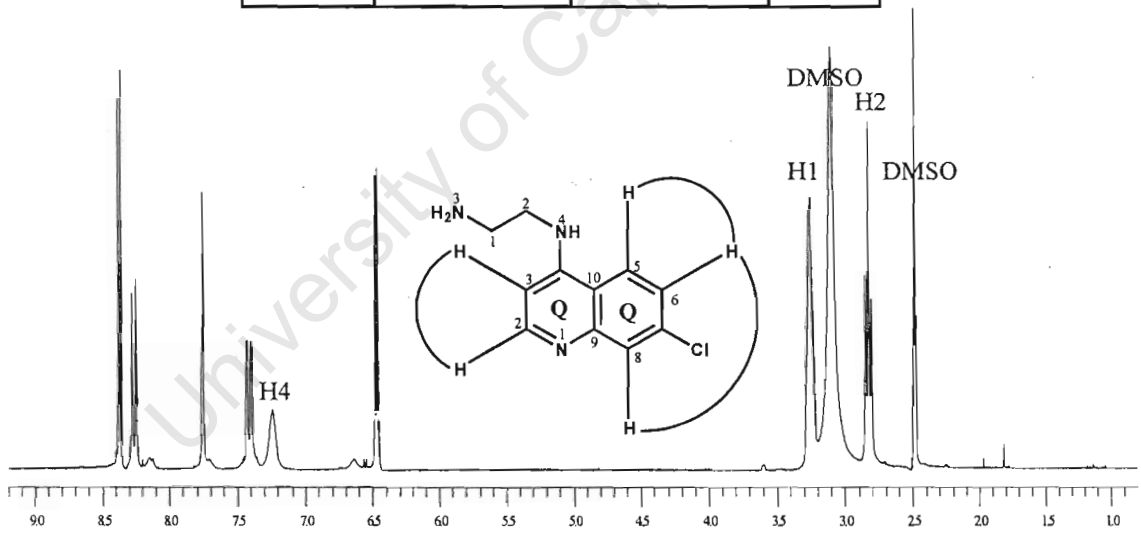

Figure 40: ^{1}H NMR Interpretation of *N*1-(7-chloro-quinolin-4-yl)-ethane-1, 2-diamine **76a**.

δ / ppm	Multiplicity	J / Hz	H#
6.53	d	5.4	H3Q
8.10	dd	2.5 and 8.8	H6Q
8.14	d	8.8	H5Q
8.42	d	5.4	H2Q
9.01	d	2.5	H8Q

δ / ppm	Multiplicity	J / Hz	H#
6.93	d	8.8	H7I
7.55	dd	2.0 and 8.8	H6I
7.76	d	2.0	H4I
7.30	br	.....	H3
®	.....	.....	H4
®	.....	.....	H6
®	.....	.....	H1I

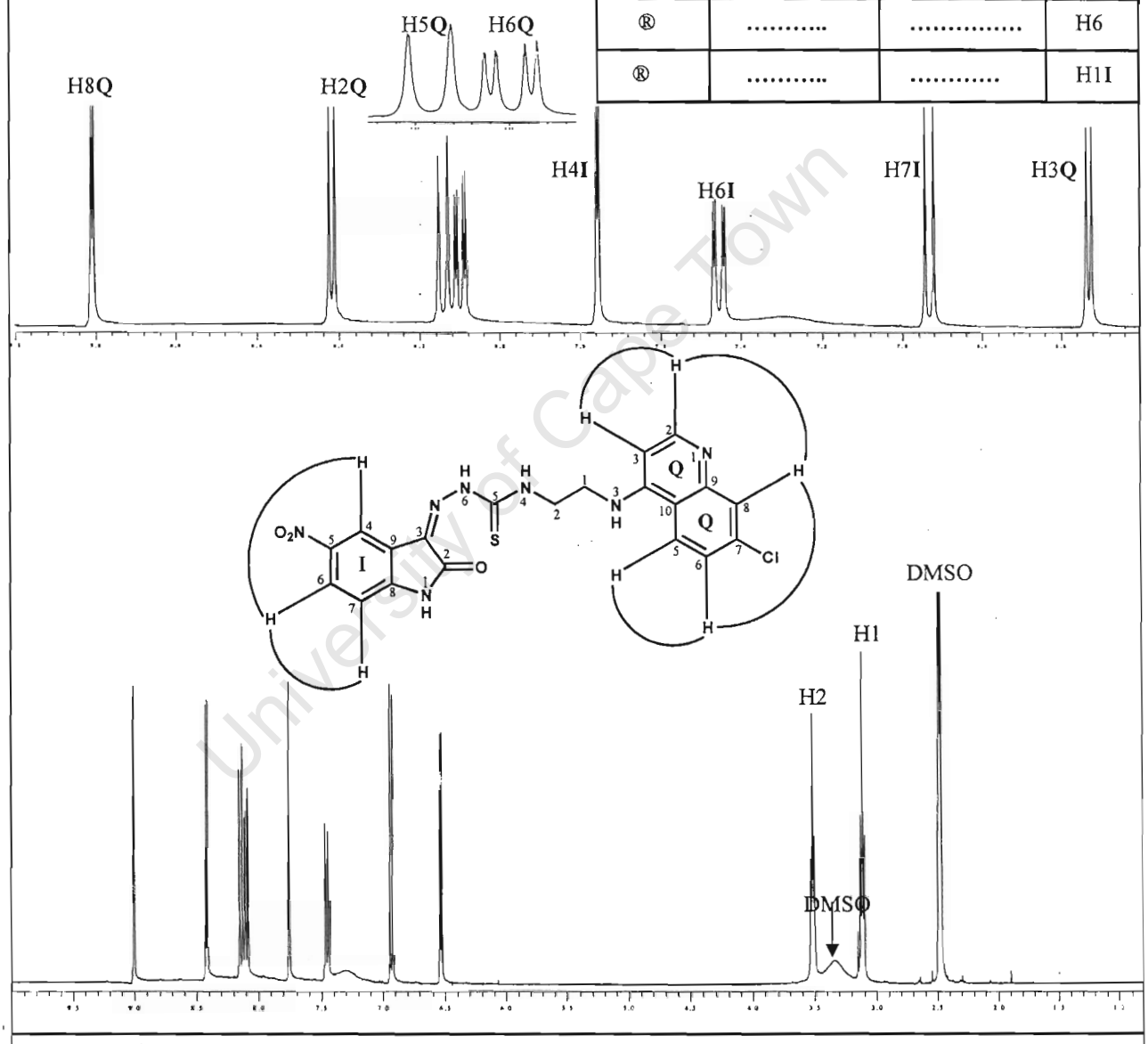

Figure 41: ^{1}H NMR interpretation of 4-aminoquinolines derivatives **79f**.

® Peaks For These Protons Were Not Revealed Due To Deuterium Exchange With DMSO-d_6

3.3.1.4 ^{1}H NMR Interpretation of 4-Aminoquinolines β-amino Alcohol **89**.

The aromatic proton peaks for target compound **89** were not well resolved at 400 MHz. As shown in Figure 42 below, some peaks are not clear leading to unresolved coupling constants, especially in region 7.40 - 7.60 ppm. Integration and chemical shift values played a key role in assigning the peaks. The labeled protons are the only identifiable protons using the information from **79f** in Figure 41. H3Q is the most shielded proton and couples (J = 7.2 Hz) with H2Q, which is the most deshielded proton. H8Q and H4I have small (long range) coupling constants of 2.4 Hz and 3.2 Hz arising from coupling to H6Q and H6I respectively.

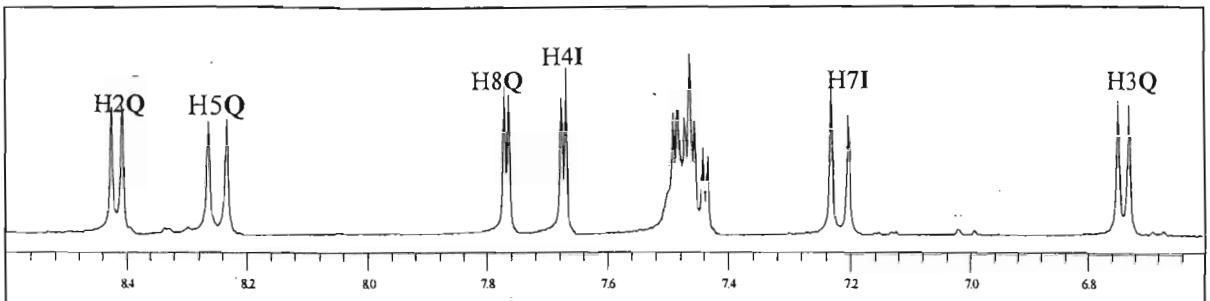

δ / ppm	Multiplicity	J / Hz	H#
δ / ppm	d	7.6	H3Q
δ / ppm	d	11.6	H7I
δ / ppm	d	3.2	H4I
δ / ppm	d	2.4	H8Q
δ / ppm	d	12.4	H5Q
δ / ppm	d	6.8	H2Q

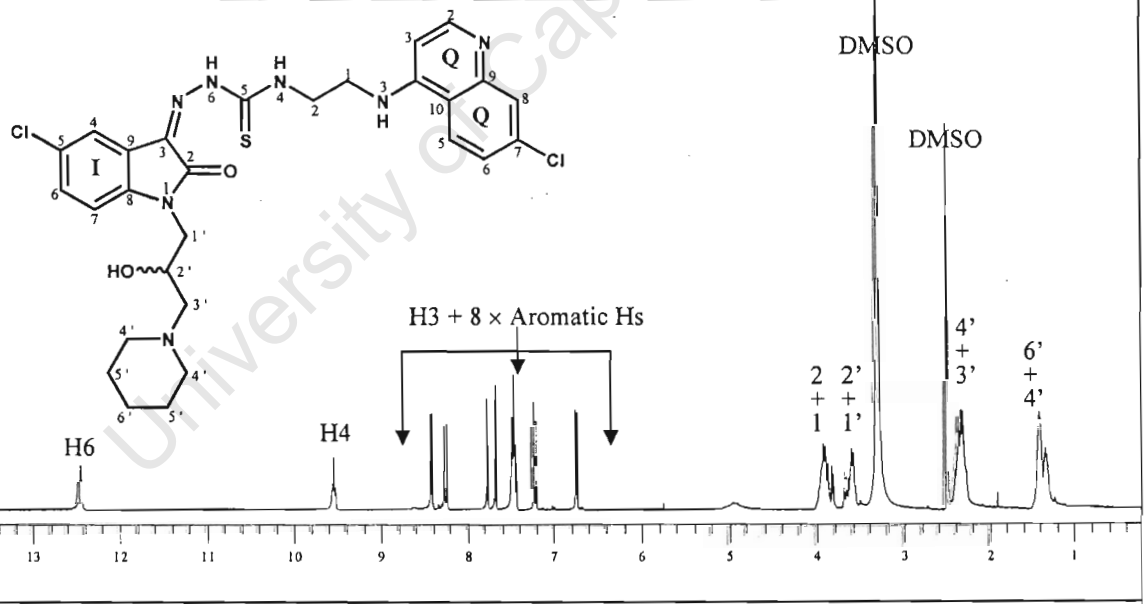

Figure 42: 1H NMR interpretation of 4-aminoquinolines β-amino alcohol **89.**

3.3.2 2D NMR Confirmation of Compounds.

The purpose of a 2D NMR for **86** and **87** (Figure 44 and 45) was to confirm the regiochemistry of epoxide (**86**) ring opening. Depending on the regiochemistry, two products **A** and **B** (**87**) are possible, Figure 43.

3.3.2.1 2D NMR Interpretation of **86**.

The 2D NMR reveals that 1' protons couple to each other and to methine proton 2'. This confirms that the two diastereotopic protons 1' are next to 2'. Both the 3' protons are also coupling to 2', implying that the methine proton is adjacent to both 1' and 3' protons, Figure 44.

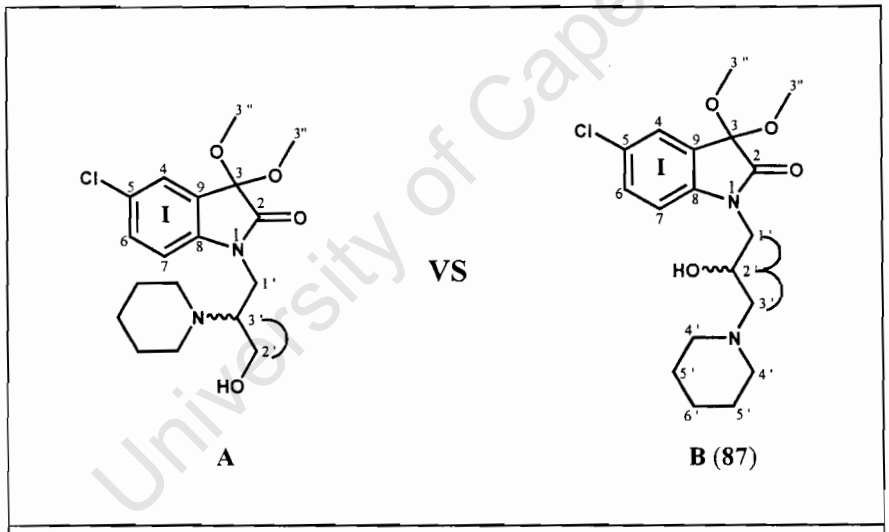

Figure 43: Illustration of two possible products **A** and **B** from opening of epoxide **86**.

3.3.2.2 2D NMR Interpretation of **87**.

Figure 45 shows that 2' is the proton bonded to -C-OH, since 2' couples to both 1' and 3' protons. This implies that epoxide ring opening occurred at the terminal carbon, giving rise to compound **87**.

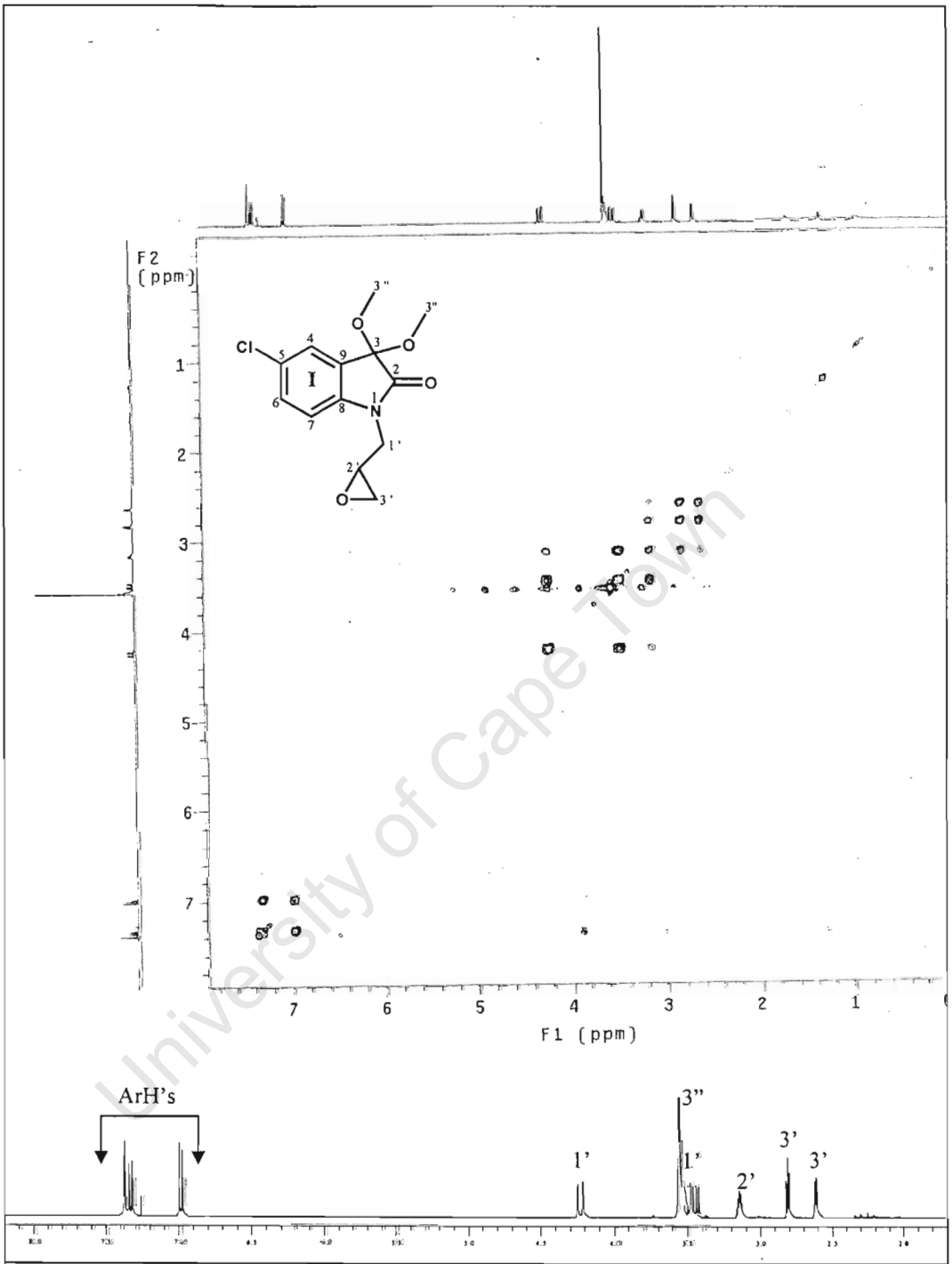

Figure 44: 2D NMR of **86**.

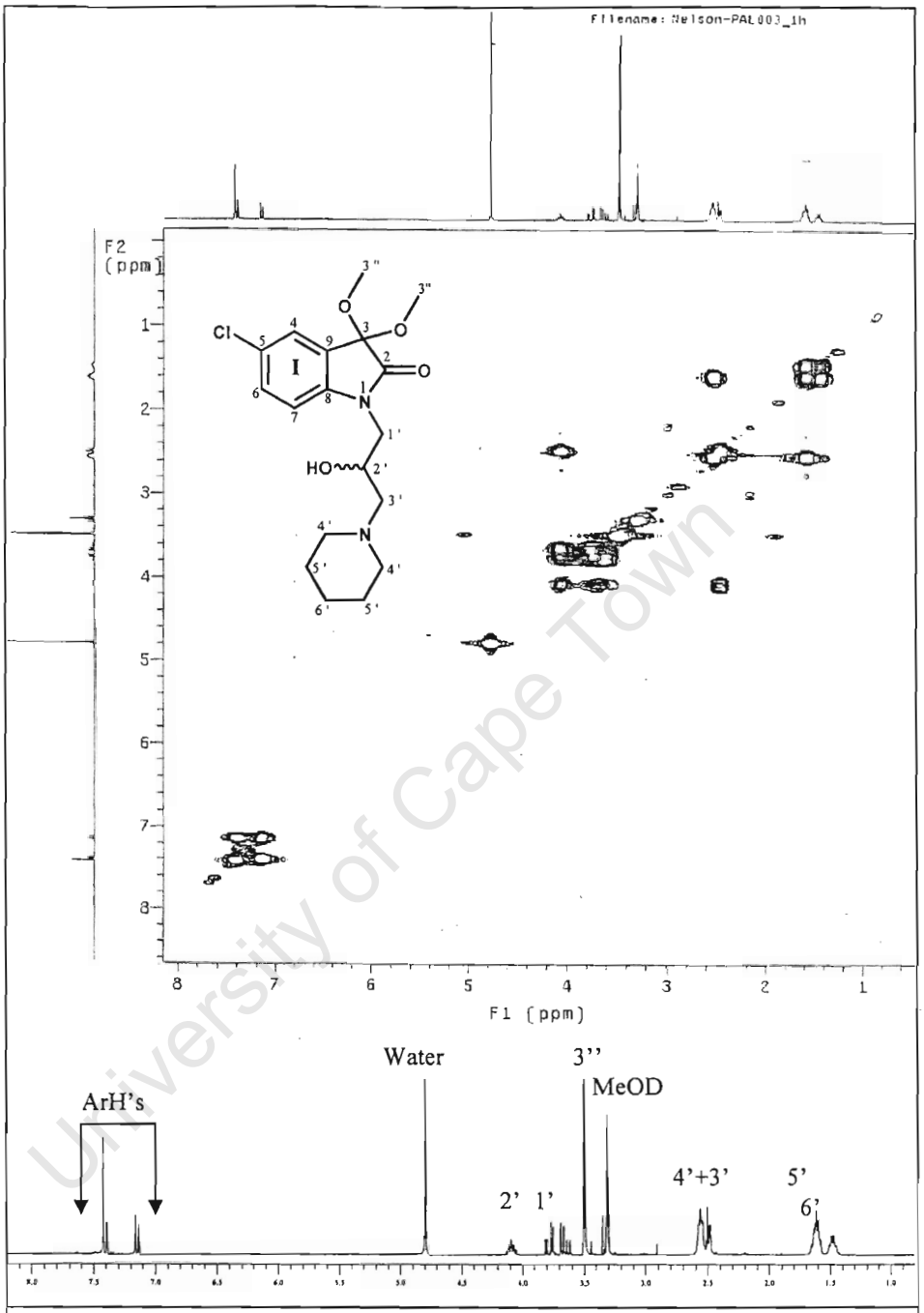

Figure 45: 2D NMR of **87**.

CHAPTER 4

BIOLOGICAL RESULTS AND DISCUSSION

4.1 PROCEDURES FOR BIOLOGICAL ASSAYS

4.1.1 Assay of Enzyme Inhibition: Falcipain-2

IC_{50}s against falcipain-2 were determined as described by Rosenthal et al [96]. Briefly, an equal amount of recombinant falcipain-2 were incubated with different concentrations of Mannich base derivatives (added from 100x stocks in dimethyl sulfoxide [DMSO]) in 100 mM sodium acetate (pH 5.5)-10 mM dithiothreitol for 30min at room temperature before addition of the substrate benzoxycarbonyl-Leu-Arg-7-amino-4-methyl- coumarin. Fluorescence was continuously monitored for 30 min at room temperature in a labsystem Fluoroskan II spectrofluorometer. IC_{50}s were determined from plots of activity over enzyme concentration with GraphPad Prism software.

4.1.2 Assay of Parasite Development: W2

Effects of inhibitors on the parasite development were determined as described earlier.[96] Synchronized W2-strain *P. falciparum* parasites[97] were cultured with compound derivatives (added from 1000x stocks in DMSO) for 48 h beginning at the ring stage. The medium was changed after 24 h, while maintaining appropriate inhibitor concentration. Giemsa-stained smears were made after 48 h, when control cultures contained nearly all ring-stage parasites. The number of new ring forms per 500 erythrocytes was counted, and compared with those of controls cultured in 0.1 % DMSO. IC_{50}s for growth inhibition were determined with GraphPad Prism software from plots of percentages of the level of parasitemia of the control relative to inhibitor concentration.

4.2 BIOLOGICAL RESULTS OF SYNTHESISED COMPOUNDS

4.2.1 Biological Results for Isatin Thiosemicarbazones 73, 78a – e

Together with the final targets, these intermediates were tested for comparison purposes against recombinant falcipain-2 (Rec-FP2) and *Plasmodium falciparum* W2 strain (P.f. W2), which is a chloroquine resistant strain (IC_{50} of chloroquine ~ 300 nM). These intermediates have different substituents at position 5 on the isatin aromatic ring except for one (**79a**) that has a methyl group at position 1. In this class of inhibitors, the effect of substituents (X = Br, Cl, F, H, Me and NO_2) at position 5 and *N*1 disubstitution of thioesters (Y = -SMe) was investigated. Results are presented in Table 5.

The change of substituents on the isatin scaffold increased activity in the order shown in Figure 46. Compound **78a** (X = Br) showed modest activity against the enzyme (IC_{50} = 7.5 μM), while compound **73** showed no activity at a concentration of 20 000 nM, suggesting that the presence of the methyl at position 1 of isatin had no effect against the enzyme at or below this concentration. Despite the modest activity of compound **78a** against FP2, it was devoid of antimalarial activity at a concentration of 20 000 nM. Indeed all other isatin thiosemicarbazone thioesters had no activity detected at a concentration of 20 000 nM against the parasite.

At 20 000 nM, all the cyclic amine derivatives were not active against Rec-FP 2. However, these derivatives had better activity against the P.f W2 strain. This lack of correlation between inhibition of FP2 and antimalarial activity in *vitro* suggests that FP2 may not be the target for these cyclic amine derivatives. Although the cyclic amines showed a better activity, introduction of a 4-aminoquinoline (7-CD-4-EDA) nucleus resulted in even much better activity against the parasite (Figure 50), demonstrating that the presence of the quinoline ring had a positive effect against P.f. W2.

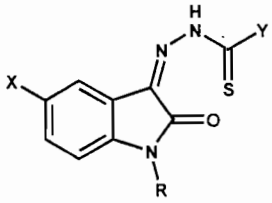

Compound	X	R	Y	IC50 (nM)		C log P
				Rec-FP2	P.f W2	
78a /AXE 9	Br	H		7506	> 20 000	3.007
78b /AXE 10	Cl	H		9318	> 20 000	2.857
78c /AXE 11	F	H		18310	> 20 000	2.287
78d /AXE 17	Me	H		9704	> 20 000	2.643
78e /AXE 12	NO_2	H		8691	> 20 000	1.887
73 /AXE 1	H	Me		> 20 000	> 20 000	3.02
74a /AXE 2	H	Me	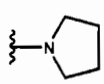	> 20 000	5951	2.897
74b /AXE 3	H	Me	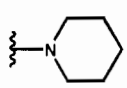	> 20 000	6201	3.456
74c /AXE 5	H	Me	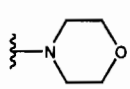	> 20 000	8750	2.1259
74d /AXE 4	H	Me	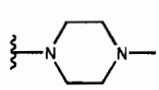	> 20 000	8217	2.6869

Table 5: Biological results of isatin and cyclic amines thiomicarbazones derivatives against Rec-FP-2 and P.f W2.

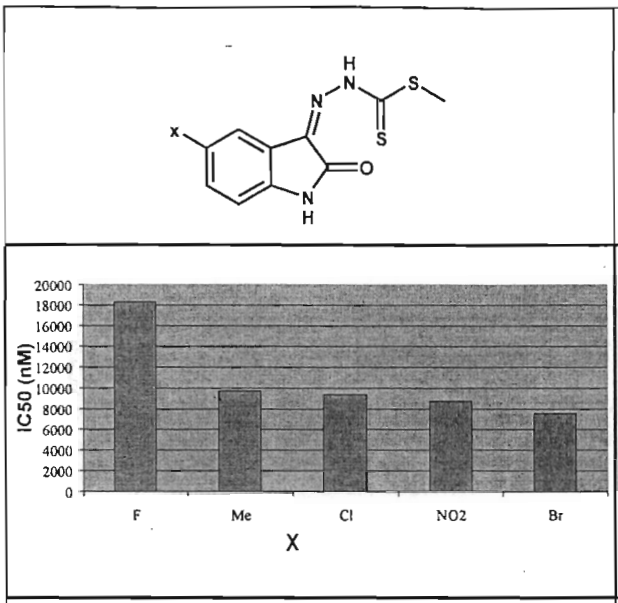

Figure 46: A plot of isatin thiosemicarbazones against Rec-FP2.

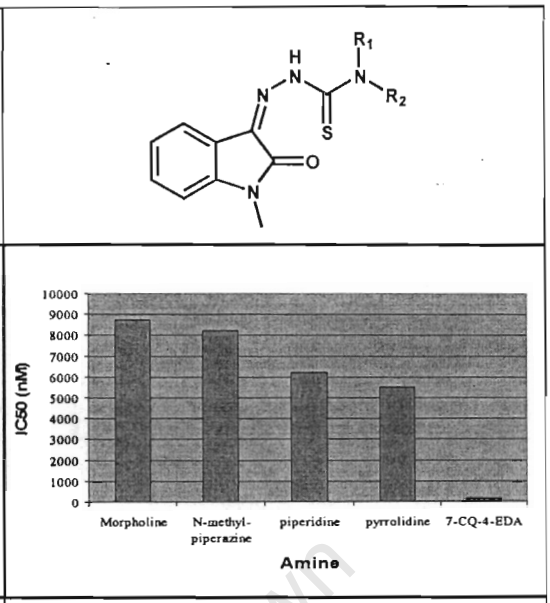

Figure 47: A plot of amino derivatives against P.f. W2.

4.2.2 Biological Results for 4-Aminoquinoline Derivatives 79a to 82f

As expected, introduction of a 4-aminoquinoline unit resulted in more active compounds, relative to simple thioester and *N*1 disubstituted derivatives presented in Table 5. The table below (Table 6) contains results of this series against the enzyme and the parasite respectively.

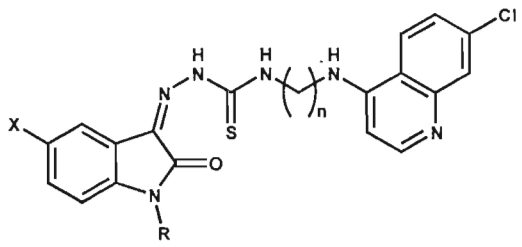

Compound	X	R	n	IC50 (nM)		C log P
				Rec-FP2	P.f. W2	
79a /AXE 6	H	Me	2	> 20 000	172.2	5.778
79b /AXE 13	Br	H	2	3648	163.5	5.71934
81b /AXE 21	Br	H	4	4503	226.8	6.7448
82b /AXE 25	Br	H	6	3417	812.8	7.8028
79c /AXE 14	Cl	H	2	6206	205.8	5.56934
81c /AXE 22	Cl	H	4	5546	205.2	6.5948
82c /AXE 26	Cl	H	6	4606	573.2	7.6528
79d /AXE 15	F	H	2	13780	168.3	4.99934
81d /AXE 23	F	H	4	14120	306.9	6.0248
82d /AXE 27	F	H	6	13210	179.1	7.0828
79e /AXE 18	Me	H	2	5625	180.7	5.35534
81e /AXE 19	Me	H	4	6227	286.1	6.3808
82e /AXE 20	Me	H	6	6117	226.6	7.4388
79f /AXE 16	NO_2	H	2	9266	215.6	4.59934
81f /AXE 24	NO_2	H	4	9836	267.7	5.6248
82f /AXE 28	NO_2	H	6	6332	451.1	6.6828

Table 6: Biological results of 4-aminoquinolines against Rec-FP-2 and P.f. W2.

Within this homologous series of isatin derivatives compounds with a two-carbon methylene spacer, (n = 2), were generally the most active against both the parasite P.f W2 (Figure 48) and the enzyme (Figure 49). With the exception of compound **79a**, all derivatives inhibited the enzyme with IC_{50} values mostly less than 10 μM. Only one compound (**79d**) had an IC_{50} above 10 μM, but even these values are below the cut off of 20 μM. Interestingly, the compound (**79a**) without activity against the enzyme has a methyl substituent at the amide nitrogen atom. This may suggest that within this series of compound methyl substitution at the amide nitrogen is detrimental to activity against the enzyme.

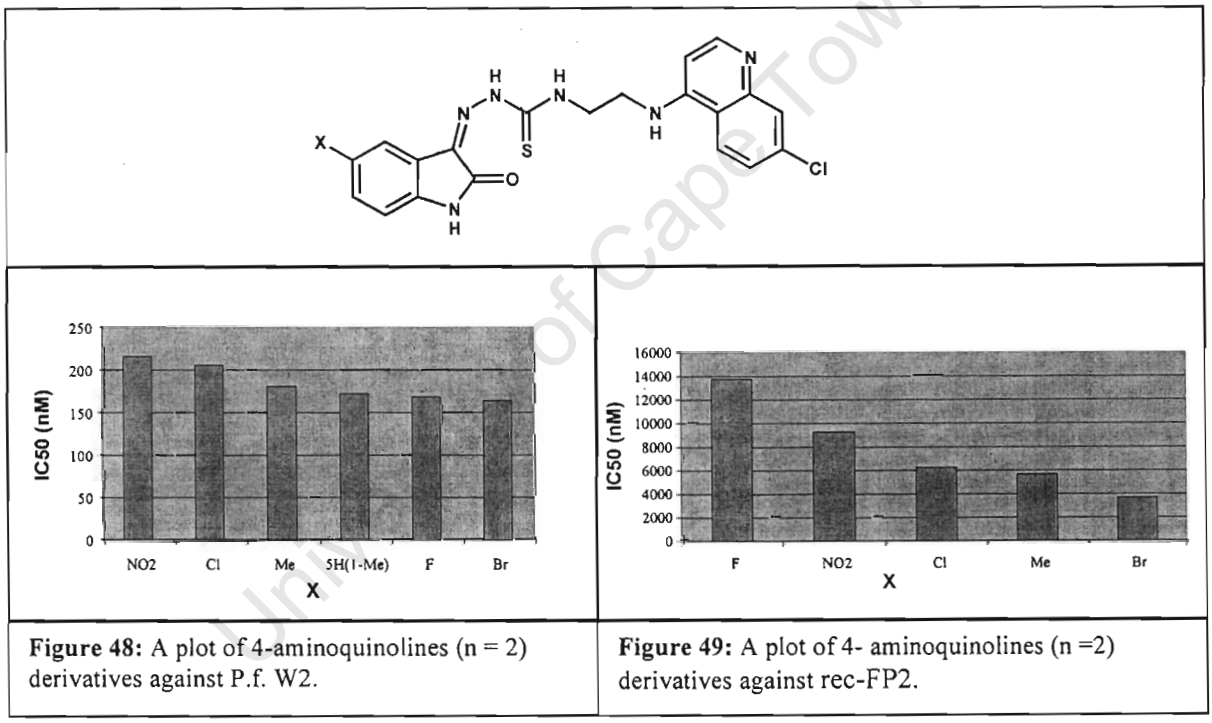

Figure 48: A plot of 4-aminoquinolines (n = 2) derivatives against P.f. W2.

Figure 49: A plot of 4- aminoquinolines (n =2) derivatives against rec-FP2.

As far as substituents (X) on the isatin aromatic ring are concerned for the two-carbon methylene spacers, the size of the halogen substituents is critical for enzyme inhibition. Bromo (X = Br) substituted derivatives were more active against the enzyme on one extreme than the fluoro (X = F) derivatives on the other extreme.

As far as activity against the parasite is concerned, the 4-aminoquinoline unit is apparently the single most important contributor since even derivatives with lower activity (e.g. **79d** with IC_{50} > 10 μM) against the presumed target enzyme showed generally comparable activity to the more active derivatives against P.f. W2. This implies that for the n = 2 series, there is no correlation between the activity of these compounds to inhibit falcipain-2 and their in *vitro* antiparasitic activity.

For the four-carbon methylene spacer, the most active compound against the parasite and the enzyme is **81c** (X = Cl) and **81b** (X = Br) respectively. Compound **81d** is the least active of all in this series against both targets. The order of increasing activity against both targets for the X substituted analogues is roughly F, Me/NO_2, Cl/Br (Figures 50 and 51).

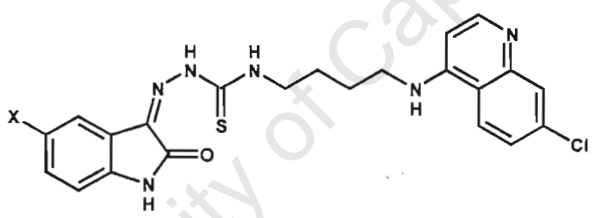

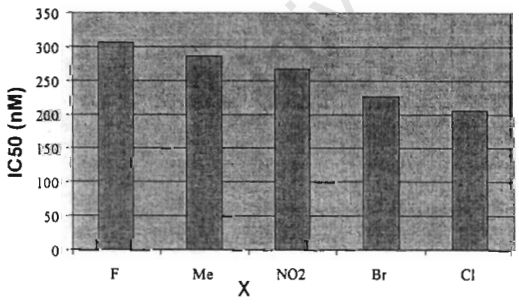

Figure 50: A plot of 4-aminoquinoline (n = 4) derivatives against P.f. W2.

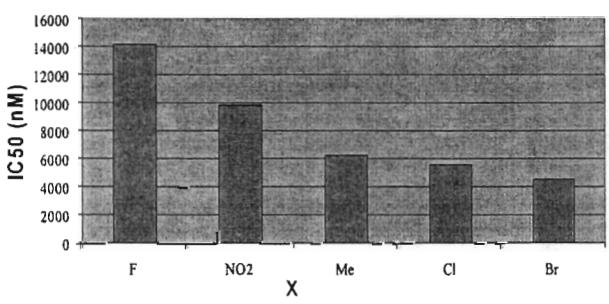

Figure 51: A plot of 4-aminoquinoline (n = 4) derivatives against FP2.

Compounds of the six-carbon methylene spacer series demonstrate a different trend against the parasite and the enzyme. Although the activity of compound **82b** (X = Br) against the enzyme is below 10 μM, it was the least active compound of all against the parasite, Figures 52 and 53.

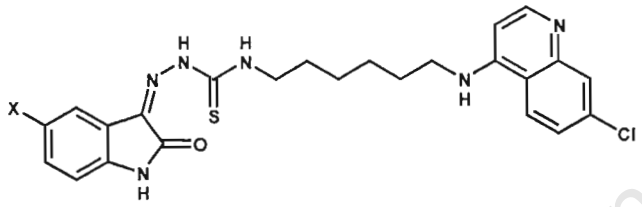

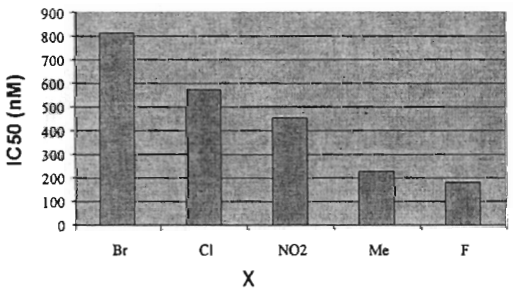

Figure 52: A plot of 4-aminoquinoline (n = 6) derivatives against Pf W2.

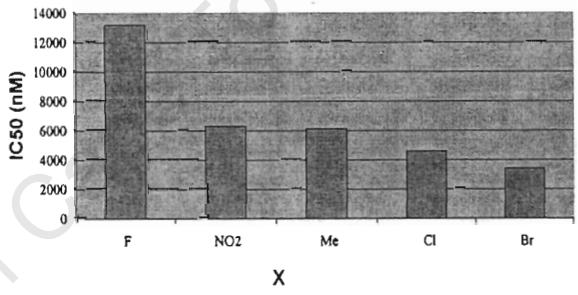

Figure 53: A plot of 4-aminoquinoline (n = 6) derivatives against FP2.

4.2.3 Summary of 4-Aminoquinoline Derivatives 79a to 82f

In summary, the results for the structure relationship studies demonstrate the influence of the substituents (X) with respect to the chain length (n).

Against the parasite, Figure 54 shows an interesting feature by substituents with respect n-carbon methylene spacer. The difference between the most and least active for each chain increases as chain length increases. For substituents Br, Cl and NO_2, the three

analogues have significant decrease in activity as the chain length increases whereas the Me and F show a decrease (from n = 2 to n = 4) and eventually an increase (from n = 4 to n = 6) in activity against the parasite with the chain length.

Against the enzyme (Figure 55) the very same trend is also observed for Br and F as well as NO_2 derivatives showing a decrease (from n = 2 to n = 4) and an increase (from n = 4 to n = 6) in activity. Me derivatives demonstrate a decrease, whereas the Cl derivatives display an increase in activity as the chain length increases.

The F derivatives behave similarly against both the parasite and the enzyme.

The most active compound is **79b** (X=Br, n=2) with an IC_{50} value of 163.5 nM against the parasite. This makes n = 2 the optimum chain length within this limited series of compounds. This compound is even superior to chloroquine whose IC_{50} value in this strain is ~ 300 nM.

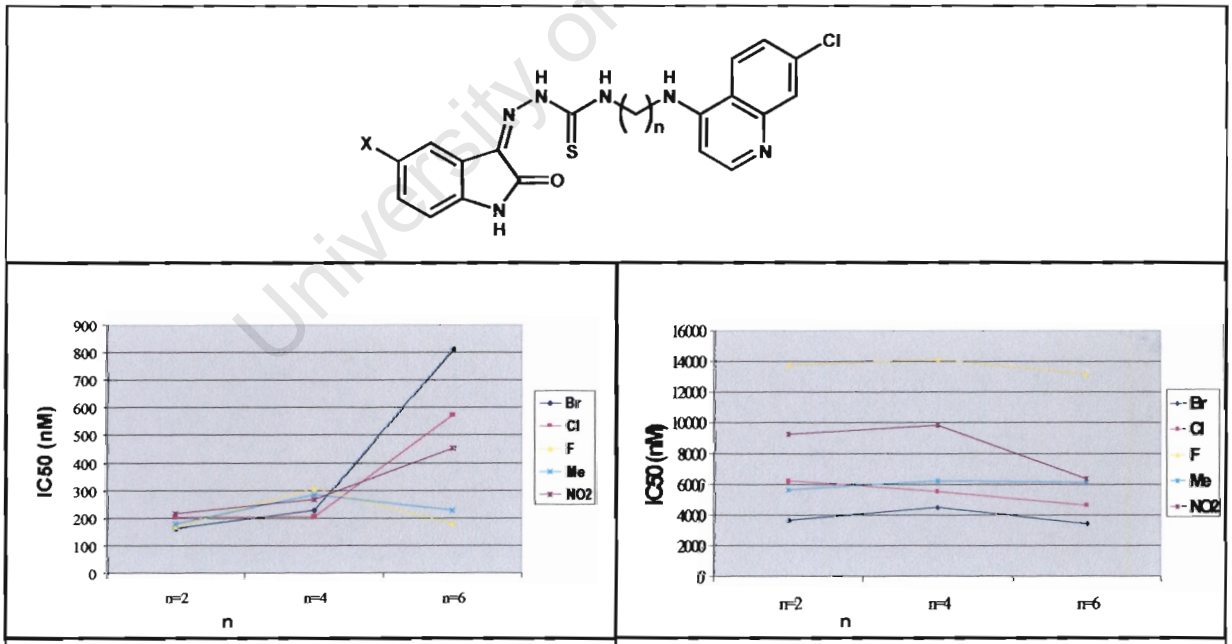

Figure 54: A plot of 4-aminoquinoline (n = 2, 4, and 6) derivatives against P.f.W2.

Figure 55: A plot of 4-aminoquinoline (n = 2, 4, and 6) derivatives against FP2.

4.2.4 Relationship between clogP and Antiplasmodial Activity of 4-Aminoquinoline Derivatives

Figure 56, shows the relationship between *C* logP (partition coefficient) and chain length of 4 aminoquinoline derivatives. *C* logP measures the lipophilicity of a molecule, which is the ability of the molecule to cross cell membranes to reach the site of action. Correlation between the degree of lipophilicity of an iron chelator and its antiplasmodial activity has been demonstrated [98]. For the 4-aminoquinolines, clogP is directly proportional to the chain length (n), as shown in Figure 56. Comparing P.f. W2 activity with clogP for each 4-aminoquinoline derivative (Br, Cl, F, Me, NO_2) a different trend is observed.

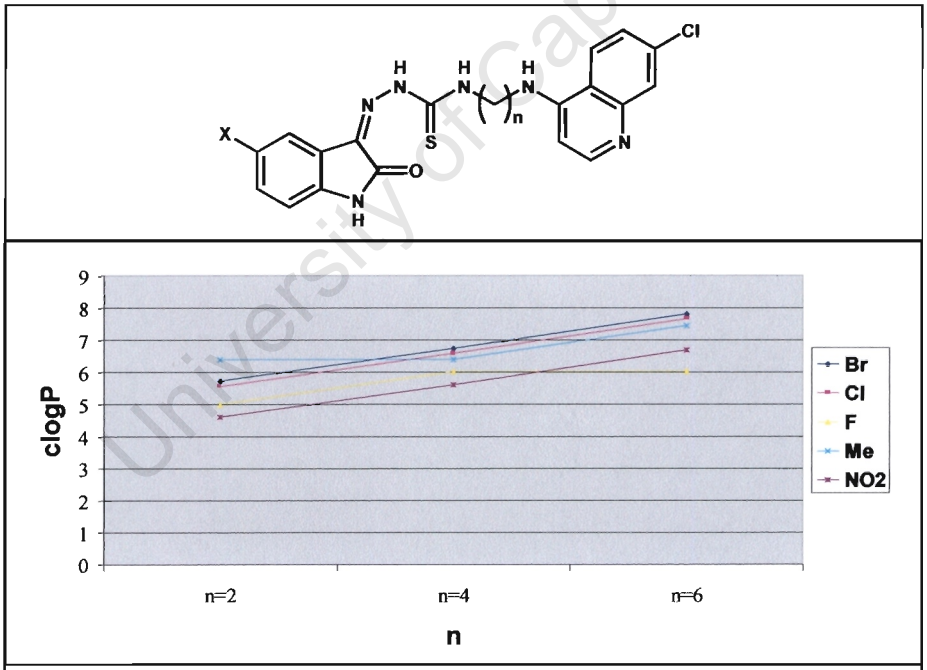

Figure 56: Clog P's of 4-aminoquinoline derivatives.

For Br, Cl and NO_2, the relationship is quite opposite i.e. the P.f W2 activity decreases while clogP increases with the length of the chain. For F and Me the activity decreases (from n = 2 to n = 4) and eventually rise (from n = 4 to n = 6), Figure 55. Overall, all 4-aminoquinolines displayed no correlation between lipophilicity and antiplasmodial activity.

4.2.5 Biological Results for 4-Aminoquinoline β-amino Alcohol.

As discussed before, this compound was designed to incorporate an amino alcohol fragment, which is a known antimalarial bioactiphore. Coupled with the 4-aminoquinoline moiety, this was envisaged to improve the antimalarial activity against P.f. W2. It was hypothesized that maximal antimalarial activity would be obtained through an additive and/or synergistic effect involving the two (amino alcohol and 4-aminoquinoline) well known antimalarial bioactiphores. Compound **89** (Table 9) was indeed found to be substantially more active (IC_{50} P.f. W2 = 19.2 nM) than the corresponding compound **79c** (IC_{50} P.f.W2 = 205.8 nM) without the amino alcohol fragment.

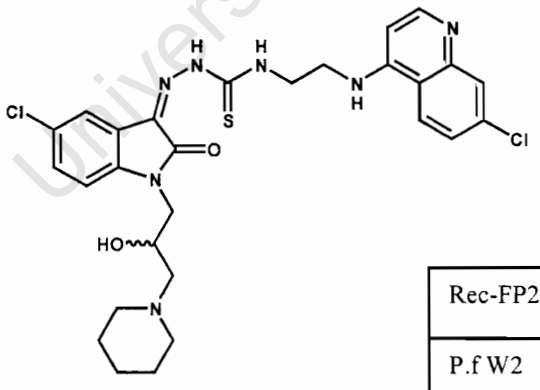

ClogP = 7.18366

Rec-FP2	16750 nM
P.f W2	19.2 nM

Table 9: Biological results for 4-aminoquinolines β-amino alcohol **89**/ AXE 8.

Relative to chloroquine, compound **89** is also substantially more active (IC_{50} for chloroquine in P.f. W2 ~ 300 nM). However, the activity of compound **89** against FP2 was modest (IC_{50} = 16750 nM) suggesting a lack of strong correlation between inhibition of FP2 and antimalarial activity in vitro.

Since compound **89** is a racemate, the antimalarial activities of the respective enantiomers need to be determined. This is in view of the following possibilities:

i) One enantiomer being active and the other has no effect or has some other biological activity.

ii) One enantiomer being more active and the other has very little effect

iii) One enantiomer being more active and the other has an antagonistic effect.

4.3 CONCLUSION

The value of attaching a 4-aminoquinoline moiety has been demonstrated in the structure-activity relationship compounds described in this work. In the homologous series, the compound (**79b**) with a two-carbon methylene spacer was found to be the most active with an IC_{50} value of 163.5 nM against both the parasite and second most active against the enzyme (IC_{50} = 3648 nM). The missing chain lengths (n = 3 or n = 5) need to be explored before the optimum chain length is decided upon.

The most active compound for the four-carbon methylene spacer, against the parasite and the enzyme is **81c** (X = Cl) and **81b** (X = Br) respectively. The order of increasing activity against both targets for the X substituted analogues was found to be roughly F, Me/NO_2, Cl/Br.

Although the activity of compound **82b** (X = Br) in six-carbon spacer is below 10 μM, it was the least active compound of all against the parasite. However, **82b** was the most active against the enzyme for all spacers within this limited series. Thus the bromo substituent is optimum especially against the enzyme.

The structure activity relationship studies designed in this project have indicated a significant effect that the chain length and substituents have on the biological activity of these derivatives. The results from structure activity relationship studies show that the substituents have a different influence with respect to the chain length. Chain length is important when it comes to the lipophilicity of a molecule. Unfortunately all 4-aminoquinolines displayed no correlation between lipophilicity and antiplasmodial activity.

Amino alcohol compound **89** was very active against the chloroquine resistant strain of the parasite. This is a significant result, which if confirmed in *vivo*, should result in a more promising novel series of 4-aminoquinoline β-amino alcohol derivatives.

4.4 FUTURE STUDIES

The biological results of the 4-aminoquinoline derivatives showing the effect of substituents and chain length should be used for further design of the new derivatives. 4-Aminoquinolines with an amino alcohol feature must be explored further but taking these substituents with their respective chain lengths into account. For example, coupled with the features of **79b** (X = Br and n = 2) a more active compound against the parasite and the enzyme may be found. In addition, further testing must be carried out against other enzyme target/s and various parasite strains with varying degrees of sensitivity and resistance to chloroquine and related quinoline drugs. Furthermore, the toxicity of these compounds in mammalian cell lines as well as the *in vivo* potency of selected compounds should be investigated.

CHAPTER 5

EXPERIMENTAL

^{1}H NMR spectra were determined in $CDCl_3$, CD_3OD or $(CD_3)_2SO$ solution on a Varian Gemini (300 MHz) or a Varian Unity Spectrometer (400 MHz), using TMS as an internal standard. The chemical shift (δ) is given in ppm relative to TMS (δ = 0.00). The coupling constant J is given in Hz. Some of the **NH** peaks were not revealed due to Deuterium exchange with DMSO-d_6

^{13}C NMR spectra were recorded on the same instruments at 75 MHz or 100 MHz in the same deuterated solvents using TMS as an internal inference. ^{13}C NMR peaks were assigned for all compounds.

Mass spectra was run from different places using the following different techniques:

From Potchestroom University, SA

FAB Mass spectra:

Micromass 70-70E double focussing magnetic sector mass spectrometer fitted with an Ion Tech B11N saddle field FAB gun (Ion Tech Ltd, Teddington, UK) and a VG11-250J data system.

The mass spectrometer was run at 6kV and the magnetic analyser scanned at a rate of 5 sec per decade over a mass range 1000 - 80 Da Xenon was used as bombardment gas at 1mA 8kV Nitrobenzyl alcohol was used as matrix (solvent). Samples were run at room temperature.

From the University of Witswatersrand, SA

EI Mass spectra:

Micromass Autospec-TOF double focussing magnetic sector mass spectrometer. All samples were run under the following operating conditions; electron energy 70eV, filament emission current 100uA, source temperature 200 °C, accelerating voltage 8kV. The magnet was scanned at a rate of 2 sec per decade (800 - 20 Da). Samples were introduced into the ion source using the standard heatable/coolable probe and heated in the range 50 - 250 °C. System fitted with Micromass OPUS data system for aquisition and acquiring of results.

Melting points were determined using a Reichert-Jung hot stage apparatus and are uncorrected

Infrared (IR) spectra were recorded in $CDCl_3$ on a satellite FTIR spectrometer, as this couldn't be possible with DMSO as in NMR.

Microanalyses were performed on a Fisons EA 1108 CHNS-O instrument.

Reactions were monitored by thin layer chromatography (tlc) using Merck F254 silica gel plates and visualized with uv light.

Column chromatography and preparative layer chromatography (plc) were performed using Merck Kieselgel 60.

Materials such as dry solvents used in reactions were purchased from commercial suppliers and used without further purification unless otherwise stated.

Numbering system used in here is not formal but for the sake of identification.

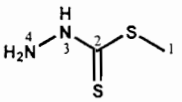

Hydrazinecarbodithioic acid methyl ester **(71)**. To an ice cooled solution of KOH (19.80 g, 0.3000 mol) in 24 ml of water and 20 ml of 2-propanol was added 98 % hydrazine hydrate (17.10 ml, 0.5490 mol). Ice-cooled carbon sulphide (18.20 ml, 0.3000 mol) was added dropwise over 2 h while maintaining the temperature of the solution below 10 °C. After the addition of ice-cooled iodomethane (18.70 ml, 0.3000 mol) over 2 h, the bright yellow mixture was stirred for an additional 1hour. The yellow colour diminished and the mixture gradually became white after iodomethane addition. Stirring was continued for an additional 90 min and the white precipitate formed was filtered. The crude product was re-crystallised from dichloromethane to give (17.60 g, 48 %) of **1** as white crystals. δ_H (300 MHz, $CDCl_3$) 2.63 (3H, s, H1), 5.44 (2H, br, H4), 9.45 (1H, br, H3); δ_C (75 MHz, DMSO-d_6) 17.5 (C1), 202.30 (C2).

GP 1: General procedure for the synthesis of amines **76a – d.**
A mixture of 4,7-dichloroquinoline (6.7500 g, 0.0341 mol), diamine (20 eq), triethylamine (0.3 eq) and potassium carbonate (0.3 eq) was stirred under reflux at 140 °C for 5 hours. The reaction mixture was then cooled and excess amine was evaporated under reduced pressure. Sodium hydroxide (150 ml), 1.0 M was added to the mixture. The resulting mixture was extracted using hot ethyl acetate (2 × 200 ml). The product was concentrated on a rotary evaporator and dried under high vacuum pump to yield the appropriate amine.

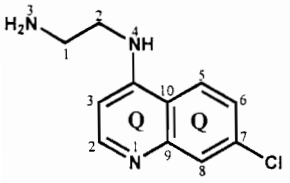

N^1-(7-Chloro-quinolin-4-yl)-ethane-1,2-diamine **(76a)**. Synthesised as per **GP 1** to give white crystals (6.7183g, 89 %). δ_H (300 MHz, DMSO-d_6) 3.01 (2H, t, *J* 6.6 Hz, H1), 3.47 (2H, t, *J* 6.6 Hz, H2), 6.56 (1H, d, *J* 6.0 Hz, H3Q), 7.24 (1H, br, H4) 7.39 (1H, dd, *J* 2.1 and 9.2 Hz, H6Q), 7.77 (1H, d, *J* 2.1 Hz, HQ8), 8.10 (1H, d, *J* 9.2 Hz, H5Q), 8.35 (1H, d, *J* 6.0 Hz, H2Q); δ_C (75 MHz, DMSO-d_6) 44.5 (C1), 45.3 (C2), 98.6

(C3Q), 117.4 (C10Q), 123.9 (C5Q), 123.9 (C6Q), 127.4 (C8Q), 133.3 (C7Q), 149.0 (C9Q), 150.2 (C4Q), 151.8 (C2Q).

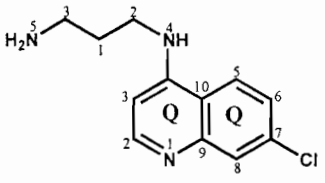

N^1-(7-Chloro-quinolin-4-yl)-propane-1,3-diamine **(76b)**. Synthesised as per **GP 1** to give yellow crystals (6.4113g, 80 %). δ_H (300 MHz, DMSO-d_6) 1.17 (2H, quint, *J* 6.9 Hz, H1), 2.70 (2H, t, *J* 6.6 Hz, H3), 3.31 (2H, t, *J* 6.9 Hz, H2), 6.45 (1H, d, *J* 5.3 Hz, H3Q), 7.42 (1H, dd, *J* 2.3 and 9.3 Hz, H6Q), 7.53 (1H, br, H4), 7.78 (1H, d, *J* 2.3 Hz, H8Q), 8.22 (1H, d, *J* 9.3 Hz, H5Q), 8.38 (1H, d, *J* 5.3 Hz, H2Q); δ_C (75 MHz, DMSO-d_6) 31.1 (C1), 38.7 (C2), 39.0 (C3), 98.5 (C3Q), 117.4 (C10Q), 123.9 (C5Q), 124.0 (C6Q), 127.4 (C8Q), 133.3 (C7Q), 149.0 (C9Q), 150.1 (C4Q), 151.9 (C2Q).

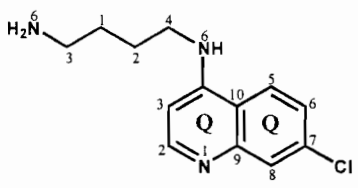

N^1-(7-Chloro-quinolin-4-yl)-butane-1,4-diamine **(76c)**. Synthesised as per **GP 1** yellow crystals (7.8119g, 92 %). δ_H (300 MHz, DMSO-d_6) 1.47 (2H, quint, *J* 6.9 Hz, H1), 1.68 (2H, quint, *J* 7.2 Hz, H2), 2.59 (2H, t, *J* 6.3 Hz, H3), 3.24 (2H, t, *J* 7.5 Hz, H4), 6.44 (1H, d, *J* 5.4 Hz, H3Q), 7.36 (1H, br, H6), 7.42 (1H, dd, *J* 2.1 and 8.9 Hz, H6Q), 7.77 (1H, d, *J* 2.1 Hz, H8Q), 8.27 (1H, d, *J* 8.9 Hz, H5Q), 8.39 (1H, d, *J* 5.4 Hz, H2Q); δ_C (75 MHz, DMSO-d_6) 25.3 (C1), 30.5 (C2), 41.2 (C3), 42.3 (C4), 98.6 (C3Q), 117.5 (C10Q), 123.9 (C5Q), 124.1 (C6Q), 127.4 (C8Q), 133.3 (C7Q), 149.1 (C9Q), 150.1 (C4Q), 151.9 (C2Q).

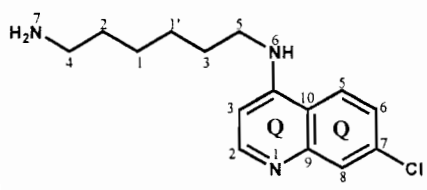

N^1-(7-Chloro-quinolin-4-yl)-hexane-1,6-diamine **(76d)**. Synthesised as per **GP 1** to give yellow crystals (8.9726g, 95 %). δ_H (300 MHz, DMSO-d_6) 1.32 (6H, m, H1+H1'+H2), 1.63 (2H, m, H3), 3.12 (4H, br, H4 + H5), 6.40 (1H, d, *J* 5.2 Hz, H3Q), 7.26 (1H, br, H6), 7.40 (1H, dd, *J* 2.0 and 9.0 Hz,

H6Q), 7.76 (1H, d, *J* 2.0 Hz, H8Q), 8.27 (1H, d, *J* 9.0 Hz, H5Q), 8.36 (1H, d, *J* 5.2 Hz, H2Q); δ_C (75 MHz, DMSO-d_6) 26.1 (C1), 26.5 (C1'), 27.8 (C2), 33.47 (C3), 41.7 (C4), 42.33 (C5), 98.5 (C3Q), 117.42 (C10Q), 123.9 (C5Q), 124.1 (C6Q), 127.4 (C8Q), 133.3 (C7Q), 149.1 (C9Q), 150.1 (C4Q), 151.8 (C2Q).

GP 2: General procedure for the synthesis of compounds **73** and **78a – e.**
The appropriate isatin (24.8201 mmol) and **71** (2eq) were mixed in 50 ml of ethanol in the presence of a catalytic (0.03 mmol) amount of acetic acid. The mixture was refluxed for 60 minutes and then allowed to cool, after which the desired intermediate was isolated.

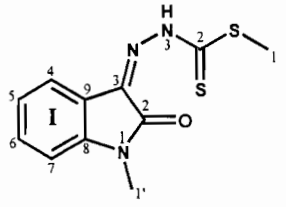

***N'-(1-Methyl-2-oxo-1,2-dihydro-indol-3-ylidene)-hydrazinecarbodithioic acid methyl ester* (73).** Synthesised as per GP 2 to give yellow crystals (6.0545g, 92 %), mp 171-173 °C. IR ($CHCl_3$) ν_{max}/cm^{-1} 1459 (Ar C=C), 1627 (C_2=S); 1639 (C_{3I}=N), 1674 (C_{2I}=O); δ_H (300 MHz, $CDCl_3$) 2.67 (3H, s, H1), 3.27 (3H, s, H1'), 6.83-7.71 (4H, m, ArH), 13.82 (1H, s, H3); δ_C (75 MHz, $CDCl_3$) 17.6 (C1), 25.7 (C1'), 109.1 (C7I), 119.4 (C5I), 119.4 (C9I), 121.3 (C4I), 123.4 (C6I), 131.6 (C8I), 144.0 (C3I), 160.6 (C2I), 202.2 (C2); HRMS (IE) Found *m/z* 265.034302 $[M+1]^+$ $C_{11}H_{11}N_3S_2O$ requires 265.034356; Found: C 49.91 %, H 4.13 %, N 15.9 % S 23.86; Anal. Calcd: C 49.79 % H 4.18 %, N 15.86 %, S 24.17 %.

GP 3: General procedure for the synthesis of **74a-d**.
A mixture of an appropriate intermediate (0.7537 mmol) and amine (4 eq) in 20 ml of methanol was stirred at room temperature for 24 hours to give a yellow/orange precipitate. The resultant precipitate was filtered and dried under high vacuum to give yellow/orange crystals, which were re-crystallised from methanol to yield the desired product.

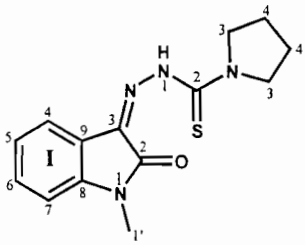

***Pyrrolidine-1-carbothioic acid, (1-methyl-2-oxo-1, 2-dihydro-idol-3-ylidene) –hydrazide* (74a).** Synthesised as per **GP 3** to give yellow crystals (0.1130g, 52 %), mp 239-241 °C. IR ($CHCl_3$) ν_{max}/cm^{-1} 1459 (Ar C=C), 1579 (C_2=S); 1639 (C_{3I}=N), 1674 (C_{2I}=O); δ_H (300 MHz, $CDCl_3$), 2.05 (4H, br m, H4), 3.28 (3H, s, H1'I), 3.86 (4H, br m, H3), 6.84-7.88 (4H, m, ArH), 13.48 (1H, s, H1); δ_C (75 MHz, $CDCl_3$) 24.0 (2×C4), 25.6 (C1'I), 30.1 (2×C3), 108.8 (C7I), 120.1 (C9I), 121.4 (C5I), 123.3 (C6I), 130.5 (C4I), 134.1 (C8I), 141.1 (C3I), 142.9 (C2I), 162.5 (C2).

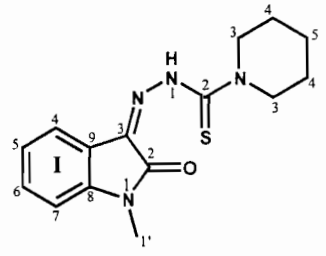

***Piperadine-1-carbothioic acid (1-methyl-2-oxo-1, 2-dihydro-indol-3-ylidene)-hydrazide* (74b).** Synthesised as per **GP 3** to give orange crystals (0.1504g, 66 %), mp 160-165 °C. IR ($CHCl_3$) ν_{max}/cm^{-1} 1459 (Ar C=C), 1579 (C_2=S); 1639 (C_{3I}=N), 1674 (C_{2I}=O); δ_H (300 MHz, $CDCl_3$) 1.68 (2H, quint, *J* 5.4 Hz, H5), 1.85 (4H, quint, *J* 5.7 Hz, H4), 3.27 (3H, s, H1'I), 3.09 (4H, t, *J* 5.7 Hz, H3), 6.81-8.43 (4H, m, ArH); δ_C (75 MHz, $CDCl_3$), 18.0 (C5I), 22.8 (2×C4), 26.1 (C1'I), 44.00 (2×C3), 108.1 (C7I), 117.6 (C9I), 123.4 (C5I), 127.7 (C6), 130.0 (C4I), 134.0 (C8I), 141.8 (C3I), 142.7 (C2I), 162.6 (C2). HRMS (IE) Found *m/z* 302.12246 $[M+1]^+$ $C_{15}H_{18}N_4SO$ requires 302.12013

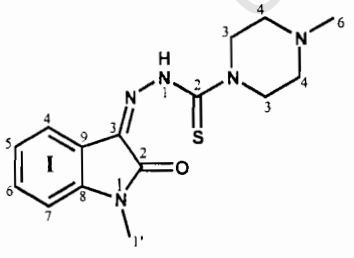

4-*Methyl-piperazine-1-carbothioic acid, (1-methyl-2-oxo-1, 2-dihydro-indol-3-ylidene)-hydrazide* (74d). Synthesised as per **GP 3** to give orange crystals (0.1340g, 56 %), mp 174-176 °C. IR ($CHCl_3$) ν_{max}/cm^{-1} 1459 (Ar C=C), 1579 (C_2=S); 1639 (C_{3I}=N), 1674 (C_{2I}=O); δ_H (300 MHz, $CDCl_3$) 2.34 (3H, s, H6), 2.55 (4H, t, *J* 5.1, H4), 3.27 (3H, s, H1'I), 4.08 (4H, t, *J* 5.1, H3), 6.80-7.74 (4H, m, ArH), 13.39 (1H, s, H1); δ_C (75 MHz, $CDCl_3$) 25.7 (C1'I), 45.7 (C6), 49.7

(2×C3), 54.5 (2×C4), 108.9 (C7I), 119.8 (C9I), 121.1 (C5I), 123.4 (C6I), 130.8 (C4I), 133.8 (C8I), 140.9 (C3I), 142.9 (C2I), 161.5 (C2).

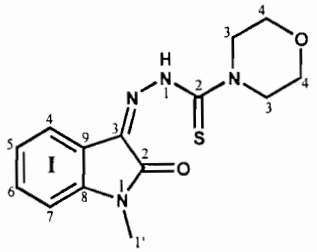

***Morpholine-4-carbothioic acid, (1-methyl-2-oxo-1,2-dihydro-1ndol-3-ylidene)-hydrazide* (74c).** Synthesised as per **GP 3** to give yellow crystals (0.1652g, 72 %), mp 164-165°C. IR ($CHCl_3$) ν_{max}/cm^{-1} 1459 (Ar C=C), 1579 (C_2=S); 1639 (C_{3I}=N), 1674 (C_{2I}=O); δ_H (300 MHz, $CDCl_3$) 3.27 (3H, s, H1'I), 3.82 (4H, t, *J* 4.2 Hz, H4), 4.07 (4H, t, *J* 5.1 Hz, H3), 6.80 (4H, m, ArH), 13.40 (1H, s, H1); δ_C (75 MHz, $CDCl_3$) 25.8 (C1'I), 50.2 (2×C3), 66.3 (2×C4), 108.9 (C7I), 119.9 (C9I), 121.1 (C5I), 123.3 (C6I), 130.9 (C4I), 134.3 (C8I), 141.0 (C3I), 142.2 (C2I), 162.5 (C2).

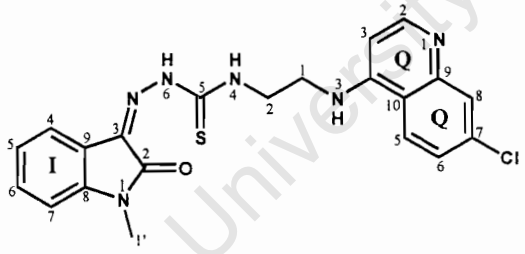

***4-(7-Chloro-quinolin-4-yl)-ethane-1,2-diamine-1-carbothioic acid (1-methyl-2-oxo-2-dihydro-indol-3-ylidene)-hydrazide* (79a).** Synthesised as per **GP 3** to give yellow crystals (0.3077g, 93 %), mp 155-156 °C. IR ($CHCl_3$) ν_{max}/cm^{-1} 1459 (Ar C=C), 1579 (Ar C=N), 1605 (C_5=S), 1639 (C_{3I}=N), 1674 (C_{2I}=O); δ_H (300 MHz, DMSO-d_6) 3.22 (3H, s, H1'I), 3.60 (2H, m, H1), 3.92 (2H, m, H2), 6.75 -8.38 (9H, m, Ar), 7.46 (1H, br, H3), 9.46 (1H, br, H4), 12.44 (1H, br s, H6); δ_C (75 MHz, DMSO-d_6) 26.4 (C1'I), 41.9 (C1), 43.1 (C2), 99.6 (C3Q), 108.1 (C10Q), 116.6 (C7I), 117.1 (C5Q), 117.9 (C9I), 118.1 (C5I), 122.2 (C6Q), 123.1 (C8Q), 126.0 (C4I), 128.0 (C6I), 130.0 (C7Q), 133.2 (C8I), 142.3 (C9Q), 143.0 (C2Q), 149.3 (C4Q), 150.3 (C3I), 152.0 (C2I), 166.6 (C5); HRMS (FAB) Found *m/z* 439.111225 $[M+1]^+$ $C_{21}H_{20}N_6SOCl$ requires 439.110784.

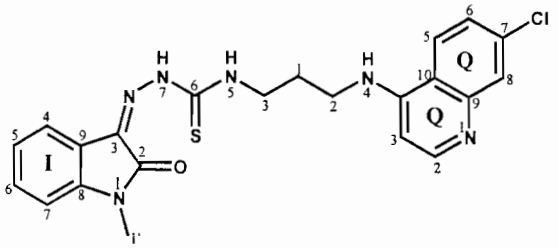

4-(7-Chloro-quinolin-4-yl)-propane-1,3-diamine-1-carbothioic acid (1-methyl-2-oxo-1,2-dihydro-indol-3-ylidene)-hydrazide **(80a)**. Synthesised as per **GP 3** to give orange crystals (0.2800g, 82 %), mp 146-149 °C. IR ($CHCl_3$) ν_{max}/cm^{-1} 1459 (Ar C=C), 1579 (Ar C=N), 1605 (C_6=S), 1639 (C_{3I}=N), 1674 (C_{2I}=O); δ_H (400 MHz, DMSO-d_6) 1.93 (2H, quint, *J* 7.2 Hz, H1), 2.95 (2H, t, *J* 7.6 Hz, H2), 3.15 (3H, s, H1'I), 3.34 (2H, t, *J* 6.8 Hz, H3), 6.48 (1H, d, *J* 5.5 Hz, H3Q), 6.94 (1H, dd, *J* 2.0 and 7.6 Hz, H6Q), 6.98 (1H, td, *J* 0.8 and J 7.6 Hz, H5I), 7.25 (1H, td, *J* 2.0 and 7.6 Hz, H6I), 7.43 (1H, dd, *J* 2.0 and 7.6 Hz, H4I), 7.77 (1H, d, *J* 2.0 Hz, H8Q), 8.21 (1H, dd, *J* 0.8 and 7.6 Hz, H7I), 8.26 (1H, d, *J* 7.6 Hz, H5Q), 8.37 (1H, d, *J* 5.5 Hz, H2Q); δ_C (100 MHz, DMSO-d_6) 17.3 (C1'I), 25.7 (C1), 25.9 (C3), 37.1 (C2), 98.6 (C3Q), 108.0 (C10Q), 116.8 (C7I), 116.9 (C5Q), 117.5 (C9I), 117.5 (C5I), 122.0 (C6Q), 123.3 (C8Q), 125.9 (C4I), 127.8 (C6I), 129.2 (C7Q), 132.9 (C8I), 142.6 (C9Q), 142.6 (C2Q), 149.5 (C4Q), 150.1 (C3I), 151.6 (C2I), 166.4 (C6)

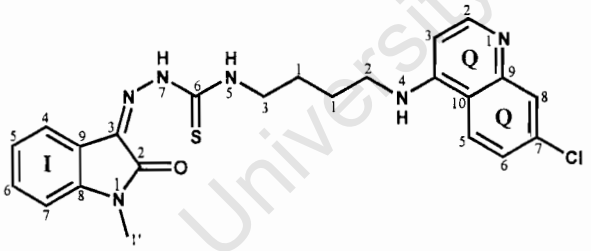

4-(7-Chloro-quinolin-4-yl)-butane-1,4-diamine-1-carbothioic acid (1-methyl-2-oxo-1,2-dihydro-indol-3-ylidene)-hydrazide **(81a)**. Synthesised as per **GP 3** to give yellow crystals (0.3203g, 91 %), mp 164-167; IR ($CHCl_3$) ν_{max}/cm^{-1} 1459 (Ar C=C), 1579 (Ar C=N), 1605 (C_6=S), 1639 (C_{3I}=N), 1674 (C_{2I}=O); δ_H (400 MHz, DMSO-d_6) 1.67 (4H, m, H1), 2.84 (2H, t, *J* 7.2 Hz, H2), 3.15 (3H, s, H1'I), 3.28 (2H, t, *J* 6.4 Hz, H3), 6.46 (1H, d, *J* 5.6 Hz, H3Q), 6.94 (1H, dd, *J* 2.4 and 7.6 Hz, H6Q), 6.98 (1H, td, *J* 2.0 and *J* 7.6 Hz, H5I), 7.24 (1H, td, *J* 2.2 and 7.6 Hz, H6I), 7.42 (1H, dd, J 2.2 and 7.6 Hz, H4I), 7.76 (1H, d, *J* 2.4 Hz, H8Q), 8.23 (1H, dd, *J* 2.0 and 7.6 Hz, H7I), 8.26 (1H, d, *J* 7.6 Hz, H5Q) 8.37 (1H, d, *J* 5.6 Hz, H2Q); δ_C (100 MHz, DMSO-d_6) 17.4 (C1'I), 24.8 (2×C1), 25.7 (C2), 25.8 (C3), 98.7 (C3Q), 108.0 (C10Q), 117.0 (C7I), 117.0 (C5Q), 117.3 (C9I), 117.4

(C5I), 121.2 (C6Q), 123.2 (C8Q), 125.7 (C4I), 127.9 (C6I), 129.4 (C7Q), 132.8 (C8I), 142.8 (C9Q), 142.8 (C2Q), 149.7 (C4Q), 150.0 (C3I), 152.0 (C2I), 166.6 (C6).

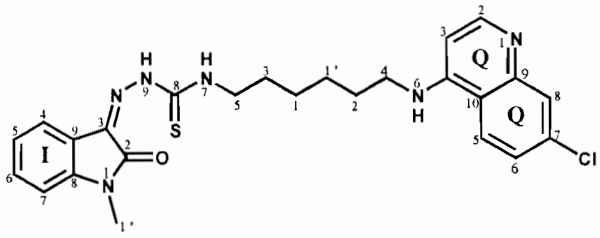

4-(7-Chloro-quinolin-4-yl)-hexane-1,6-diamine-1-carbothioic acid (1-methyl-2-oxo-1,2-dihydro-indol-3-ylidene)-hydrazide **(82a)** Synthesised as per **GP 3** to give orange crystals (0.3545g, 95 %), mp 174-176 °C. IR ($CHCl_3$) ν_{max}/cm^{-1} 1459 (Ar C=C), 1579 (Ar C=N), 1605 (C_8=S), 1639 (C_{3I}=N), 1674 (C_{2I}=O); δ_H (400 MHz, DMSO-d_6) 1.36 (4H, m, H1+H1'), 1.54 (2H, quint, *J* 7.6 Hz, H2), 1.630 (2H, quint, *J* 6.8, H3), 2.79 (2H, t, *J* 7.6 Hz, H4), 3.17 (3H, s, H1'I), 3.23 (2H, t, *J* 6 Hz, H5), 6.42 (1H, d, *J* 5.6 Hz, H3Q), 6.94 (1H, dd, *J* 2.0 and 7.6 Hz, H6Q), 6.98 (1H, td, *J* 0.8 and J 7.6 Hz, H5I), 7.24 (1H, td, *J* 2.1 and 7.6 Hz, H6I), 7.41 (1H, dd, *J* 2.1 and 7.6 Hz, H4I), 7.55 (1H, d, *J* 2.0 Hz, H8Q), 8.24 (1H, dd, *J* 0.8 and 7.6 Hz, H7I), 8.27 (1H, d, *J* 7.6 Hz, H5Q), 8.36 (1H, d, *J* 5.6 Hz, H2Q); δ_C (100 MHz, DMSO-d_6) 17.4 (C1'I), 25.7 (C1'), 25.8 (C1), 26.1 (C2), 26.5 (C3), 27.1 (C4), 27.6 (C5), 98.6 (C3Q), 108.1 (C10Q), 117.4 (C7I + C5Q), 117.5 (C9I), 117.5 (C5I), 121.9 (C6Q), 124.1 (C8Q), 126.2 (C4I), 127.5 (C6I), 129.2 (C7Q), 133.4 (C8I), 142.6 (C9Q), 142.6 (C2Q), 149.6 (C4Q), 150.0 (C3I), 151.8 (C2I), 166.5 (C6).

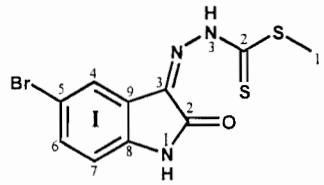

N-(5-Bromo-2-oxo-1,2-dihydro-indol-3-ylidene)-hydrazinecarbodithioic acid methyl ester **(78a).** Synthesised as per **GP 2** to give yellow crystals (2.3667g, 81 %), mp 257-259°C. IR ($CHCl_3$) ν_{max}/cm^{-1} 1459 (Ar C=C), 1627 (C_2=S); 1639 (C_{3I}=N), 1674 (C_{2I}=O); δ_H (400MHz, DMSO-d_6) 2.63 (3H, s, H1), 6.90 (1H, d, *J* 8.4, H7I), 7.55 (1H, dd, *J* 2.2 and 8.4, H6I), 7.60 (1H, d, *J* 2.2 Hz, H4I), 11.32 (1H, s, H3), 13.83 (1H, s, H1I); δ_C (100 MHz, $CDCl_3$) 17.9 (C1), 112.1 (C7I), 114.1 (C5I), 119.1

(C9I), 126.2 (C4I), 130.8 (C6I), 135.1 (C8I), 143.0 (C3I), 162.7 (C2I), 202.4 (C2); HRMS (IE) Found *m/z* 328.929189 $[M+1]^+$ $C_{10}H_8N_3S_2OBr$ requires 328.929217

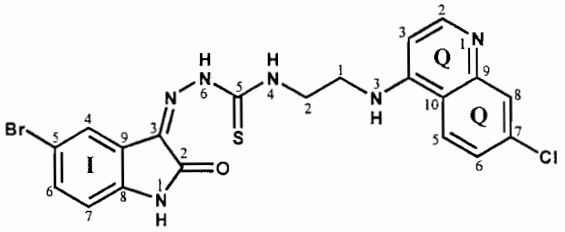

4-(7-Chloro-quinolin-4-yl)-ethane-1,2-diamine-1-carbothioic acid (5-bromo-2-oxo-1,2-dihydro-indol-3-ylidene)-hydrazide **(79b)**. Synthesised as per **GP 3** to give red crystals (0.2837g, 93 %), mp 220-223 °C. IR ($CHCl_3$) ν_{max}/cm^{-1} 1459 (Ar C=C), 1579 (Ar C=N), 1605 (C_5=S), 1639 (C_{3I}=N), 1674 (C_{2I}=O); δ_H (400MHz, DMSO-d_6) 3.12 (2H, t, *J* 6.4 Hz, H1), 3.58 (2H, t, *J* 6.4 Hz, H2), 6.63 (1H, d, *J* 5.6 Hz, H3Q), 6.73 (1H, d, *J* 8.4 Hz, H7I), 6.90 (1H, dd, *J* 2.0 and 8.4 Hz, H6I), 7.30 (1H, dd, *J* 1.8 and 8.6 Hz, H6Q), 7.55 (1H, br, H3) 7.57 (1H, br, H4) 7.60 (1H, d, *J* 2.0 Hz, H4I), 7.80 (1H, d, *J* 1.8 Hz, H8Q), 8.22 (1H, d, *J* 8.6 Hz, H5Q), 8.48 (1H, d, *J* 5.6, H2Q), 8.34 (1H, s, H6), 10.45 (1H, s, H1I); δ_C (100 MHz, DMSO-d_6) 38.1 (C1), 39.0 (C2), 111.6 (C3Q), 114 (C10Q), 117.8 (C5I), 120.5 (C5Q), 122.2 (C7I), 123.9 (C9I), 125.1 (C6Q), 125.6 (C8Q), 126.4 (C4I), 128.7 (C6I), 133.5 (C7Q), 138 (C8I), 149.9 (C9Q), 151.1 (C4Q), 152.7 (C2Q), 155.8 (C3I), 162.8 (C2I), 167.5 (C5); HRMS (FAB) Found *m/z* 504.014688 $[M+1]^+$ $C_{20}H_{18}N_6SOBrCl$ requires 504.013470.

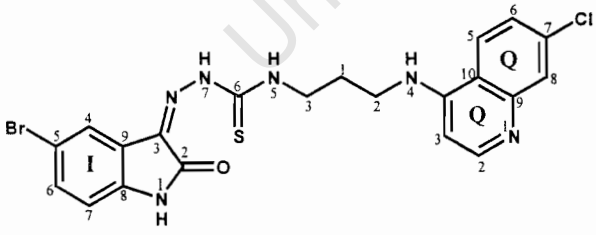

4-(7-Chloro-quinolin-4-yl)-propane-1,3-diamine-1-carbothioic acid (5-bromol-2-oxo-1,2-dihydro-indol-3-ylidene)-hydrazide **(80b)**. Synthesised as per **GP 3** to give yellow crystals (0.2634g, 84 %), mp 167-170 °C. IR ($CHCl_3$) ν_{max}/cm^{-1} 1459 (Ar C=C), 1579 (Ar C=N), 1605 (C_6=S), 1639 (C_{3I}=N), 1674 (C_{2I}=O); δ_H (400 MHz, DMSO-d_6) 1.90 (2H, quint, *J* 7.2 Hz, H1) 2.90 (2H, t, *J* 7.6 Hz, H2), 3.32 (2H, t, *J* 6.8 Hz, H3) 6.47 (1H, d, *J* 5.6 Hz, H3Q) 6.79 (1H, d, *J* 8.4 Hz, H7I) 7.34 (1H, dd, *J* 1.8 and 8.4 Hz, H6I) 7.37 (1H, dd, *J* 2.0 and 9.2 Hz, H6Q) 7.73 (1H, d, *J* 1.8 Hz, H4I), 8.06 (1H, d, *J* 9.2

Hz, H5Q) 8.27 (1H, d, *J* 2.0 Hz, H8Q) 8.30 (1H, d, *J* 5.6 Hz, H2Q); δ_C (100 MHz, DMSO-d_6) 26.0 (C1), 37.1 (C2), 39.3 (C3), 108.2 (C3Q), 111.1 (C10Q), 116.7 (C5I), 117.4 (C5Q), 119.9 (C7I), 124.1 (C9I), 124.4 (C6Q), 128.1 (C8Q), 130.7 (C4I), 133.4 (C6I),138.8 (C7Q), 140.1 (C8I), 149.0 (C9Q), 149.8 (C4Q), 151.8 (C2Q), 155.8 (C3I), 162.9 (C2I), 167.2 (C6).

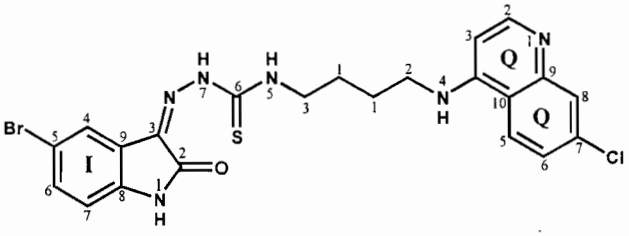

4-(7-Chloro-quinolin-4-yl)-butane-1,4-diamine-1-carbothioic acid (5-bromo-2-oxo-1,2-dihydro-indol-3-ylidene)-hydrazide **(81b)**. Synthesised as per **GP 3** to give yellow crystals (0.3157g, 98 %), mp 195-197 °C. IR ($CHCl_3$) ν_{max}/cm^{-1} 1459 (Ar C=C), 1579 (Ar C=N), 1605 (C_6=S), 1639 (C_{3I}=N), 1674 (C_{2I}=O); δ_H (400MHz, DMSO-d_6), 1.64 (4H, br, H1), 2.82 (2H, t, *J* 6.8 Hz, H2), 3.26 (2H, t, *J* 6.8 Hz, H3), 6.46 (1H, d, *J* 5.6 Hz, H3Q), 6.75 (1H, d, *J* 8.2 Hz, H7I), 7.29 (1H, dd, *J* 2.0 and 8.2 Hz, H6I), 7.40 (1H, dd, *J* 2.4 and 9.2 Hz, H6Q), 7.69 (1H, d, *J* 2.0 Hz, H4I), 8.26 (1H, d, *J* 9.2 Hz, H5Q), 8.06 (1H, d, *J* 5.2 Hz, H2Q), 8.29 (1H, d, *J* 2.4 Hz, H8Q); δ_C (100 MHz, DMSO-d_6), 25.7 (2×C1), 39.7 (C2), 42.5 (C3), 111.8 (C3Q), 113.5 (C10Q), 118.2 (C5I), 120.8 (C5Q), 124.7 (C7I), 124.7 (C9I), 128.2 (C6Q), 128.8 (C8Q), 131.3 (C4I) 134.1 (C6I), 134.6 (C7Q), 140.8 (C8I), 149.8 (C9Q), 150.8 (C4Q), 152.5 (C2Q), 155.2 (C3I), 162.0 (C2I), 168.0 (C6); HRMS (FAB) Found *m/z* 530.029779 $[M+1]^+$ $C_{22}H_{20}N_6SOBrCl$ requires 530.029120.

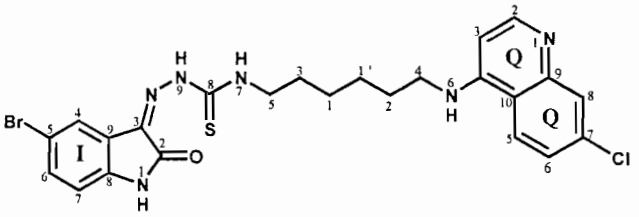

4-(7-Chloro-quinolin-4-yl)-hexane-1,6-diamine-1-carbothioic acid (5-bromo-2-oxo-1,2-dihydro-indol-3-ylidene)-hydrazide **(82b)**. Synthesised as per **GP 3** to give orange crystals (0.2204g, 65 %) mp 169-173 °C. IR ($CHCl_3$) ν_{max}/cm^{-1} 1459 (Ar C=C), 1579 (Ar C=N), 1605 (C_8=S), 1639 (C_{3I}=N), 1674 (C_{2I}=O); δ_H (300MHz, DMSO-d_6) 1.38 (4H, quint, *J* 3.6 Hz, H1+ H1'), 1.57 (2H, quint, *J* 6.6 Hz, H2), 1.66 (2H, quint, *J* 6.9 Hz, H3), 2.82 (2H, t, *J* 7.2 Hz, H4), 3.26 (2H, t, *J* 6.9 Hz, H5), 6.45 (1H, d, *J* 5.4 Hz, H3Q), 6.79 (1H, d, *J* 8.7 Hz, H7I), 7.25 (1H, br, H6), 7.32 (1H, dd, *J* 2.1 and 8.7 Hz, H6I), 7.44 (1H, dd, *J* 2.1 and 9.3 Hz, H6Q), 7.79 (1H, d, *J* 2.1 Hz, H4I), 8.28 (1H, d, *J* 9.3 Hz, H5Q), 8.34 (1H, d, *J* 2.1 Hz, H8Q) 8.40 (1H, d, *J* 5.4 Hz, H2Q); δ_C (75 MHz, DMSO-d_6) 25.5 (C1), 26.0 (C1'), 26.9 (C2), 27.5 (C3), 40.3 (C5), 42.2 (C4), 111.0 (C3Q), 112.7 (C10Q), 117.4 (C5I), 119.9 (C5Q), 123.9 (C7I), 124.0 (C9I), 127.3 (C6Q), 128.0 (C8Q), 130.7 (C4I), 133.3 (C7Q), 134.0 (C6I), 141.0 (C8I), 148.7 (C9Q), 149.2 (C4Q), 150.1 (C2Q), 155.6 (C3I), 161.9 (C2I), 167.7 (C8); HRMS (FAB) Found *m/z* 559.068904 $[M+1]^+$ $C_{24}H_{25}N_6SOBrCl$ requires 559.068245.

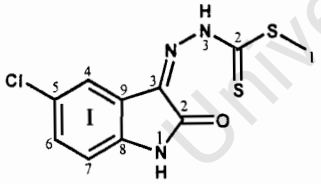

N-(5-Chloro-2-oxo-1,2-dihydro-indol-3-ylidene)-hydrazinecarbodithioic acid methyl ester **(78b).** Synthesised as per **GP 2** to give yellow crystals (2.9901g, 95 %), mp 260-262 °C. IR ($CHCl_3$) ν_{max}/cm^{-1} 1459 (Ar C=C), 1627 (C_2=S); 1639 (C_{3I}=N), 1674 (C_{2I}=O); δ_H (300MHz, DMSO-d_6) 2.63 (3H, s, H1), 6.96 (1H, d, *J* 8.1 Hz, H7I), 7.45 (1H, dd, *J* 2.4 and 8.1 Hz, H6I), 7.49 (1H, d, *J* 2.4 Hz, H4I), 11.44 (1H, s, H3), 13.88 (1H, s, H1I); δ_C (75 MHz, DMSO-d_6) 17.0 (C1), 112.4 (C7I), 113.3 (C5I), 120.9 (C9I), 126.8 (C4I), 131.5 (C6I), 134.2 (C8I), 141.9 (C3I), 162.1 (C2I), 201.4 (C2); HRMS (IE) Found *m/z* 284.979822 $[M+1]^+$ $C_{10}H_8N_3S_2OCl$ requires 284.979733.

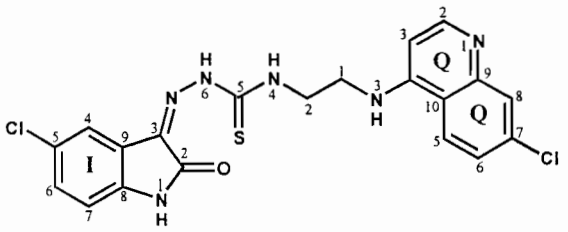

***4-(7-Chloro-quinolin-4-yl)-ethane-1,2-diamine-1-carbothioic acid (5-chloro-2-oxo-1,2-dihydro-indol-3-ylidene)-hydrazide* (79c)**. Synthesised as per **GP 3** to give yellow crystals (0.3022g, 94 %), mp 201-203 °C. IR ($CHCl_3$) ν_{max}/cm^{-1} 1459 (Ar C=C), 1579 (Ar C=N), 1605 (C_5=S), 1639 (C_{3I}=N), 1674 (C_{2I}=O); δ_H (300MHz, DMSO-d_6), 3.15 (2H, t, *J* 6.3 Hz, H1), 3.54 (2H, t, *J* 6.3 Hz, H2), 6.55 (1H, d, *J* 5.7 Hz, H3Q), 6.79 (1H, d, *J* 8.1 Hz, H7I), 7.19 (1H, dd, *J* 2.4 and 8.1 Hz, H6I), 7.48 (1H, dd, *J* 2.3 and 9.0 Hz, H6Q), 7.8 (1H, d, *J* 2.4 Hz, H4I), 8.18 (1H, d, *J* 9.0 Hz, H5Q), 8.26 (1H, d, *J* 2.3 Hz, H8Q), 8.44 (1H, d, *J* 5.7 Hz, H2Q), 10.40 (1H, s, H1I); δ_C (75 MHz, DMSO-d_6) 38.2(C1), 39.9 (C2), 111.2 (C3Q), 113.5 (C10Q), 118.2 (C5I), 120.1 (C5Q), 124.8 (C7I), 125.0 (C9I), 125.6 (C6Q), 126.1 (C8Q), 128.1 (C4I), 129.9 (C6I), 134.3 (C7Q), 140.5 (C8I), 149.5 (C9Q), 150.5 (C4Q), 152.5 (C2Q), 154.6 (C3I), 159.7 (C2I) 167.9 (C5); HRMS (FAB) Found *m/z* 460.063874 $[M+1]^+$ $C_{20}H_{18}N_6SOCl_2$ requires 460.063987.

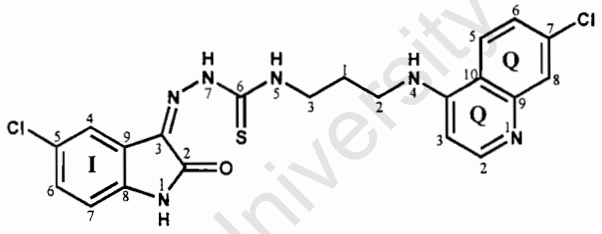

***4-(7-Chloro-quinolin-4-yl)-propane-1,3-diamine-1-carbothioic acid (5-chloro-2-oxo-1,2-dihydro-indol-3-ylidene)-hydrazide* (80c)** Synthesised as per **GP 3** to give yellow crystals (0.2485g, 75 %), mp 158-161 °C. IR ($CHCl_3$) ν_{max}/cm^{-1} 1459 (Ar C=C), 1579 (Ar C=N), 1605 (C_6=S), 1639 (C_{3I}=N), 1674 (C_{2I}=O); δ_H (300 MHz, DMSO-d_6) 1.91 (2H, quint, *J* 6.6 Hz, H1), 2.92 (2H, t, *J* 7.5 Hz, H2), 3.35 (2H, t, *J* 6.6 Hz, H3), 6.48 (1H, d, *J* 5.7 Hz, H3Q), 6.98 (1H, d, *J* 9.0 Hz, H7I), 7.44 (1H, dd, *J* 2.3 and 9.0 Hz, H6I), 7.78 (1H, d, *J* 2.3 Hz, H4I), 8.12 (1H, dd, *J* 3.0 and 8.9 Hz, H6Q), 8.24 (1H, d, *J* 8.9 Hz, H5Q), 8.40 (1H, d, *J* 5.7 Hz, H2Q), 9.07 (1H, d, *J* 3.0 Hz, H8Q); δ_C (75 MHz, DMSO-d_6), 26.5 (C1), 37.3 (C2), 39.3 (C3), 108.2 (C3Q), 112.0 (C10Q), 117.4 (C5I), 118.0 (C5Q), 120.6 (C7I), 124.0 (C9I), 124.8 (C6Q), 127.4 (C8Q), 130.0 (C4I), 133.3 (C6I), 139.2 (C7Q), 141.6 (C8I), 146.2 (C9Q), 149.0 (C4Q), 149.7 (C2Q), 156.7 (C3I), 162.5 (C2I), 167.7 (C6).

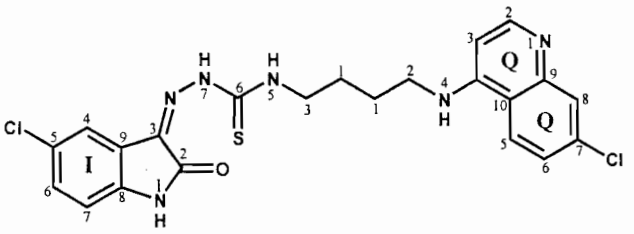

4-(7-Chloro-quinolin-4-yl)-butane-1,4-diamine-1-carbothioic acid (5-chloro-2-oxo-1,2-dihydro-indol-3-ylidene)-hydrazide **(81c)**. Synthesised as per **GP 3** to give yellow crystals (0.2797g, 82 %), mp 195-197 °C. IR ($CHCl_3$) ν_{max}/cm^{-1} 1459 (Ar C=C), 1579 (Ar C=N), 1605 (C_6=S), 1639 (C_{3I}=N), 1674 (C_{2I}=O); δ_H (300MHz, DMSO-d_6) 1.67 (4H, br, H1), 2.84 (2H, t, *J* 6.6 Hz, H2), 3.29 (2H, t, *J* 6.6 Hz, H3), 6.48 (1H, d, *J* 5.3 Hz, H3Q), 6.81 (1H, d, *J* 8.1 Hz, H7I), 7.20 (1H, dd, *J* 2.3 and 8.1 Hz, H6I), 7.46 (1H, dd, *J* 2.4 and 8.9 Hz, H6Q), 7.78 (1H, d, *J* 2.3 Hz, H4I), 8.25 (1H, d, *J* 8.9 Hz, H5Q), 8.27 (1H, d, *J* 2.4 Hz, H8Q), 8.39 (1H, d, *J* 5.3 Hz, H2Q); δ_C (75 MHz, DMSO-d_6), 24.8 (2×C1), 38.7 (C3), 41.7 (C2), 110.6 (C3Q), 114.4 (C10Q), 119.4 (C5I), 123.9 (C5Q), 124.0 (C7I), 124.9 (C9I), 125.3 (C6Q), 127.4 (C8Q), 130.0 (C4I), 133.4 (C6I), 134.9 (C7Q), 139.7 (C8I), 149.0 (C9Q), 150.0 (C4Q), 151.8 (C2Q), 156.0 (C3I), 162.7 (C2I), 167.3 (C6); HRMS (FAB) Found *m/z* 487.088633 $[M+1]^+$ $C_{22}H_{21}N_6SOCl_2$ requires 487.087462.

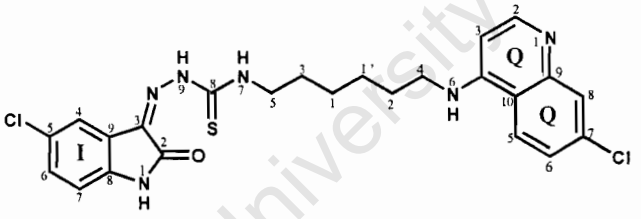

4-(7-Chloro-quinolin-4-yl)-hexane-1,6-diamine-1-carbothioic acid (5-chloro-2-oxo-1,2-dihydro-indol-3-ylidene)-hydrazide **(82c)**. Synthesised as per **GP 3** to give yellow crystals (0.2814g, 78 %), mp 128-131 °C. IR ($CHCl_3$) ν_{max}/cm^{-1} 1459 (Ar C=C), 1579 (Ar C=N), 1605 (C_8=S), 1639 (C_{3I}=N), 1674 (C_{2I}=O); δ_H (400MHz, DMSO-d_6) 1.38 (4H, quint, *J* 4.0 Hz, H1 + H1'), 1.56 (2H, quint, *J* 7.2 Hz, H2), 1.66 (2H, quint, *J* 6.8 Hz, H3), 2.79 (2H, t, *J* 7.2 Hz, H4), 3.26 (2H, t, *J* 7.2 Hz, H5), 6.43 (1H, d, *J* 5.6 Hz, H3Q), 6.70 (1H, d, *J* 8.2 Hz, H7I), 7.14 (1H, br s, H6) 7.16 (1H, dd, *J* 2.0 and 8.2 Hz, H6I), 7.40 (1H, dd, *J* 2.0 and 8.8 Hz, H6Q), 7.76 (1H, d, *J* 2.0 Hz, H4I), 8.24 (1H, d, *J* 8.8 Hz, H5Q), 8.28 (1H, d, *J* 2.0 Hz, H8Q), 8.38 (1H, d, *J* 5.6 Hz, H2Q); δ_C (100 MHz, DMSO-d_6) 25.6(C1), 26.0 (C1'), 26.9 (C2), 27.0 (C3), 40.3 (C5), 42.4 (C4), 111.2 (C3Q), 112.9 (C10Q), 118.2 (C5I), 120.3 (C5Q), 124.9 (C7I), 125.8

(C9I), 127.9 (C6Q), 129.9 (C8Q), 131.9 (C4I), 132.8 (C7Q), 134.2 (C6I), 139.3 (C8I), 148.1 (C9Q), 150.0 (C4Q), 150.1 (C2Q), 154.1 (C3I), 162.4 (C2I), 167.2 (C8); HRMS (FAB) Found *m/z* 515.110876 $[M+1]^+$ $C_{24}H_{25}N_6SOCl_2$ requires 515.118762.

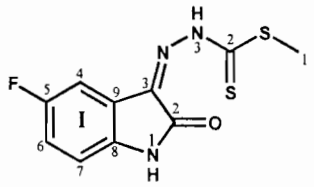

***N-(5-Fluoro-2-oxo-1,2-dihydro-indol-3-ylidene)-hydrazinecarbodithioic acid methyl ester* (78c).** Synthesised as per **GP 2** orange crystals (2.3160g, 71 %), mp 236-238 °C. IR ($CHCl_3$) ν_{max}/cm^{-1} 1459 (Ar C=C), 1627 (C_2=S); 1639 (C_{3I}=N), 1674 (C_{2I}=O); δ_H (400MHz, DMSO-d_6) 2.61 (3H, s, H1), 6.90 – 7.30 (3H, m, Ar), 11.34 (1H, s, H3), 13.90 (1H, s, H1I); δ_C (100 MHz, DMSO-d_6) 17.1 (C1), 112.4 (C7I), 112.5 (C5I),119.4 (C9I), 128.7 (C4I), 130.3 (C6I), 134.7 (C8I), 139.5 (C3I), 162.4 (C2I), 201.4 (C2); HRMS (IE) Found *m/z* 269.009198 $[M+1]^+$ $C_{10}H_8N_3S_2OF$ requires 269.009284.

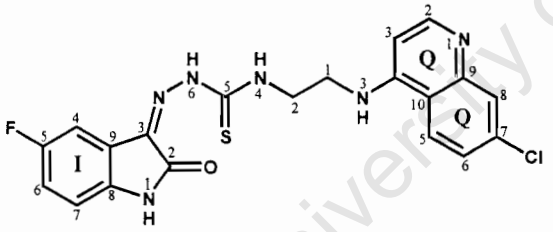

***4-(7-Chloro-quinolin-4-yl)-ethane-1,2-diamine-1-carbothioic acid (5-fluoro-2-oxo-1,2-dihydro-indol-3-ylidene)-hydrazide* (79d).** Synthesised as per **GP 3** to give yellow crystals (0.3223g, 98 %), mp 197-198 °C. IR ($CHCl_3$) ν_{max}/cm^{-1} 1459 (Ar C=C), 1579 (Ar C=N), 1605 (C_5=S), 1639 (C_{3I}=N), 1674 (C_{2I}=O); δ_H (400MHz, DMSO-d_6) 3.10 (2H, t, *J* 6.4 Hz, H1), 3.52 (2H, t, *J* 6.6 Hz, H2), 6.52 –8.50 (8H, m, Ar), 7.28 (1H, br, H3), 7.89 (1H, br, H4); δ_C (100 MHz, DMSO-d_6) 37.4 (C1), 38.7 (C2), 112.5 (C3Q), 114.6 (C10Q), 117.5 (C5I), 118.7 (C5Q), 124.0 (C7I), 124.2 (C9I), 125.7 (C6Q), 125.9 (C8Q), 127.4 (C4I), 133.5 (C6I), 134.4 (C7Q), 138.7 (C8I), 149 (C9Q), 151.8 (C4Q), 155.9 (C2Q), 156.0 (C3I),162.8 (C2I), 167.7 (C5).

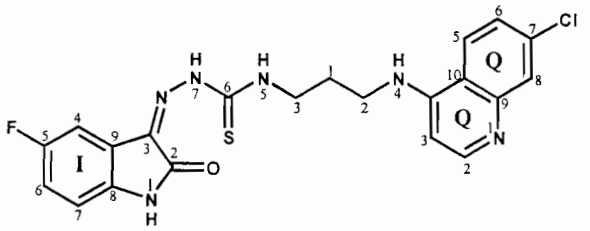

4-(7-Chloro-quinolin-4-yl)-propane-1,3-diamine-1-carbothioic acid (5-fluoro-2-oxo-1,2-dihydro-indol-3-ylidene)-hydrazide **(80d)**. Synthesised as per **GP 3** to give yellow crystals (0.2409g, 71 %), mp 164-166 °C. IR ($CHCl_3$) ν_{max}/cm^{-1} 1459 (Ar C=C), 1579 (Ar C=N), 1605 (C_6=S), 1639 (C_{3I}=N), 1674 (C_{2I}=O); δ_H (300 MHz, DMSO-d_6) 1.95 (2H, quint, *J* 7.5 Hz, H1) 2.98 (2H, t, *J* 8.1 Hz, H2) 3.36 (2H, t, *J* 7.5 Hz, H3) 6.50 – 8.40 (8H, m, Ar); δ_C (75 MHz, DMSO-d_6) 25.3 (C1), 37.1 (C2), 38.9 (C3), 109.8 (C3Q), 112.6 (C10Q), 115.0 (C5I), 117.4 (C5Q), 118.7 (C7I), 124.0 (C9I), 124.1 (C6Q), 127.4 (C8Q), 130.5 (C4I), 133.4 (C6I), 139.0 (C7Q), 140.1 (C8I), 149.0 (C9Q), 149.9 (C4Q), 151.7 (C2Q), 155.9 (C3I), 159.0 (C2I), 167.9 (C6).

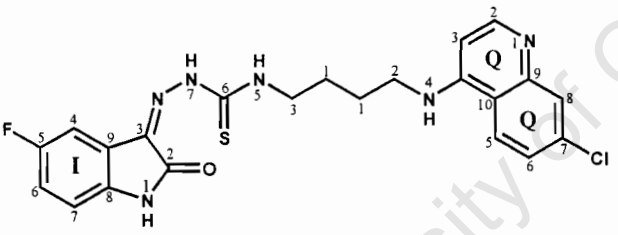

4-(7-Chloro-quinolin-4-yl)-butane-1,4-diamine-1-carbothioic acid (5-fluoro-2-oxo-1,2-dihydro-indol-3-ylidene)-hydrazide **(81d)**. Synthesised as per **GP 3** to give yellow crystals (0.3462g, 99 %), mp 181-182 °C. IR ($CHCl_3$) ν_{max}/cm^{-1} 1459 (Ar C=C), 1579 (Ar C=N), 1605 (C_6=S), 1639 (C_{3I}=N), 1674 (C_{2I}=O); δ_H (400MHz, DMSO-d_6), 1.70 (4H, m, H1), 2.86 (2H, t, *J* 5.1 Hz, H2), 3.29 (2H, t, *J* 5.1 Hz, H3), 6.46 (1H, d, *J* 5.6 Hz, H3Q), 6.72-8.20 (6H, m, Ar), 8.38 (1H, d, *J* 5.6 Hz, H2Q); δ_C (100 MHz, DMSO-d_6) 25.7 (2×C1), 39.6 (C3), 42.5 (C2), 110.5 (C3Q), 113.3 (C10Q), 115.4 (C5I), 118.2 (C5Q), 123.6 (C7I), 124.6 (C9I), 124.7 (C6Q), 128.2 (C8Q), 130.1 (C4I), 134.1 (C6I), 135.6 (C7Q), 138.1 (C8I), 149.8 (C9Q), 150.8 (C4Q), 152.6 (C2Q), 155.6 (C3I), 159.4 (C2I), 168.5 (C6).

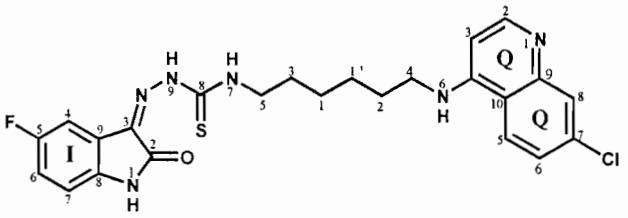

4-(7-Chloro-quinolin-4-yl)-hexane-1,6-diamine-1-carbothioic acid (5-fluoro-2-oxo-1,2-dihydro-indol-3-ylidene)-hydrazide **(82d).** Synthesised as per **GP 3** to give yellow crystals (0.3631g, 98 %), mp 150-153 °C. IR ($CHCl_3$) ν_{max}/cm^{-1} 1459 (Ar C=C), 1579 (Ar C=N), 1605 (C_8=S), 1639 (C_{3I}=N), 1674 (C_{2I}=O); δ_H (300MHz, DMSO-d_6) 1.33(4H, m, H1 + H1'), 1.52 (2H, quint, *J* 6.6 Hz, H2), 1.61 (2H, quint, *J* 7.5 Hz, H3), 2.77 (2H, t, *J* 7.5 Hz, H4), 3.22 (2H, t, *J* 6.6 Hz, H5), 6.40 – 8.4 (8H, m, Ar), 7.31 (H, br, H6); δ_C (75 MHz, DMSO-d_6), 25.6 (C1), 26.1 (C1'), 26.4 (C2), 27.0 (C3), 40.3 (C5), 42.2 (C4), 109.8 (C3Q), 111.6 (C10Q), 117.4 (C5I), 118.7 (C5Q), 124.9 (C7I), 125.9 (C9I), 126.1 (C6Q), 127.4 (C8Q), 130.0 (C4I), 133.4 (C7Q), 134.0 (C6I), 140.0 (C8I), 149.0 (C9Q), 150.1 (C4Q), 151.8 (C2Q), 156.0 (C3I), 159.0 (C2I), 167.8 (C8); HRMS (FAB) Found *m/z* 500.155206 $[M+1]^+$ $C_{24}H_{26}N_6SOClF$ requires 500.156137.

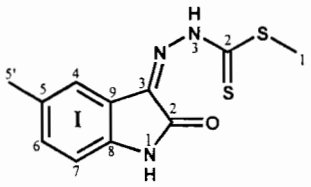

N-(5-Methyl-2-oxo-1,2-dihydro-indol-3-ylidene)-hydrazinecarbodithioic acid methyl ester **(78d).** Synthesised as per **GP 2** to give yellow crystals (2.5028g, 76 %), mp 229-233 °C. IR ($CHCl_3$) ν_{max}/cm^{-1} 1459 (Ar C=C), 1627 (C_2=S); 1639 (C_{3I}=N), 1674 (C_{2I}=O); δ_H (400MHz, DMSO-d_6) 2.29 (3H, s, H5'), 2.62 (3H, s, H1), 6.82-7.38 (3H, m, Ar), 11.07 (1H, s, H3), 13.93 (1H, s, H1I); δ_C (100 MHz, DMSO-d_6), 17.8 (C1), 21.1 (C5 '), 111.9 (C7I), 112.8 (C5I), 121.0 (C9I), 127.8 (C4I), 130.4 (C6I), 133.5 (C8I), 141.8 (C3I), 163.1 (C2I), 201.9 (C2); HRMS (IE) Found *m/z* 265.034442 $[M+1]^+$ $C_{11}H_{11}N_3S_2O$ requires 265.034356.

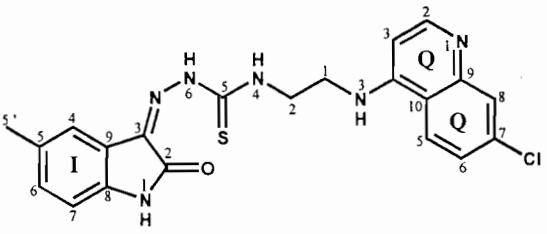

4-(7-Chloro-quinolin-4-yl)-ethane-1,2-diamine-1-carbothioic acid (5-methyl-2-oxo-1,2-dihydro-indol-3-ylidene)-hydrazide **(79e)**. Synthesised as per **GP 3** to give yellow crystals (0.3143g, 95 %), mp 204-206 °C. IR ($CHCl_3$) ν_{max}/cm^{-1} 1459 (Ar C=C), 1579 (Ar C=N), 1605 (C_5=S), 1639 (C_{3I}=N), 1674 (C_{2I}=O); δ_H (400MHz, DMSO-d_6) 2.30 (3H, s, H5'I), 3.10 (2H, t, *J* 6.4 Hz, H1), 3.51 (2H, t, *J* 6.4 Hz, H2), 6.53 (1H, d, *J* 5.2 Hz, H3Q), 6.67 (1H, d, *J* 7.8 Hz, H7I), 6.97 (1H, dd, *J* 2.0 and 7.8 Hz, H6I), 7.30 (1H, dd, *J* 1.2 and 9.0 Hz, H6Q), 7.78 (1H, d, *J* 2.0 Hz, H4I), 8.06 (1H, d, *J* 1.2 Hz, H8Q), 8.17 (1H, d, *J* 9.0 Hz, H5Q), 8.42 (1H, d, *J* 5.2 Hz, H2Q); δ_C (100 MHz, DMSO-d_6) 21.5 (C5'I), 38.7 (C1), 39.7 (C2), 109.9 (C3Q), 111.2 (C10Q), 118.2 (C5I), 119.1 (C5Q), 123.3 (C7I), 123.9 (C9I), 124.7 (C6Q), 126.1 (C8Q), 128.1 (C4I), 130.2 (C6I),134.2 (C7Q), 140.1 (C8I), 149.8 (C9Q), 150.9 (C4Q), 152.5 (C2Q), 156.2 (C3I), 162.4 (C2I), 168.2 (C5).

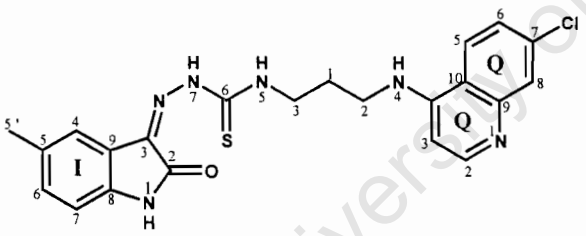

4-(7-Chloro-quinolin-4-yl)-propane-1,3-diamine-1-carbothioic acid (5-methyl-2-oxo-1,2-dihydro-indol-3-ylidene)-hydrazide **(80e)**. Synthesised as per **GP 3** to give yellow crystals (0.2936g, 86 %), mp 157-162 °C; IR ($CHCl_3$) ν_{max}/cm^{-1} 1459 (Ar C=C), 1579 (Ar C=N), 1605 (C_6=S), 1639 (C_{3I}=N), 1674 (C_{2I}=O); δ_H (300 MHz, DMSO-d_6) 1.96 (2H, quint, *J* 7.5 Hz, H1), 2.29 (3H, s, H5'I), 2.98 (2H, t, *J* 8.1 Hz, H2), 3.36 (2H, t, *J* 6.6 Hz, H3), 6.49 – 8.40 (8H, m, Ar); δ_C (75 MHz, DMSO-d_6) 20.8 (C5'I), 25.9 (C1), 37.0 (C2), 39.3 (C3), 109.2 (C3Q), 111.0 (C10Q), 117.4 (C5I), 118.2 (C5Q), 121.2 (C7I), 123.9 (C9I), 125.0 (C6Q), 127.4 (C8Q), 129.6 (C4I), 133.4 (C6I), 139.2 (C7Q), 140.7 (C8I), 148.9 (C9Q), 149.8 (C4Q), 151.7 (C2Q), 157.7 (C3I), 162.2 (C2I), 167.8 (C6).

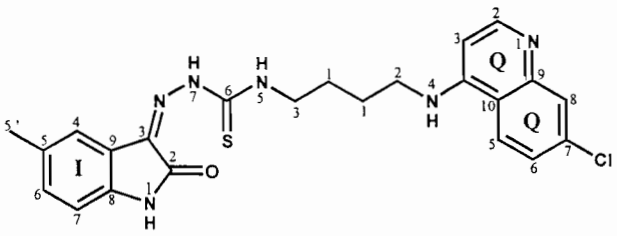

4-(7-Chloro-quinolin-4-yl)-butane-1,4-diamine-1-carbothioic acid (5-methyl-2-oxo-1,2-dihydro-indol-3-ylidene)-hydrazide **(81e)**. Synthesised as per **GP 3** to give yellow crystals (0.3309g, 94 %), mp 177-180 °C. IR ($CHCl_3$) ν_{max}/cm^{-1} 1459 (Ar C=C), 1579 (Ar C=N), 1605 (C_6=S), 1639 (C_{3I}=N), 1674 (C_{2I}=O); δ_H (400MHz, DMSO-d_6), 1.69 (4H, m, H1), 2.24 (3H, s, 5'I), 2.86 (2H, t, *J* 7.2 Hz, H2), 3.29 (2H, t, *J* 6.8 Hz, H3), 6.46 (1H, d, *J* 5.2 Hz, H3Q), 6.68 (1H, d, *J* 8.0 Hz, H7I), 6.97 (1H, dd, *J* 2.0 and 8.0 Hz, H6I), 7.40 (1H, dd, *J* 2.4 and 9.0 Hz, H6Q), 7.76 (1H, d, *J* 2.0 Hz, H4I), 8.08 (1H, d, *J* 2.4 Hz, H8Q) 8.22 (1H, d, *J* 9.0 Hz, H5Q), 8.38 (1H, d, *J* 5.2 Hz, H2Q); δ_C (75 MHz, DMSO-d_6) 20.8 (C5'I), 24.9 (2×C1), 38.7 (C3), 41.3 (C2), 109.1 (C3Q), 113.5 (C10Q), 117.4 (C5I), 118.3 (C5Q), 123.9 (C7I), 124.0 (C9I), 127.1(C6Q), 127.4 (C8Q), 130.0 (C4I), 134.9 (C6I), 135.3 (C7Q), 139.2 (C8I), 149.0 (C9Q), 150.0 (C4Q), 151.8 (C2Q), 154.9 (C3I), 161.9 (C2I), 167.2 (C6); HRMS (FAB) Found *m/z* 467.142342 $[M+1]^+$ $C_{23}H_{24}N_6SOCl$ requires 467.142084.

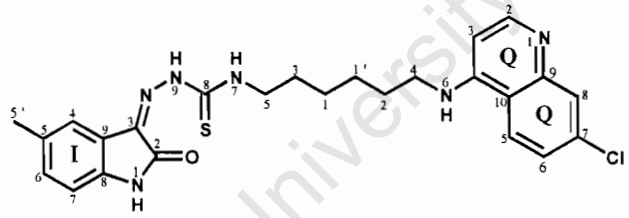

4-(7-Chloro-quinolin-4-yl)-hexane-1,6-diamine-1-carbothioic acid (5-methyl-2-oxo-1,2-dihydro-indol-3-ylidene)-hydrazide **(82e)** Synthesised as per **GP 3** to give yellow crystals (0.2724g, 73 %), mp 203-205 °C. IR ($CHCl_3$) ν_{max}/cm^{-1} 1459 (Ar C=C), 1579 (Ar C=N), 1605 (C_8=S), 1639 (C_{3I}=N), 1674 (C_{2I}=O); δ_H (300MHz, DMSO-d_6) 1.33 (4H, m, H1 + H1'), 1.53 (2H, quint, *J* 6.6 Hz, H2), 1.61 (2H, quint, *J* 6.6 Hz, H3), 2.21 (3H, s, H5'), 2.77 (2H, t, *J* 7.2 Hz, H4), 3.21 (2H, t, *J* 6.9 Hz, H5), 6.42 (1H, d, *J* 5.6 Hz, H3Q), 6.70 (1H, d, *J* 8.1 Hz, H7I), 6.98 (1H, dd, *J* 1.8 and 8.1 Hz, H6I), 7.24 (1H, br, H6), 7.39 (1H,dd, *J* 3 and 8.7 Hz, H6Q), 7.76 (1H, d, *J* 1.8 Hz, H4I), 8.04 (1H, d, *J* 3 Hz, H8Q), 8.22(1H, d, *J* 8.7 Hz, H5Q), 8.34 (1H, d, *J* 5.6 Hz, H2Q); δ_C (75 MHz, DMSO-d_6) 20.8 (C5'I), 25.6 (C1), 26.1 (C1'), 27.1 (C2), 27.6 (C3), 40.3 (C5), 42.2 (C4), 109.2 (C3Q), 111.5 (C10Q), 117.4 (C5I), 118.3 (C5Q), 124.0 (C7I),

124.1 (C9I), 127.1 (C6Q), 127.4 (C8Q), 129.6 (C4I), 134.0 (C7Q), 135.4 (C6I), 139.2 (C8I), 140.6 (C9Q), 149.0 (C4Q), 150.0 (C2Q), 155.8 (C3I), 162.4 (C2I), 167.0 (C8); HRMS (FAB) Found *m/z* 496.181987 $[M+1]^+$ $C_{25}H_{29}N_6SOCl_4$ requires 496.181209.

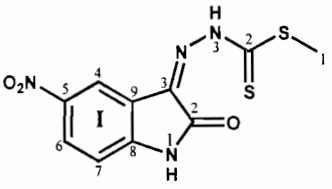

***N-(5-Nitro-2-oxo-1,2-dihydro-indol-3-ylidene)-hydrazinecarbodithioic acid methyl ester* (78e).** Synthesised as per **GP 3** to give red crystals (2.6838g, 87 %), mp 250-252 °C. IR ($CHCl_3$) ν_{max}/cm^{-1} 1459 (Ar C=C), 1627 (C_2=S); 1639 (C_{3I}=N), 1674 (C_{2I}=O); δ_H (300MHz, DMSO-d_6), 2.66 (3H, s, H1), 7.16 (1H, d, *J* 8.6, H7I), 8.21 (1H, d, *J* 2.4 Hz, H4I) 8.30 (1H, dd, *J* 2.4 and 8.6, H6I), 11.93 (1H, s, H3), 13.75 (1H, s, H1I); δ_C (75 MHz, DMSO-d_6) 17.2 (C1), 111.6 (C7I), 115.6 (C5I), 120.1 (C9I), 127.8 (C4I), 131.3 (C6I), 133.5 (C8I), 142.8 (C3I), 162.6 (C2I), 201.8 (C2); HRMS (IE) Found *m/z* 296.003802 $[M+1]^+$ $C_{10}H_8N_4S_2O_3$ requires 296.003783.

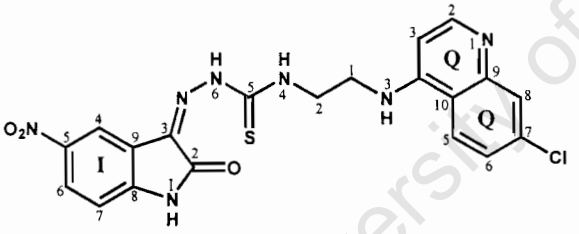

***4-(7-Chloro-quinolin-4-yl)-ethane-1,2-diamine-1-carbothioic acid (5-nitro-2-oxo-1,2-dihydro-indol-3-ylidene)-hydrazide* (79f).** Synthesised as per **GP 3** to give yellow crystals (0.3045g, 96 %), mp 227-228 °C. IR ($CHCl_3$) ν_{max}/cm^{-1} 1459 (Ar C=C), 1579 (Ar C=N), 1605 (C_5=S), 1639 (C_{3I}=N), 1674 (C_{2I}=O); δ_H (400MHz, DMSO-d_6) 3.11 (2H, t, *J* 6.4 Hz, H1), 3.52 (2H, t, *J* 6.4 Hz, H2), 6.53 (1H, d, *J* 5.4 Hz, H3Q), 6.93 (1H, d, *J* 8.8 Hz, H7I), 7.30 (1H, m, H3) 7.55 (1H, dd, *J* 2.0 and *J* 8.8 Hz, H6I), 7.76 (1H, d, *J* 2.0 Hz, H4I), 8.10 (1H, dd, *J* 2.5 and 8.8 Hz, H6Q), 8.14 (1H, d, *J* 8.8 Hz, H5Q) 8.42 (1H, d, *J* 5.4 Hz, H2Q), 9.01 (1H, d, *J* 2.5 Hz, H8Q); δ_C (100 MHz, DMSO-d_6) 37.4 (C1), 38.7 (C2), 109.0 (C3Q)117.4 (C10Q), 117.9 (C5I), 120.6 (C5Q), 124.0 (C7I), 124.2 (C9I), 124.8 (C6Q), 127.3 (C8Q)128.6 (C4I), 131.6 (C6I), 135.1 (C7Q), 141.6 (C8I), 148.7 (C9Q), 149.7 (C4Q), 151.7 (C2Q), 155.8 (C3I), 161.9 (C2I), 167.6 (C5); HRMS (FAB) Found *m/z* 471.088952 $[M+1]^+$ $C_{20}H_{18}N_7SO_3Cl$ requires 471.088037

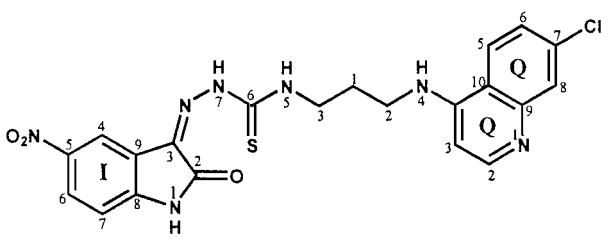

4-(7-Chloro-quinolin-4-yl)-propane-1,3-diamine-1-carbothioic acid (5-nitro-2-oxo-1,2-dihydro-indol-3-ylidene)-hydrazide **(80f)**. Synthesised as per **GP 3** to give orange crystals (0.2352g, 72 %), mp 160-164 °C. IR ($CHCl_3$) ν_{max}/cm^{-1} 1459 (Ar C=C), 1579 (Ar C=N), 1605 (C_6=S), 1639 (C_{3I}=N), 1674 (C_{2I}=O); δ_H (300 MHz, DMSO-d_6) 1.91 (2H, quint, *J* 7.5 Hz, H1) 2.92 (2H, t, *J* 7.5 Hz, H2) 3.35 (2H, t, *J* 6.6 Hz, H3) 6.48 (1H, d, *J* 6.0 Hz, H3Q) 6.85 (1H, d, *J* 8.0 Hz, H7I) 7.20 (1H, dd, *J* 2.1 and 8.0 Hz, H6I) 7.44 (1H, dd, *J* 2.1 and 9.2 Hz, H6Q) 7.79 (1H, d, *J* 2.1 Hz, H4I) 8.24 (1H, d, *J* 9.2 Hz, H5Q) 8.27 (1H, d, *J* 2.1 Hz, H8Q) 8.40 (1H, d, *J* 6.0 Hz, H2Q); δ_C (100.6 MHz, DMSO-d_6), 26.6 (C1), 37.4 (C2), 38.7 (C3), 110.6 (C3Q), 112.0 (C10Q), 117.4 (C5I), 117.9 (C5Q), 119.4 (C7I), 124.0 (C9I), 124.1 (C6Q), 128.0 (C8Q), 131.0 (C4I), 133.4 (C6I), 139.7 (C7Q), 141.3 (C8I), 149.0 (C9Q), 149.9 (C4Q), 151.8 (C2Q), 156.0 (C3I), 160.9(C2I), 167.4 (C6).

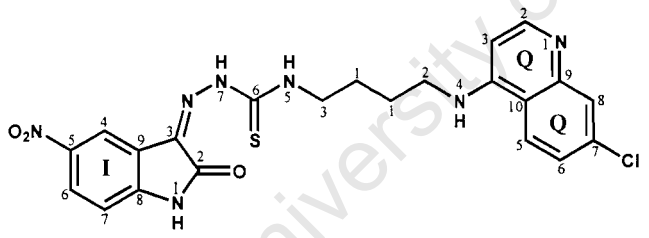

4-(7-Chloro-quinolin-4-yl)-butane-1,4-diamine-1-carbothioic acid (5-nitro-2-oxo-1,2-dihydro-indol-3-ylidene)-hydrazide **(81f)**. Synthesised as per **GP 3** to give yellow crystals (0.3260g, 97 %), mp 217-219 °C. IR ($CHCl_3$) ν_{max}/cm^{-1} 1459 (Ar C=C), 1579 (Ar C=N), 1605 (C_6=S), 1639 (C_{3I}=N), 1674 (C_{2I}=O); δ_H (300MHz, DMSO-d_6) 1.67 (4H, m, H1), 2.84 (2H, t, *J* 6.3 Hz, H2), 3.29 (2H, t, *J* 5.7 Hz, H3), 6.48 (1H, d, *J* 5.9 Hz, H3Q), 6.97 (1H, d, *J* 9.0 Hz, H7I), 7.44 (1H, dd, *J* 2.4 and 9.0 Hz, H6I), 7.78 (1H, d, *J* 2.4 Hz, H4I), 8.12 (1H, dd, *J* 2.9 and 8.9 Hz, H6Q), 8.24 (1H, d, *J* 8.9 Hz, H5Q), 8.39 (1H, d, *J* 5.2 Hz, H2Q), 9.07 (1H, d, *J* 2.9 Hz, H8Q); δ_C (75 MHz, DMSO-d_6) 24.8 (C1), 38.7 (C3), 41.7 (C2), 109.1 (C3Q), 114.0 (C10Q), 117.4 (C5I), 118.0 (C5Q), 123.6 (C7I), 124.0 (C9I), 124.8 (C6Q), 127.4 (C8Q), 129.9 (C4I), 134.1 (C6I), 135.8

(C7Q), 141.0 (C8I), 149.0 (C9Q), 150.0 (C4Q), 151.8 (C2Q), 155.2 (C3I), 162.8 (C2I), 167.6 (C6).

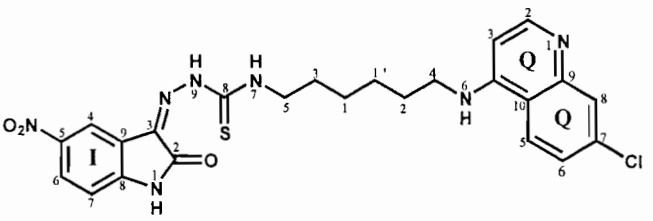

4-(7-Chloro-quinolin-4-yl)-hexane-1,6-diamine-1-carbothioic acid (5-nitro-2-oxo-1,2-dihydro-indol-3-ylidene)-hydrazide **(82f)**. Synthesised as per **GP 3** to give orange crystals (0.3267g, 92 %), mp 198-200 °C; IR ($CHCl_3$) ν_{max}/cm^{-1} 1459 (Ar C=C), 1579 (Ar C=N), 1605 (C_8=S), 1639 (C_{3I}=N), 1674 (C_{2I}=O); δ_H (300MHz, DMSO-d_6) 1.38 (4H, quint, *J* 3.6 Hz, H1 + H1'), 1.56 (2H, m, *J* 7.2 Hz, H2), 1.66 (2H, quint, *J* 7.5 Hz, H3), 2.81 (2H, t, *J* 7.2 Hz, H4), 3.26 (2H, t, *J* 6.6 Hz, H5), 6.44 (1H, d, *J* 5.4 Hz, H3Q), 6.98 (1H, d, *J* 8.9 Hz, H7I), 7.26 (1H, br, H6), 7.43 (1H, dd, *J* 2.6 and 8.9 Hz, H6I), 7.78 (1H, d, *J* 2.1 Hz, H4I), 8.12 (1H, dd, *J* 3.0 and 8.7 Hz, H6Q), 8.26 (1H, d, *J* 8.7 Hz, H5Q), 8.39 (1H, d, *J* 5.4 Hz, H2Q), 9.91 (1H, d, *J* 3 Hz, H8Q); δ_C (75 MHz, DMSO-d_6) 25.5 (C1), 26.0 (C1'), 27.0 (C2), 27.5 (C3), 40.3 (C5), 42.2 (C4), 109.5 (C3Q), 113.8 (C10Q), 117.3 (C5I), 118.0 (C5Q), 124.5 (C7I), 125.9 (C9I), 127.0 (C6Q), 127.7 (C8Q), 129.2 (C4I), 133.9 (C7Q), 135.3 (C6I), 139.0 (C8I), 146.7 (C9Q), 148.8 (C4Q), 150.1 (C2Q), 154.6 (C3I), 162.7 (C2I), 167.7 (C8); HRMS (FAB) Found *m/z* 525.134801 $[M+1]^+$ $C_{24}H_{24}N_7SO_3Cl$ requires 525.134987.

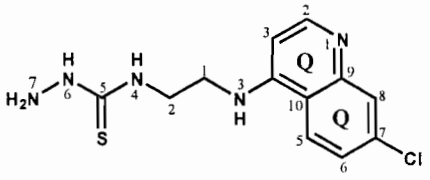

4-(7-Chloro-quinolin-4-yl)-ethane-1,2-diamine-1-carbothioic acid hydrazide **(83)**. A mixture of **1** (0.500 g, 1.6904 mmol) and **76a** (1.8140g, 8.1826 mmol) were refluxed in 30 ml of methanol for 24 hours to give a yellow heterogenous mixture after cooling to room temperature. The solvent was removed by filtration to give yellow crystals, which were re-crystallised from methanol to yield (0.6293 g, 52 %), mp 106-164 °C. IR ($CHCl_3$) ν_{max}/cm^{-1} 1459 (Ar C=C), 1579 (Ar C=N), 1605 (C_5=S); δ_H

(400MHz, DMSO-d_6) 3.82 (2H, br, H1), 4.48 (2H, br, H2), 6.64 (2H, d, *J* 5.4 Hz, H3Q), 7.43 (1H, dd, *J* 2.0 and 9.0 Hz, H6Q), 7.78 (1H, d, *J* 2.0 Hz, H8Q), 8.23 (1H, d, *J* 9.0 Hz, H5Q), 8.38 (1H, d, *J* 5.4 Hz, H2Q); δ_C (100 MHz, DMSO-d_6) 41.0 (C1), 42.9 (C2), 98.8 (C3Q), 117.3 (C10Q), 123.9 (C5Q), 124.0 (C6Q), 127.5 (C8Q), 133.3 (C7Q), 148.9 (C9Q), 150.1 (C4Q), 151.9 (C2Q), 169.4 (C5). HRMS (IE) Found *m/z* 295.06591 $[M+1]^+$ $C_{12}H_{14}ClN_5S$ requires 295.06584;

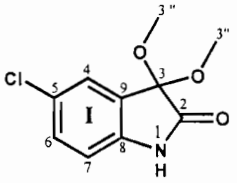

5-*Chloro*-3,3-*dimethyoxy*-1,3-*dihydro-indol*-2-*one* (85). A suspension of 5-chloroisatin (2.0000 g, 0.01101 mol), catalytic amount *p*-toluene sulfonic acid and trimethyl orthoformate (36.15 ml, 0.3304 mol) in 60 ml of anhydrous methanol was refluxed for 48 h. The solvent was then removed under reduced pressure and the residue dissolved in dichloromethane and washed with saturated aqueous $NaHCO_3$. The organic layer was dried with $MgSO_4$, concentrated and purified by chromatography on silica gel (eluent: MeOH:DCM 1:10) to yield the *ketal* **85** as light brown crystals (1.5545g, 62 %), mp 143-146 °C. IR ($CHCl_3$) ν_{max}/cm^{-1} 1459 (Ar C=C), 1674 (C_{2I}=O); δ_H (400MHz, $CDCl_3$) 3.56 (6H, s, H3''), 6.83 (1H, d, *J* 8.0 Hz, H7I), 7.28 (1H, dd, *J* 2.0 and 8.0 Hz, H6I), 7.37 (1H, d, *J* 2.0 Hz, H4I); δ_C (100 MHz, $CDCl_3$) 50.89 (C3''), 97.2 (C7I), 112.0 (C3I), 125.5 (C6I), 126.8 (C9I), 128.2 (C5I), 130.6 (C4I), 139.0 (C8I), 172.9 (C2I). HRMS (IE) Found *m/z* 227.034963 $[M+1]^+$ $C_{10}H_{10}ClNO_3$ requires 227.034921; Found: C 52.95 %, H 4.19 %, N 5.99 %; Anal. Calcd: C 52.76 %, H 4.43 %, N 6.15 %.

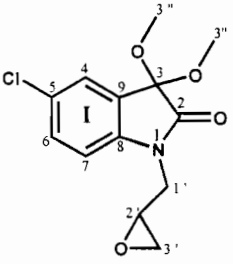

5-*chloro*-3,3-*dimethoxy*-1-*oxiranylm ethyl*-1,3-*dihydro-indol*-2-*one* (86). 5-Chloro-3, 3-dimethoxy-1, 3-dihydro-indol-2-one **85** (1.5000 g, 6.5894 mmol) and KF/Al_2O_3 (5 eqs by mass) were suspended in 60 ml of CH_2Cl_2. 1-Chloro-2, 3-epoxypropane (2.1 ml, 26.3574 mmol) was then added and the reaction was stirred at room temperature for 48 h. The mixture was then filtered and the resulted liquid was

concentrated under high vacuum to give the *epoxide* **86** as a yellow to green oil (1.2152g, 65 %). IR ($CHCl_3$) ν_{max}/cm^{-1} 1459 (Ar C=C), 1674 (C_{2I}=O); δ_H (400 MHz, $CDCl_3$) 2.62 (1H, dd, *J* 2.4 and 4.8 Hz, H3'), 2.81 (1H, t, *J* 4.8 Hz, H3'), 3.14 (1H, m, H2'), 3.47 (1H, dd, *J* 6.0 and 15.2 Hz, H1'), 3.55 (3H, s, H3''), 3.56 (3H, s, H3''), 4.23 (1H, dd, *J* 2.8 and 15.2 Hz, H1'), 6.99 (1H, d, *J* 8.4 Hz, H7I), 7.33 (1H, dd, *J* 2.0 and 8.4 Hz, H6I), 7.38 (1H, d, *J* 2.0 Hz, H4I); δ_C (100 MHz, $CDCl_3$) 41.8 (C3'), 44.72 (C2'), 49.8 (C1'), 50.9 (C3''), 96.7 (C7I), 111.1 (C3I), 125.1 (C6I), 126.3 (C9I), 128.4 (C5I), 130.6 (C4I), 141.2 (C8I), 170.4 (C2I);.

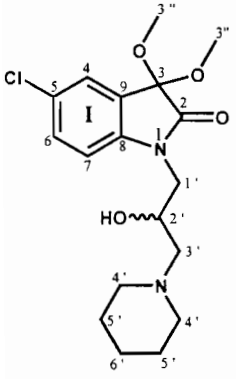

5-Chloro-1-(2-hydroxy-3-piperidin-1-yl-propyl)-3,3-dimethoxy-1,3-dihydro-indol-2-one **(87).** A solution of 5-chloro-3,3-dimethoxy-1-oxiranylmethyl-1,3-dihydro-indol-2-one **86** (1.0000 g, 3.5247 mmol) and piperidine (0.70 ml, 7.0495 mmol) in 50 methanol was refluxed for 12 hrs. The solvent was removed under reduced pressure and column chromatography (SiO_2, MeOH: CH_2Cl_2, 1:9) yielded **87** as light brown oil (0.7671g, 59 %). R_f 0.23; IR ($CHCl_3$) ν_{max}/cm^{-1} 1459 (Ar C=C), 1674 (C_{2I}=O); δ_H (300 MHz, CD_3OD) 1.46 (2H, quint, *J* 6.8 Hz, H6'), 1.61 (4H, quint, *J* 5.1 Hz, H5'), 2.48 (2H, m, H3'), 2.53 (4H, t, *J* 5.4 Hz, H4'), 3.49 (3H, s, H3''), 3.50 (3H, s, H3''), 3.64 (1H, dd, *J* 6.9 and 15 Hz, H1'), 3.77 (1H, dd, *J* 4.4 and 15 Hz, H1'), 4.09 (1H, m, H2'), 7.30 (1H, d, *J* 8.4 Hz, H7I), 7.38 (1H,dd, *J* 2.0 and 8.4 Hz, H6I), 7.40 (1H, d, *J* 2.0 Hz, H4I); δ_C (75.45 MHz, $CDCl_3$) 24.9 (C6'), 26.4 (2×C5'), 51.4 (C3''), 52.0 (C1'), 56.0 (2×C4'), 63.8 (C3'), 67.0 (C2'), 98.3 (C7I), 112.8 (C3I), 126.1 (C6I), 127.8 (C9I), 129.2 (C5I), 131.6(C4I), 141.3 (C8I), 172.6 (C2I).

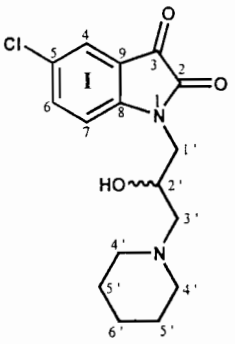

5-Chloro-1-(2-hydroxy-3-piperadin-1-yl-propyl)-1H-indole-2-3-dion **(88).** 5-Chloro-1-(2-hydroxy-3-piperidin-1-yl-propyl)-3,3-dimethoxy-1,3-dihydro-indol-2-one **87** (0.5 g, 1.54 mmol) was dissolved in a mixture of 1 ml concentrated HCl and 9 ml acetone. The red solution was stirred at room temperature for 3 hrs monitered by TLC. The resulted salt was dissolved 2M Na_2CO_3, extracted with CH_2Cl_2 and column chromatography (SiO_2, MeOH: CH_2Cl_2, 1:9) yielded the *ketone* **88** (97 %) of red crystals. R_f 0.35; mp 147-149 °C; IR ($CHCl_3$) ν_{max}/cm^{-1} 1459 (Ar C=C), 1674 (C=O), 1702 (C=O); δ_H (300MHz, $CDCl_3$) 1.45 (2H, quint, *J* 6 Hz, H6'), 1.56 (4H, quint, *J* 5.1 Hz, H5'), 2.31 (4H, m, H4'), 2.58 (2H, m, H3'), 3.62 (H, dd, *J* 6 and 14.6 Hz, H1'), 3.87 (H, dd, *J* 3.9 and *J* 14.6 Hz, H1'), 3.98 (H, m, H2'); δ_C (75.45 MHz, $CDCl_3$) 24.0 (C6'), 26.0 (2×C5'), 53.6 (2×C4'), 54.5 (C1'), 61.4 (C3'), 65.7 (C2'), 98.5 (C7I), 124.7 (C6I), 125.8 (C9I), 129.4 (C5I), 131.2 (C4I), 139.6 (C8I), 172.4 (C2I), 184.4 (C3I); HRMS (EI) Found *m/z* 322.108474 $[M+1]^+$ $C_{16}H_{19}N_2O_3Cl$ requires 322.108420. Found: C 59.23 %, H 5.78 %, N 8.41 %, Anal. Calcd: C 59.34 % H 5.93 %, N 8.68 %.

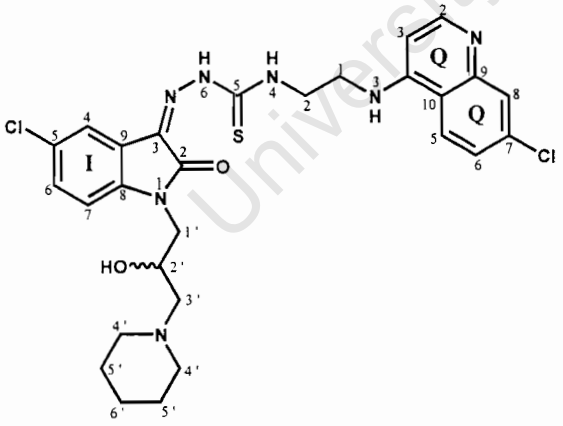

4-(7-Chloro-quinolin-4-yl)-ethane-1,2-diamine-1-carbothioic acid [5-chloro-1-(2-hydroxy-3-piperidin-1-yl-propyl)-2-oxo-1,2-dihydro-indol-3-ylidene]-hydrazide **(89)**. A solution of the ketone **88** (0.4000g, 1.2392 mmol) and **83** (0.7331g, 2.4784 mmol) in 15 methanol was refluxed for 48 hrs monitored by TLC. The solvent was removed under reduced pressure and column chromatography (SiO_2, MeOH: CH_2Cl_2, 1:9) yielded **89** as yellow crystals (0.3395g, 11 %), mp 240-241 °C. R_f 0.21; IR ($CHCl_3$) ν_{max}/cm^{-1} 1459 (Ar C=C), 1579 (Ar C=N), 1605 (C_5=S), 1639 (C_{3I}=N), 1674 (C_{2I}=O); δ_H (300MHz, $CDCl_3$), (2H, br, H6'), 1.41 (4H, br, H5'), 2.31 (2H, br, H3'), 2.36 (4H, br, H4'), 3.61 (3H, m,

H2'+H1'), 3.91 (4H, m, H1+H2), 6.73-8.42 (8H, m, Ar) 7.46 (1H, t, *J* 2.7Hz, H3), 9.54 (H, t, *J* 5.4 Hz, H4), 12.45 (1H, s, H6); δ_C (100.6 MHz, DMSO-D6), 24.5 (C6'), 26.2 (2×C5'), 41.7 (C2), 43.2 (2×C4'), 45.7 (C1), 55.4 (C1'), 63.7 (C3'), 65.6 (C2'), 99.6 (C3Q), 113.7 (C10Q), 118.2 (C5I), 118.2 (C5Q), 120.5 (C7Q), 121.7 (C9I), 124.8 (C6Q), 127.5 (C8Q), 128.2 (C4I), 130.9 (C6I), 136.2 (C7I), 141.9 (C8Q), 143.6 (C9I), 149.7 (C4Q), 150.8 (C2Q), 152.5 (C3I), 161.5 (C2I), 168.4 (C5); HRMS (FAB) Found *m/z* 601.179653 $[M+1]^+$ $C_{28}H_{33}N_7SO_2Cl_2$ requires 601.179351; Found: C 56.19 %, H 5.75 %, N 15.31 %, S 4.75; Anal. Calcd: C 56.00 % H 5.20 %, N 16.33 %, 5.34 %.

REFERENCES

1) Bruce-Chwatt, L. J., Essential malariology. 2nd ed. London, William Heineman Medical Books Ltd, **1985**.

2) Sullivan, D. J., *International Journal for Parasitology*, **2002**, *32*, 1645-1653.

3) Moreau, S., Perly, B. and Biguet, *J. Biochimie*. **1982**, *64*, 1015-1025.

4) Ziegler, J., Linck, R. and Wright, D., W. *Curr. Med. Chem*. **2001**, *8*, 17-189.

5) Egan, T. J., *Exp. Opin. Ther. Patents*., **2001**, *11*, 185-209.

6) Egan, T. J., *Min. Rev. Med. Chem*., **2001**, *1*, 113-123.

7) Meshnick, S.; Dobson, M.; *Antimalarial Chemotherapy. Mechanisms of Action, Resistance and New Directions in Drug Discovery* (ed, Rosenthal, P.J.) 15-26 (Human, Totowa, New Jersey, **2001**).

8) Ridley, R.G., *Nature*, **2002**, *415*, 686.

9) Report No. WHO/CDS/RBM/2001.33 (World Health Organisation, Geneva, **2001**).

10) Clark, A. M., *Pharm. Res.*, **1996**, *13*, 801.

11) Newman, D. J.; Cragg, G. M.; and Snader, K. M.; *Nat. Prod. Rep.*, **2000**, *17*, 215-234.

12) Grabley, S.; Thiericke, R.; *Adv. Biochem. Eng./ Biotech.*, **1999**, *64*, 104.

13) Arvigo, R.; Balick, M.; Rainforest Remedies, Lotus Press, Twin Lakes, **1993**.

14) Grifo, F.; Newman, D.; Fairfield, A. S.; Bhattacharya, B.; Grupenhoff, J. T., In The Origins of Prescrition Grugs, ed. F. Grifo and J. Rosenthal, Island Press, Washington, D.C., **1997**, p. 131.

15) da Silva J. F. M.; Garden, S. J.; Pinto, A. C.; *J. Braz. Chem..Soc*., **2001**, *12*(3), 273-324.

16) Guo, Y.; Chen, F.; *Zhongcaoyao,* **1986**, *17*(8), *(CA 104: 213068f).*

17) Wei, L.; Wang, Q.; Liu, X., *Yaowu fenxi Zazhi,* **1982**, *2*, 288., (*CA 98:95726b*).

18) Ichia, M.; Palumbo, A.; Prota, G., *Tetrahedron*., **1998**, *44*, 6441.

19) Palumbo, A.; Ischia, M.; Misuraca, G.; Prota, G.; *Biocim. Biophhys. Acta.*, **1989**, *990*, 297.

20) Halket, J..M.; Watkins, P. J.; Przyborowska, A.; Goodwin, B.L.; Clow, A.;

Glover, V.; Sandler, M., *J. Chromatogr.* **1991**, *562*, 279.

21) Imam, S. A.; Varma, R. S., *Experientia*, **1975**, *31*, 1287.

22) Varma, R. S.; Khan, I. A., *Polish J. Pharmacol. Pharm.* **1977**, *29*, 549.

23) Lyer, R. A.; Hanna, P. E., *Bioorg. Med. Chem. Lett.* **1995**, *5*, 89.

24) Webber, S. E.; Tikhe, J.; Worland, S. T.; Fuhrman, S. A.; Hendrickson, T. F.; Matthews, D.A.; Love, R. A.; Patick, A. K.; Meador, J. W.; Ferre, R. A.; Brown, E. L.; Deslie, D. M.; Ford, C. E.; Binford, S. L., *J. Med. Chem.*, **1996**, *39*, 5072.

25) Shuttleworth, S. J.; Nasturica, D.; Gervais, C.; Siddiqui, M. A.; Rando, R. F.; Lee, N., *Bioorg. Med. Chem. Lett.*, **2000**, *10*, 2501.

26) Chiyanzu, I.; Hansell, E.; Gut, J.; Rosenthal, P. J.; McKerrow, J. H.; Chibale K., *Bioorg. Med. Chem. Lett.*, **2003**, *13*, 3527 – 3530.

27) Alam M.; Younas M.; Zafar M.A.; Naeem *P., J. Sci. Ind. Res.*, **1989**, *32*, 246. *(CA 112:7313u).*

28) Kapadia G.J.; Shuka Y.N.; Basak S.P.; Sokoloski E.A.; Fales H.M., *Tetrahedron*, **1980,** *36*, 2441.

29) Loloiu G.; Maior O., *Rev. Roum. Chim.* **1997**, *42*, 67.

30) Ijaz A.S.; Alam M.; Ahmad B., *Indian J. Chem. Sect.* B, **1994**, *33B*, 288.

31) Gassman P.G., *Ger. Offen.* 3, 000, **1980.** 338, *(CA 93:P204455g).*

32) Gassman P.G.; Cue B.W., Jr. US 4186132, **1980**. *(CA 92:P165220j.)*

33) Gassman P.G., US 4252723 **1981**. *(CA 93:P204455g).*

34) Pinto A.C.; Silva F.S.Q.; Silva R.B., *Tetrahedron Lett.*, **1994,** *35*, 8923.

35) Muchowski J.M.; Nelson P.H., *Tetrahedron Lett.*, **1980**, *21*, 4585.

36) Collino, F.; Volpe, S., *Bull. Chim. Farm.*, **1982**, *121*, 408, (CA 98:143360b).

37) da Silva J. F. M.; Garden, S. J.; Pinto, A. C., *J. Braz. Chem..Soc.*, **2001**, *12*(3), 273-324.

38) Gopal, M.; Srivastava, G.; Pande, U. C.; Tiwari, R. D., *Microhim Acta*, **1977**, 215.

39) Niera, D.; de Domínguez, G.; Rosenthal, P. J., *Blood*, **1996**, *87*, 4448-4454.

40) Gabay, T.; Ginsburg, H., *Exp. Parasitol.*, **1993**, *77*, 261-272.

41) Rubin, H.; Salem, J. S.; Li, L-S.; Yang, F.; Mama, S.; Wang, Z.; Fisher, A.; Hamann, C. S.; Cooperman, B. S., *Proc. Natl. Acad. Sci.* USA, **1993**, *90*, 9280.

42) Surolia, N.; Padmanaban, G., *Biochem. Biophys. Res. Commun.* **1992**, *187*,

744.

43) Awamahasakda W.; Ittarat, I.; Chang, C.C.; McElroy, P.; Meshnick, S.R., *Mol. Biochem. Parasitol.* **1994**, *67*, 183-191.

44) Orijih, A. U.; Banyal, H. S.; Chevli, R.; Fitch, C. D., *Science*, **1981**, *214*, 667.

45) Lecaille F.; Brömme D., *Chem. Rev.*, **2002**, *102*, 4459-4488.

46) Turk, D.; Guncar, G.; Turk, P.; Turk, B., *J. Biol. Chem.*, **1998**, *279*, 137 – 147.

47) Giles N.M.; Watts A.B.; Giles G.I.; Fry F.H.; Littlechild J.A.; Jacobs C., *Chem. Biol*, **2003**, *10*, 677-693.

48) Park O.K.; Bauerie R., *J. Bacteriol*, **1999**, *181*, 1636-1642.

49) Schroder, E.; Philiphs, C.; Garman, E.; Harlos, K.; Crawford, C., *FEBS Lett.*, **1993**, *315*, 38.

50) Lalonde, J M.; Zhao, B.; Smith, W. W.; Janson, C.A.; DesJarlais, R. L.; F.; Tomaszek, T. A.; Carr, J. T.; Thompson, S. K.; Oh, H-J.; Yamashita, D. S.; Veber, D.; Abdel-Meguid, S.S., *J. Med. Chem.*, **1998**, *41*, 4567.

51) Marquis, R. W.; Yamashita, D. S.; Ru, Y.; LoCastro, S. M.; Oh, K. F.; Erhard, K. F.; Des Jarlais, R. L.; Head, M. S.; Smith, W. W.; Zhao, B.; Janson, C. A.; Abdel-Meguid, S.S.; Tomaszek, T. A; Levy, M. A.; Veber, D. F., *J. Med. Chem.*, **1998**, *41*, 3563.

52) Marquis, R. W., *Annual Reports in Medicinal Chemistry*, **2000**, *35*, 309.

53) Votta, B. J.; Levy, M. A.; Badger, A.; Bradbeer, J.; Dodds, R.A.; James, I.E.; Thompson, S.; Bossard, M. J.; Carr, T.; Connor, J. R.; Tomaszek, T. A.; Szewczuk, L.; Drake, F. H.; Veber, D. F.; Gowen, M. J., *J. Bone Miner. Res.*, **1997**, *12*, 1396.

54) Conroy, J. L.; Sanders, T. C.; Seto, C. T.; *J. Amer. Chem. Soc.*, **1997**, *119*, 4285.

55) Conroy, J. L.; Abato, P.; Ghosh, M.; Austermuhle, M. I.; Kiefer, M. R.; Seto, C. T., *Tet. Lett.*, **1998**, 8253.

56) Dragovich, P. S.; Zhou, R.; Webber, S. E.; Prins, T. J.; Kwok, A. K.; Okano, K.; Fuhrman, S. A.; Zalman, L. S.; Maldonado, F. C.; Brown, E. L.; Meador III, J. W.; Patik, A. K.; Ford, C. E.; Binford, S. L.; Mattews, D. A.; Ferre, R. A.; Worland, S. T., *Bioorg. Med. Chem. Lett.*, **2000**, *10*, 45.

57) Lee, D.; Long, S.A.; Adams, J. L.; Chan, G.; Vaidya, K. S.; Francis, T. A.; Kikly, K.; Winkler, J. D.; Sung, C-M.; Debouck, C.; Richardson, S.; Levy, M. A.; DeWolf, W. E.; Keler, P. M.; Tomaszek, T.; Head, M. S.; Ryan, M. D.; Haltiwanger, R. C.; Liang, P-H.; Janson, C. A.; McDevitt, P. J.; Johanson, K.; Concha, N. O.; Chan, W.; Abdel-Meguid, S. S.; Badger, A. M.; Lark, M. W.; Nadeau, D. P.; Suva, L. J.; Gowen, M.; Nuttall, M. E., *J. Biol. Chem.* In Press.

58) Matthews, D.A.; Dragovich, P, S.; Webber, S. E.; Fuhrman, S. A.; Patrik, A. K.; Zalman, L. S.; Hendrikson, T. F.; Love, R. A.; Prins, T. J.; Marakovits, J. T.; Zhou, R.; Tikhe, J.; Ford, C. E.; Meador, J. W.; Ferre, R. A.; Brown, E. L.; Binford, S. L.; Brothers, M. A.; DeLisle, D. M.; Worland, S. T.; *Proc. Natl. Acad. Sci.*, **1999**, *96*, 11000.

59) Patick, A. K.; BinFord, S. L.; Brothers, M. A.; Jackson, R. L.; Ford, C. E.; Diem, M. D.; Maldonado, F.; Dragovich, P. S.; Zhou, R.; Prins, T. J.; Fuhrman, S. A.; Meador, J. W.; Zalman, L. S.; Matthews, D. A.; Worland, S. T.; A*ntimicrob. Agents Chemother.*, **1999**, *43*, 3193.

60) Riese, R. J.; Mitchell, R. N.; Villadangos, J. A.; Shi, G-P.; Plamer, J. T.; Karp, E. R.; DeSanctis, D. T.; Ploegh, H. L.; Chapman, H. A., *J. Clin. Invest.*, **1998**, *101*, 2351.

61) Rosenthal, P. J.; Olson, J. E.; Lee, G. K.; Palmer, J. T.; Klaus, J. L.; Rasnick, *Antimocrob Agents Chemother.*, **1996**, *40*, 1600.

62) Kranz, A.; *Methods in Enzymology*, **1994**, *47*, 656.

63) Krantz A.; *Advances in Medicinal Chemicinal*, **1992**, *1*, 235.

64) Bagio, R.; Shi, Y-Q.; Wu, Y-Q.; Abeles, R. H.; *Biochemistry*, **1996**, *35*, 3351.

65) Venkatraman, S.; Kong, J-s.; Nimkar, S.; Wang, Q. M.; Aube, J.; Hanzlik, R. P.; *Bioorg. Med. Chem. Lett.*; **1999**, *9*, 577.

66) Thomson, S. K.; Halbert, S.M.; Bossaed, M. J.; Tomaszek, T. A.; Levy, M. A.; Zhao, B.; Smith, W.W.; Abdel-Megud, S. S.; Janson, C. A.; D'Alessio, K. J.; McQueney, M. S.; Amegadzie, B. Y.; Hanning, C. R.; DesJarlais, R. L.; Briand, J.; Sarkar, S. K.; Huddleston, M. J.; Ijames, C. F.; Carr, S. A.; Garnes, K. T.; Shu, A.; Heys, J. R.; Bradbeer, J.; ZembryKi, D.; LeeRykaczewki, L.; James, I. E.; Lark, M. L.; Drake, F. H.; Gowen, M.; Gleason, J. G.; Veber, D. F.; *Proc. Natl, Acad. Sci.* USA, **1997**, *94*, 14249.

67) Rosenthal, P. J.; Meshnick, S.R., *Mol. Biochem. Parasitol.* **1996**, *83,* 131-139.

68) Yayon, A.; Vande Waa, J.A.; Yayon, M., Geary, T.G., *J. Protozool.* **1983**, *30,* 642-647.

69) Slater, A.F.G., *Exp. Parasitol.* **1992**, *74,* 392.

70) Egan T.J.; Combrinck J.M.; Egan J.; Hearne G.R.; Marques H.M.; Ntenteni S., Sewell B.T.; Smith P.J.; Talor D.; van Schalkwyk D.A.; Walden J.C., *Biochem. J.*, **2002**, *365,* 343-347.

71) Gluzman, I.Y.; Francis, S.E.; Oksman., A.; Smith, C.E.; Duffin, K.L; Golberg, D.E., *J.Clin. Invest.* **1994**, *93,* 1602-1608.

72) Francis, S. E.; Gluzman, I. Y.; Oksman, A.; Banerjee, D.; Golberg, D.E., *Mol. Biochem. Parasitol.* **1996**, *83,* 89-200.

73) Salas, F.; Fichmann, J.; Lee, G.K.; Scott, M.D.; Rosenthal, P.J. *Infect. Immun.* **1995**, *63,* 2120-2125.

74) Carrell, R.W.; Winterbourn, C.C.; Rachmilewitz, E. A. *Br. J. Haematol.* **1994**, *30,* 259-264.

75) Misra, H. P.; Fridovich, I. *J. Biol. Chem.* **1972**, *247,* 6960-6962.

76) Hunt, N.H.; Stocker, R. *Blood Cells*, **1990**, *16,* 499-526.

77) Golberg, D.E.; Slater, A.F.G.; Beavis, R.; Chait, B.; Cerami, A.; Henderson, G.B. *J. Exp. Med.* **1991**, *173,* 961-969.

78) Beychok, S.; Tyuma, I.; Benesch, R. E.; Benesch, R., *J. Biol. Chem.* **1967**, *242,* 2460.

79) Kolakovich, K.A.; Gluzman, I.Y.; Duffin, K.L Golberg, D.E., *Mol. Biochem. Parasitol.*, **1997**, *87,* 123-135.

80) Dorn, A.; Stoffel, H.; Matile, H.; Rubendorf, R.; Ridley, R.G. *Nature*, **1995**, *374,* 269-271.

81) Slater, A.F.G;. Cerami, A. *Nature*, **1992**, *355,* 167-169.

82) Bendrat, K.; Berger, B.J.; Cerami, A., *Nature*, **1995**, *378,* 138.

83) Sullivan, D. J.; Gluzman, I. Y.; Golberg, D.E., *Science*, **1996**, *271,* 219-222.

84) Slater, A.F.G.; Cerami, A., *Int. Pat. Appl.* PCT/US92/11279, **1993**.

85) Pagola S.; Stephens P.W.; Bohle D.S.; Kosar A.D.; Madsen S.K., *Nature*, **2000**, *404,* 307.

86) Bohle S.D.; Stephens P.W.; Dinnebier R.E.; Madsen S.K., *J. Biol. Chem.* **1997**, *272,* 713.

87) Sumpter, W. C., *Chem. Rev.*, **1954**, *34*, 407.

88) Finch R.A.; Liu M.C.; Cory A.H.; Cory J.G.; Sartorelli A.C., *Adv. Enzyme Regul.*, **1999**, *39,* 3-12.

89) Klayman D.L.; Bartosevich J.F.; Grffin T.S.; Mason C.J.; Scovill J.P., *J. Med. Chem.*, **1979**, *22,* 855-862.

90) Wilson, H.R.; Revankar, G. R.; Tolman, R. L., *J. Med. Chem.*, **2002**, *45*, 2695-2707.

91) Du X.; Guo C.; Hansell E.; Dyole P.S.; Caffrey C.R.; Holler T.P.; McKerrow J.H.; Cohen F.E., *J. Med. Chem.*, **2002**, *45*, 2695-2707.

92) Barret, A.; Salvesen, G., *Proteinase Inhibitors*, Eds. Elsevier Amsterdam, **1986**, *19*, 3 – 22.

93) Sweeney, D.; Raymer, M. L.; Lockwood, T. D., *Biochem. Pharmacol.*, **2003**, *66*, 663-677.

94) Sridhar, S. K.; Saravanan, M.; Ramesh, A., *Eur. J. Med. Chem.*, **2001**, *36*,

615-625.

95) Klayman, D. L.; Bartoservich, J. F.; Griffin, T. S.; Mason, C. J.; and Scovill, J. P. *J. Med. Chem.* **1979**, 22, 855-862.

96) Li, R.; Kenyon, G. L.; Cohen, F. E.; Chen, X.; Gong, B.; Dominguez, J. N.; Davidson, E.; Kurzban, G.; Miller, R. E.; Nuzum, E. O.; Rosenthal, P. J.; McKerrow, J. H. *J. Med. Chem.* **1995**, *38*, 5031.

97) Shenai, B. R.; Sijwali, P. S.; Singh, A.; Rosenthal, P. J., *J. Biol. Chem.* **2000**, *275*, 29000.

98) Pradines, B.; Rlain, J. M.; Ramiadrasoa, F.; Fusai, T.; Mosnier, J.; Rogier, C; Daries, W; Baret, E.; Kunesch, G; LeBras, J; Parzy, D., *J.Antimicrob. Chemother.* **2002**, *50*, 177-187.

UNIVERSITY OF CAPE TOWN

MEDICINAL CHEMISTRY RESEARCH GROUP- 2004

BACK ROW (standing): Boniface Mbewe, Chitalu Musonda, Alexander Dauth, Nelson Ntuli, Frank Chouteau, Richard Gessner, Susan Yeh, Claire Tacon, Aloysiuns Nchinda.

FRONT ROW (standing): Tzu-Shean (Jamy) Feng, Carrie-Ann Molneaux, Mengistead Bereketead G, Fereidoon Daryaee, Natasha October, Riyad Domingo.

SEATED: Kelly Chibale.